

Steering towards stiffness

A preliminary analysis method for local deformations in a yacht structure caused by wave-induced loads

L. van der Linde

Technische Universiteit Delft



Steering towards stiffness

A preliminary analysis method for local deformations in a yacht structure caused by wave-induced loads

by

L. van der Linde

to obtain the degree of Master of Science
at the Delft University of Technology,
to be defended publicly on Monday June 3, 2019 at 14:00.

Student number: 4229363
Project duration: 01-11-2018 until 03-06-2019
Thesis committee: Ir. J. Sinke, TU Delft, chair
Dr. ir. J.M.J.F. van Campen, TU Delft, supervisor
Dr. ir. G.N. Saunders-Smits, TU Delft
Ir. M. van Wijngaarden, Feadship/De Voogt Naval Architects

An electronic version of this thesis is available at <http://repository.tudelft.nl/>.

Preface

This master thesis is an attempt to provide Feadship/De Voogt Naval Architects with more accurate and practical insights in the longitudinal stiffness of their designed and manufactured superyachts. Considering my background in aerospace engineering, it shows that engineering knowledge crosses the boundaries of different industries and that the combination of different views and backgrounds strengthens development. It was great to work for my research amid people that are building the dreams of future superyacht owners and it gave me a glimpse into a world that only a very small percentage of the world is ever going to be part of.

I wish to express my gratitude to Dr. Julien van Campen for all his support and guidance that set my focus on the subjects of importance. Also, the availability for questions, feedback, interest and the trips to Feadship are highly appreciated. For my supervision at Feadship I would like to express my gratitude to Ir. Martijn van Wijngaarden and for giving me practical advice on improvement of my work by setting realistic targets.

To all my friends I would like to say thank you for the necessary distractions, drinks and support during the last few months. A special thanks goes to my girlfriend Tamar for believing in me during my thesis and my complete master's degree. The enjoyable moments and laughing together kept me positive and allowed me to write a thesis that I am proud of. Finally, I am grateful to my parents that cared for me all those years and gave their unconditional support that made it possible to study in Delft.

*L. van der Linde
Delft, June 2019*

Nomenclature

Acronyms

APP	Aft perpendicular
CoG	Center of Gravity
EDW	Equivalent Design Wave
FE	Finite Element
FEA	Finite Element Analysis
FEM	Finite Element Method
FPP	Front perpendicular
ISSC	International Ship and Offshore Structures Congress
JONSWAP	Joint North Sea Wave Observation Project
MPR	Most Probable max Response
P-M	Pierson-Moskowitz
RANS	Reynolds-Averaged Navier-Stokes
RAO	Response Amplitude Operator
SDA	Significant Double Amplitude
SSC	Special Service Craft
SWBM	Still Water Bending Moment
SWSF	Still Water Shear Force
TR	Target response
VBM	Vertical Bending Moment
WBM	Wave Bending Moment

Greek symbols

β	Heading angle	°
γ	Peak shape parameter	-
λ	Wave length	m
ω	Warping displacement	m
ω	Wave frequency	rads ⁻¹
ω_e	Encounter frequency	rads ⁻¹
ω_{EDW}	Equivalent Design Wave frequency	rads ⁻¹
ϕ	Cross-sectional rotation	rad

ϕ	Phase angle	rad
ϕ	Roll angle	°
ψ	Yaw angle	°
σ	Spectral width parameter	-
σ_ζ	Root mean square wave elevation	m
θ	Cross-sectional rotation	rad
θ	Pitch angle	°
ε	Phase angle	rad
ζ	Surface elevation	m
ζ_a	Wave amplitude	m
ζ_{max}	Most probable maximum amplitude	m
Roman symbols		
A	Area	m ²
A_v	Vertical projected area	m ²
A_γ	normalising factor	-
B	Yacht beam	m
C	Restoring matrix	-
C_b	Block coefficient	-
D	Hydrodynamic body motion force	N
D	Yacht depth	m
E	Froude-Krylov force	N
E	Young's modulus	Pa
F	Force	N
G	Shear modulus	Pa
g	Gravitational constant	9.81 ms ⁻²
H	Transfer function	-
H	Water depth	m
H	Wave height	m
H_s	Significant wave height	m
I	Inertial force	N
I	Moment of inertia	m ⁴
J	Torsional constant	m ⁴
K	Stiffness matrix	-
k	Shear correction factor	-

k	Wave number	rad m^{-1}
l	Element length	m
L_r	Rule length	m
L_{oa}	Length overall	m
L_{pp}	Length between perpendiculars	m
L_{wl}	Length waterline	m
M	Bending moment	Nm
M	Mass matrix	-
m_n	Spectral moment	-
M_x	Torque	Nm
N	Number of wave cycles	-
Q	Internal shear load	N
q	Distributed load	Nm^{-1}
R	Hydro-static restoring force	N
r	Response	-
S	Wave (variance density) spectrum	$\text{m}^2 \text{s}$
S_r	Response (variance density) spectrum	-
T	Wave period	s
T	Yacht draught	m
t	Thickness	m
T_z	Mean zero-crossing period	s
t_{exp}	Exposure time to sea state	s
u	Axial displacement	m
u	Displacement field	m
V	Shear force	m
V	Yacht speed	kts
w	Displacement	mm
x	Longitudinal location	m

Abstract

The superyacht industry faces an increasing trend of larger dimensions, more open spaces, larger hull openings and more exotic shapes. This puts more effort on the structural design of the yachts to maintain the high luxury standard that distinguishes superyachts from commercial marine vessels. Especially longitudinal stiffness is important, since the luxurious interior and delicate systems installed in a superyachts are not allowed to cause creaking noises or be damaged. Inevitably, a structure deforms elastically and knowledge on the magnitude of these deformations is required to be able to design the structure in accordance with the high comfort standards belonging to superyacht customers. Experimental observations show a direct link to the yacht sailing in waves and interior movement due to an elastically deforming structure. Therefore knowledge on the sea state that causes the loads and an accurate structural model that represents the yacht structure is essential in predicting the deformations that occur during operation. The aim of this thesis is to establish a method that can provide more insights in the magnitude of the structural deflections and rotations in operating conditions of Feadship superyachts to use for risk assessment and provides guidance on clearances or connections that should be used for interior instalment.

The determination of deformations considers the wave-induced loads acting on the hull structure and the structural characteristics of the yacht. A potential flow strip method is used in this thesis to determine the linear response of a yacht to a sea state represented by a standard JONSWAP spectrum. A regular equivalent design wave is used to obtain design load distributions that represent the most extreme or most probable loading distribution the yacht experiences for a set of operation parameters such as heading angle and speed. The yacht structure is modelled excluding the superstructure as a Timoshenko beam including shear deformations and torsion and its global and local deformation response is verified with commercial software. Validation is done by comparison of the structural response of the beam model with a 3D detailed Finite Element (FE) model response of a test case yacht subjected to classification society rule loads. The design load distributions are then applied to the beam model to obtain global and local deformation estimates of the yacht structure in a realistic sea state. The deformations can be compared to limit values to indicate structural risks and provide magnitude for the clearances and connections that should be adopted for the interior.

The operational load distributions derived with the equivalent design waves match in shape and order of magnitude with the rule design loads. Maximum vertical and horizontal bending moments are observed to be amidships and the maximum torque is observed to be more aft at approximately 25% of the length between perpendiculars. The equivalent design wave can generate concurrent load distributions that occur for heading angles smaller than 180° to indicate what deformations occur in or out of phase with each other.

The beam model showed good agreement with the 3D FE model for the global displacements and rotations for the vertical and horizontal and the longitudinal rotation for the torque. Including the shear deformations in the beam model resulted in an increase of 20% for the maximum vertical displacement, reducing the stiffness significantly. The local response is derived from the global response and three main deformation components are calculated: the bulging, expansion/contraction of horizontal structural elements caused by vertical bending and the vertical displacement due to torsion of the hull girder. The local deformation components are compared to the deformation in the 3D FE model and a good agreement is found.

The operational load distributions and the beam model are combined to create a longitudinal distribution of the deformation components that can indicate whether excessive deformation will occur in a longitudinal section of the yacht. Also, the deformation components can directly indicate what measures should be taken to install the interior with proper clearance or connections.

Contents

Abstract	ix
1 Introduction	1
1.1 Aim and scope	1
1.2 Research questions	2
1.3 Thesis structure	2
2 Literature review	3
2.1 Yacht definitions and loading	3
2.1.1 Geometry	3
2.1.2 Hull loading	4
2.2 Wave theory	5
2.2.1 Wave definition	6
2.2.2 Regular waves	7
2.2.3 Irregular waves.	7
2.2.4 Wave spectra	8
2.2.5 Standard wave spectra	8
2.3 Short term wave statistics	9
2.4 Seakeeping analysis	10
2.4.1 Linear response analysis	11
2.4.2 Strip method	12
2.4.3 Response to an irregular seaway	13
2.4.4 Internal loads	14
2.4.5 Equivalent Design Wave	15
2.4.6 Non-linearity's in seakeeping analysis	15
2.5 Structural modelling	16
2.5.1 Euler-Bernoulli beam theory.	17
2.5.2 Timoshenko beam theory	17
2.5.3 Shear correction factor.	18
2.6 Finite Element Analysis	18
2.7 Load transfer to structural model	19
2.8 Summary and discussion	20
3 Operational wave-induced loads	23
3.1 Test case	24
3.2 Linear response analysis	24
3.2.1 Internal loads	25
3.2.2 The response spectrum	26
3.3 Equivalent Design Wave	29
3.3.1 Equivalent Design Wave features.	29
3.3.2 The target response	30
3.3.3 Load distributions	33
3.3.4 Applicability for structural response	34
3.4 Summary	36
4 Structural response	39
4.1 Finite Element model	40
4.2 Beam model verification	41
4.3 Property determination.	42
4.4 Global response.	44
4.4.1 Load cases	45

4.4.2	3D FE model description.	47
4.4.3	Validation results and discussion	48
4.5	Local response	50
4.5.1	Vertical bending response	51
4.5.2	Torsional response	56
4.6	Local deformations with design loads.	58
4.6.1	Risk analysis	62
4.6.2	Clearance analysis	64
4.7	Solutions for response improvements.	66
4.8	Summary	67
5	Conclusions	69
6	Recommendations for future work	71
	Bibliography	73
A	Two-noded Timoshenko beam element	77
B	Siemens NX 11 cross-sectional property performance	79



Introduction

Feadship is specialised in the design, engineering and manufacturing of luxurious superyachts for the wealthy few percent of the worlds population. The preliminary design of these superyachts is performed by Feadship subsidiary: De Voogt Naval Architects and is subjected to high performance, appearance and comfort standards. In yacht building, the stylist of the in- and exterior has a major role in safeguarding the desirable design for the customer while the engineer has to fit the boat around the stylish design and make it safe and with sufficient structural integrity [22]. This is very different from the 'function-over-looks' approach used in the commercial ship industry. From the point of an optimal design, the structural engineer thus has much less freedom, though the yacht still has to meet all the certification strength requirements from the classification societies, such as Lloyd's Register. These classification societies provide prescriptive empirical design rules, that include maximum allowed shear and moment envelopes for the strength assessment of the hull. In normal operation, loads close to these extreme envelopes are not to be expected, especially not for superyachts, that operate in relatively calm waters.

The wave-induced loads in normal operating conditions do not lead to strength issues in general, but these loads do cause elastic deflections of the yacht structure. The deflections or movement of the structure relative to the interior can cause e.g. creaking of interior, but also damage to glass walls or windows without proper clearance. The perceived comfort level on a yacht can be improved by proper analysis of the elastic deflections and their effect on the interior creaking. In other words, this considers a study to the stiffness of the yacht structure.

Solutions exist to solve the discomforting effects of a deflecting yacht structure: e.g. the design of the interior can be adapted to dampen the effects, appropriate clearances can be applied during interior instalment and/or the structure itself can be stiffened. For a proper solution trade-off and risk assessment, knowledge on the magnitude of the deflections is required. At Feadship, no capacity currently exists to obtain realistic estimates of the deflections of the yacht structure under operational conditions in the preliminary design phase. Load cases provided by classification societies only provide extreme loading conditions instead of operating conditions and no method is available to calculate the structural response at relevant locations.

The creaking of interior caused by a deflecting yacht structure is unacceptable for a high-quality superyacht and realistic estimates of the deflections are therefore worth investigating to minimise their occurrence and thereby improving the perceived comfort level on Feadship superyachts.

1.1. Aim and scope

The analysis of structural deflections due to wave-induced loads in operating conditions is a complex situation that consists of vertical and horizontal bending, torsion and in-plane deformation of the yacht structure. All these responses can result to some degree to the deflecting yacht structure that can come in contact with interior and cause creaking or damage. This thesis work aims to establish a method that can provide more insights in the magnitude of the structural deflections and rotations in operating conditions of yachts to use for risk assessment and gives magnitudes of required clearances and interior connections to minimise discomfort of the Feadship customer. The knowledge on the longitudinal bending and torsion stiffness of Feadship super yachts should hereby increase and the research objective considered in this work to contribute to these developments is:

To include the effect of operational wave-induced loads on a yacht structure in the preliminary design phase by creating a structural model that incorporates major structural elements and identifies structural limit states that can indicate excessive local deformations and/or predict required interior clearances.

The approach in this thesis work to achieve this goal can be divided in two main subjects: the derivation of operational wave-induced load distributions that act on the yacht structure and the modelling of the yacht structure using methods suitable for the preliminary design. The yacht structure is modelled as a non-prismatic beam that includes shear deformations and torsion. The wave-induced loads are determined by a linear response analysis using a strip theory potential flow analysis. The two main subjects are combined to study the response of the yacht in an operational sea state environment to obtain information on the deformations that can be expected in a realistic operating scenario.

1.2. Research questions

The research is guided by two main research questions, each with the necessary sub-questions. The first research question (I) concerns the first main subject of the operational wave-induced loads and is regarded in Chapter 3. The second main research (II) question concerns the second main subject of the structural model and its accuracy, which is regarded in Chapter 4.

- I What is the relevant operational wave-induced load distribution of a yacht in relation to the longitudinal stiffness and how does it compare to the rule design loads?
 - a *For what heading angles and mean-zero crossing periods of the sea state do the individual internal load components have the largest response?*
 - b *At what longitudinal location should the peak response be taken as target response to determine the load distributions with the Equivalent Design Waves (EDW's)?*
- II Can the response of the 1D beam model be used to indicate excessive deformations in new designs and/or obtain useful predictions for interior clearance?
 - a *What is the influence of the method to determine the cross-sectional property distribution of the yacht?*
 - b *What is the accuracy of the global response and the local (room) response of a 1D beam model of a yacht compared to a 3D FEM response?*
 - c *Is there a significant influence of the shear deformations in the results or is a more simple beam theory that neglects these deformations sufficient?*

1.3. Thesis structure

The main body of this document starts with the literature review in Chapter 2. For readers with a non-maritime background the necessary concepts and ship terminology that are relevant to understand the research work are discussed. The chapter contains also an introduction to linear wave theory, irregular waves and wave spectra. Furthermore, an introduction is provided in the seakeeping abilities or seaworthiness of a marine vessel for understanding the linear response analysis used in combination with the strip method potential flow analysis. At last, structural modelling capabilities are discussed for ships and examples are given for their performance and applicability in relation to this thesis work.

In Chapter 3, the linear response analysis method is described that defines the response of a test case yacht to an irregular sea in the frequency spectrum. Design load distributions are derived for the vertical and horizontal bending and the torque based on the response results from the linear response analysis.

Chapter 4 considers the structural modelling of the yacht structure with 1D Timoshenko beam elements, programmed in the Python programming language. The accuracy of this model is determined by comparison with a 3D Finite Element (FE) model of a test case yacht. The design load distributions from Chapter 3 are then applied to the beam model to determine the global and local deformations that occur in the yacht for an actual seaway. These deformation components are then used as example of structural risk assessment and clearance analysis to be used for new yachts.

Conclusions on the work performed in this thesis are given in Chapter 5 including answers to the research questions to determine if the research objective is met. Recommendations are given in Chapter 6 by the author for future work based on the work in this document.

2

Literature review

From the viewpoint of structural engineering, commercial shipping puts a focus on strength and fatigue assessment by probabilistic load analysis. The operational envelope of superyachts is quite different and the yachts usually do not encounter the extreme loading conditions that are taken into account for commercial vessels. For certification of superyachts, the structural strength and integrity is always necessary, though, often with less extensive structural analysis performed as compared to commercial vessels. In contrast to commercial marine vessels, the longitudinal stiffness gets more focus for superyachts, due to the luxurious nature of the interior and the customer comfort that is expected. The inherent nature of a structure to deform elastically under a load must be taken into account to make sure that the interior inside the yacht does not creak or get damaged. This research aims to predict the magnitude of the deflecting yacht structure for risk management and to account for them during the detailed design phases. This combines two main subject as indicated in Chapter 1: the operational wave-induced loads of yachts and the structural modelling of the yacht structure.

For readers without a maritime background, general yacht or ship definitions and loading conditions are given in Section 2.1 for a basis to understand the terminology in this work. It is followed by an introduction to linear wave theory in Section 2.2 including the mathematical descriptions of the ocean surface that is used to describe the wave statistics in Section 2.3. The determination of the hydrodynamic loads that act on a ship due to waves (the wave-induced loads) are part of the maritime field called seakeeping and is presented in Section 2.4. Seakeeping analysis considers the determination of the seakeeping abilities of a ship and can be used to derive load distributions. In Section 2.5 the modelling of ship structures is discussed with examples of methods used in literature for the preliminary design phases. The non-prismatic nature of the yacht hull structure requires numerical methods such as the Finite Element Method (FEM) to obtain more accurate results, which is shortly discussed in Section 2.6. The transfer of the load distributions to a structural model such as a Finite Element (FE) model is less straightforward for a free floating structure than for a static object and therefore a short discussion is given in Section 2.7. At last, the literature study is summarized and discussed in Section 2.8.

2.1. Yacht definitions and loading

A yacht is a special category of motorised ships built for leisure or representative purposes. Many similarities exist with commercial or professional ships, though more emphasis is put on their comfort, appearance and luxury instead of design functionality and efficiency. For Feadships, the term superyacht is more appropriate, which is in general defined as a yacht of ≥ 25 m. Yacht specific literature is scarce, because most literature on ships has its origin in the commercial shipping industry, though in general the same principles and definitions are applicable. The words: ship, yacht and superyacht are therefore used interchangeably in this work.

2.1.1. Geometry

The geometry of a yacht can be described in many different parameters and the main geometry dimensions used in this work are given in Figure 2.1. The aft perpendicular is the vertical line through the rudder post and the front perpendicular is the vertical line that intersects the forward side of the ships bow at the waterline.

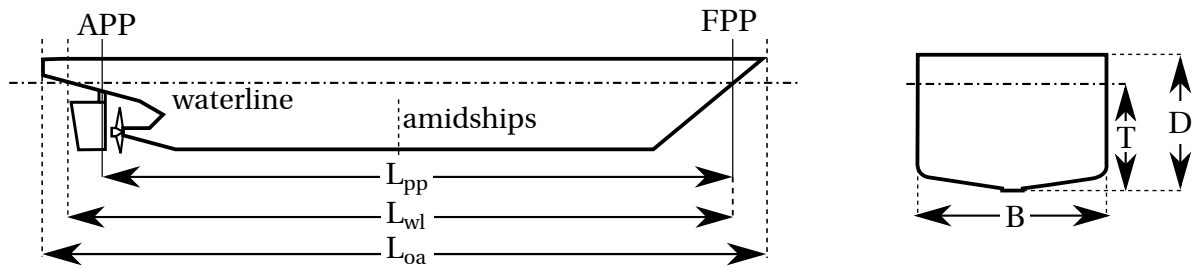


Figure 2.1: Yacht geometry definitions: APP = aft perpendicular, FPP = front perpendicular, L_{pp} = length between perpendiculars, L_{wl} = length on waterline, L_{oa} = length overall, B = beam, T = draught and D = depth

2.1.2. Hull loading

In this study, the loads related to the water pressure on the hull are regarded. This water pressure results in three important moment distributions in the hull: the vertical bending moment, the horizontal bending moment and the moment of torsion or torque. The vertical bending moment is the most important load component [52] and consists of a hydrostatic and hydrodynamic component. The hydrostatic component is a result of the fact that the mass distribution is generally not equal to the upward force of the water (buoyancy). The difference between the two forces results in the internal Still Water Shear Force (SWSF) and Still Water Bending Moment (SWBM). This process is illustrated in Figure 2.2

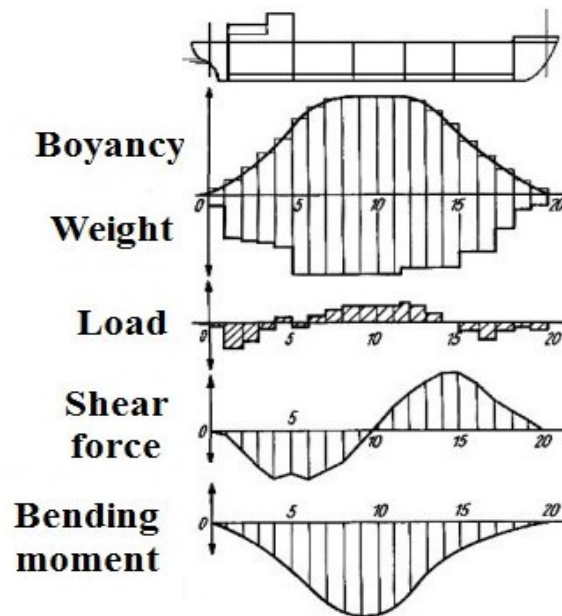


Figure 2.2: Determination of the still water shear force and bending moment distributions along the length of a ship. [63]

In a dynamic situation, i.e. the ship lies in water with waves, the hydrodynamic pressure of the water causes an additional bending moment to the still water bending moment called the Wave Bending Moment (WBM). The superposition of the SWBM and WBM results in the total Vertical Bending Moment (VBM) as given in Eq. (2.1).

$$VBM = SWBM + WBM \quad (2.1)$$

The WBM can be negative or positive and if the resulting VBM of Eq. (2.1) is positive, the hull girder¹ is in a so-called *hogging* state. The hull is bent longitudinally concave downwards by the forces acting on it. If the VBM is negative, the hull girder is said to be in a *sagging* state where the hull is bent longitudinally concave upward. The hogging and sagging states of the global hull girder are illustrated in Figure 2.3.

¹The theoretical box girder formed by the continuous longitudinal members of the hull of a ship

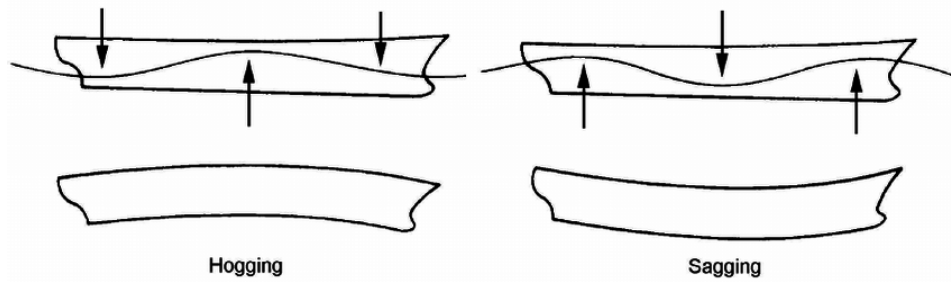


Figure 2.3: Hogging and sagging states of a ship hull girder. [18]

For structural analysis, the maximum value of the wave bending moment is an important design parameter for ultimate strength assessment. In ship design, the wave bending moments and shear forces are usually given by empirical relations that are specified by classification societies such as Lloyd's Register. These relations are defined based on geometrical properties of the yacht and different rules exist for different ship types. Yachts manufactured at Feadship fall into the Lloyd's Register G6 Special Service Craft category. The rules are considered conservative estimates of the maximum loads a yacht encounters in its service life, because they are generally applicable and not yacht specific.

The torque on the hull girder is illustrated in Figure 2.4, where the ship is located in between two wave crests and an asymmetric pressure distribution on the hull results in the wave-induced torque M_x in the hull. The same asymmetric pressure distribution results in horizontal shear forces and consequently the Horizontal Bending Moment (HBM).

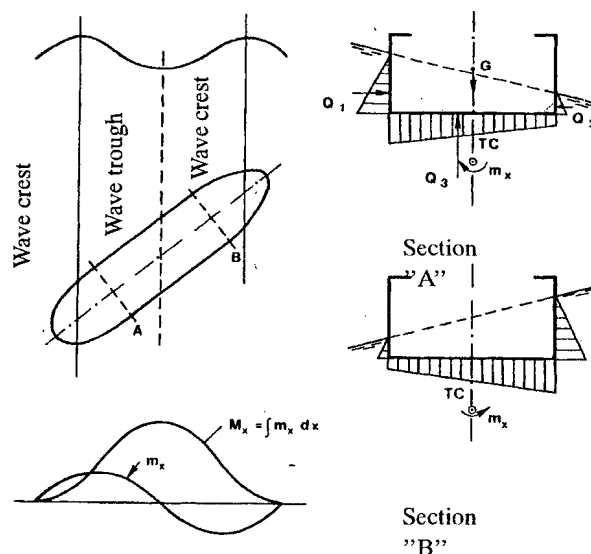


Figure 2.4: The wave-induced torque M_x on a ship's hull. [33]

In addition to the design rules, direct hydrodynamic analysis can also be performed to analyse the wave bending moments, torque and shear forces occurring due to waves. In broader terms, hydrodynamic analysis is performed as part of a seakeeping analysis, which considers the seakeeping abilities or seaworthiness of a marine vessel as will be discussed in Section 2.4. Seakeeping can be seen as the response to the ocean waves and therefore wave theory is regarded first in Section 2.2.

2.2. Wave theory

For understanding of the hydrodynamic loads, it is important to understand what is causing these loads and what the theories are that describe the waves mathematically. In this section an introduction to the definitions and mathematical principles of (linear) wave theory are given, which are required for a proper under-

standing of the hydrodynamic seakeeping analysis.

2.2.1. Wave definition

Ocean waves are classified in different categories of wave period with different amounts of energy. It depends on the type of maritime structure, which ones are to be taken into account. For ships and yachts, the high energy, wind generated gravity waves with a period of 1/4 s to 30 s are the most relevant. [6]

In marine engineering, there is a distinction with an elevation of the ocean surface and a wave. A surface elevation is the instantaneous elevation of the ocean surface in a time record relative to a zero water level and a wave is the total profile of the surface elevation between two successive zero-crossings. In Figure 2.5 an example of a time record of water surface elevation can be seen. Here a downward-zero crossing is given, i.e. one wave is defined being in between two successive downward crossings of the mean surface elevation, which is essentially the average water height with respect to the sea bottom. A zero-upward crossing is also possible as a wave definition. For statistical purposes there is no difference between the two. [27]

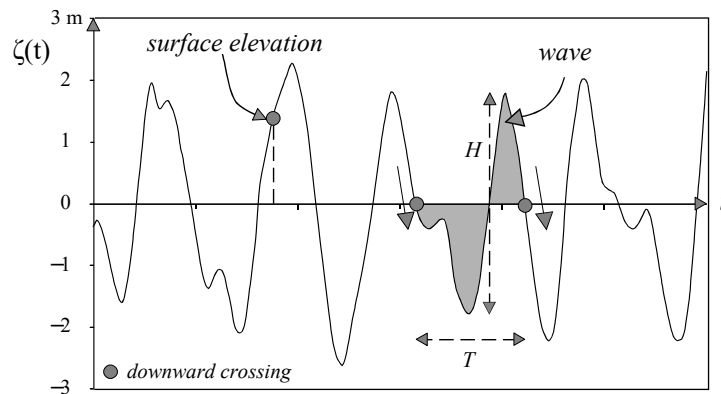


Figure 2.5: A time record of surface elevation and a wave definition. Indicated are the wave period T and wave height H . Modified from [27]

The time record in Figure 2.5 is representative for wind generated gravity waves and is very irregular in nature. Despite this irregular nature, it is common to regard this surface as the superposition of many regular harmonic waves with their own wave length, amplitude, frequency and direction of motion as visualised in figure Figure 2.6.

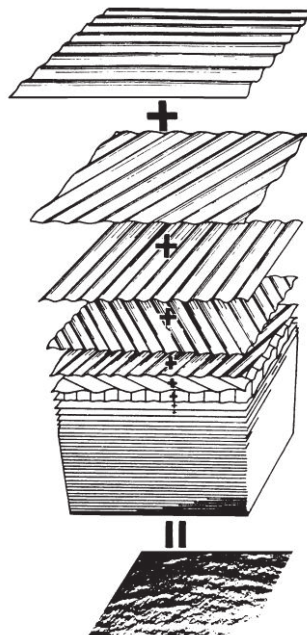


Figure 2.6: The ocean surface described as the sum of many simple, long crested harmonic waves. [56]

This superposition concept makes it possible to describe the irregular ocean surface with simple mathematical descriptions of regular waves, which is discussed in Section 2.2.2.

2.2.2. Regular waves

In Figure 2.7 a regular or harmonic wave can be seen including common wave characteristic definitions. A propagating wave in the x - direction can be described mathematically by Eq. (2.2). Here the wave elevation above the mean ocean surface ζ is a function of the wave amplitude ζ_a in meter, the wave number k in rad/m, x location in the direction of movement in meter, wave frequency ω in rad/s and t the moment in time in s of a certain point on the wave.

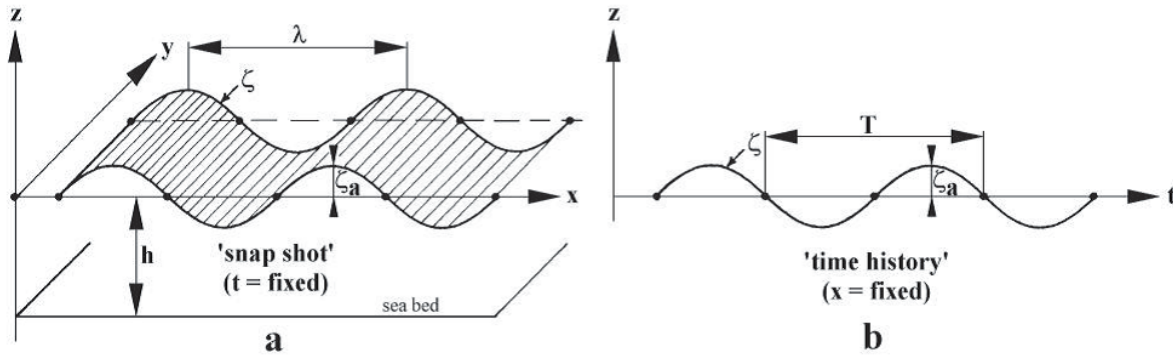


Figure 2.7: The definitions of a harmonic wave for a) a fixed time and b) a time history view of the surface elevation.[36]

$$\zeta(t) = \zeta_a \cos(kx - \omega t) \quad (2.2)$$

From linear wave theory, Eq. (2.3) gives the wave length λ as function of the wave number k , which is determined by the dispersion relation for infinite depth (or deep) water given in Eq. (2.4), with wave frequency ω_0 and gravitational constant $g = 9.81 \text{ m/s}^2$. The wave frequency can also be related to the wave period T according to Eq. (2.5). Combining equations 2.3 - 2.4, the wavelength can be expressed as function of the wave frequency in Eq. (2.6), which is applicable if infinite water depth is assumed. For a more detailed description of linear wave theory and derivation of the equations the reader is referred to Holthuijsen [27].

$$\lambda = \frac{2\pi}{k} \quad (2.3)$$

$$\omega^2 = gk \quad (2.4)$$

$$\omega = \frac{2\pi}{T} \quad (2.5)$$

$$\lambda = \frac{2\pi g}{\omega^2} \quad (2.6)$$

2.2.3. Irregular waves

The ocean surface is irregular, which means it is not periodical and not repeating itself in time and space and an example of an irregular wave record was given in Figure 2.5. There are several statistical parameters that can be used to describe such an irregular wave record, of which the most common one is the significant wave height H_s . It is defined as the mean of the highest one-third of waves in the wave record. Hence j in Eq. (2.7) is not the number of a respective wave in the time record, but the rank number of the wave, based on wave height [27]. This seems like an arbitrary choice, but has a historical reason. In the past, wave height records were visual estimates of experienced observers at sea and the estimates tend to be biased to the higher waves in the record [6].

$$H_{1/3} = \frac{1}{N/3} \sum_{j=1}^{N/3} H_j \quad (2.7)$$

2.2.4. Wave spectra

In Figure 2.6 the concept was mentioned to regard the irregular ocean surface elevation as the superposition of multiple regular waves with different frequencies, amplitudes and phases. This is actually a means to treat the ocean surface as a stochastic process to be able to characterise its properties. A one-dimensional surface elevation time signal can be described by a Fourier series, i.e. the sum of N regular wave components as seen in Eq. (2.8). Note that a time signal is the surface elevation at at one location, hence the x -component in Eq. (2.2) is not present for one harmonic wave in the Fourier series.

$$\zeta(t) = \sum_{n=1}^N \zeta_{a_n} \cos(\omega_n t + \varepsilon_n) \quad (2.8)$$

An assumptions that is implied in the sum of regular waves concept is that the surface elevation is a stationary Gaussian process, the regular wave components are not dependent on each other and the wave amplitudes of each component are Rayleigh distributed (providing that the wave frequency bandwidth is not too wide). With the Fourier analysis of the time record, an amplitude spectrum can be created, which is a discrete function of the amplitudes corresponding to frequencies. A continuous function is required to fully characterise the ocean surface. Therefore this amplitude spectrum is transformed into a continuous variance density spectrum (which is from now on referred to as *wave spectrum* for convenience). For more details on the intermediate steps and the origin and validity of the variable distributions, the reader is referred to Bosboom and Stive [6] or Holthuijsen [27].

The wave spectrum is a one-dimensional spectrum. This means that the waves propagate in one direction (e.g. in x -direction as in Figure 2.7) and are long-crested. In reality, waves also propagate in the y -direction, assuming a level horizontal water surface, thus a more complete representation of the ocean surface would be to use a two-dimensional wave spectrum, or short-crested sea. The definition of the long-, and short-crested seas can be seen in Figure 2.8. Though functions exist to scale the one-dimensional wave spectrum to approximate a two-dimensional wave spectrum [28], in marine engineering usually the long-crested sea's are used as design seas to reduce analysis complexity.

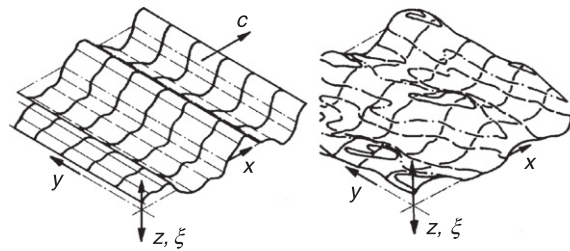


Figure 2.8: Long-crested (left) and short-crested (right) seaways. [4]

2.2.5. Standard wave spectra

In previous sections, a random time record is taken as a basis. This time record is usually not available for engineering applications and therefore standard spectra are developed based on observed properties of ocean surface elevation. The shape of these spectra are based on one or more parameters that are often used to describe the measurements of wave heights and periods. For example, *scatter diagrams* are available that contain the measured significant wave heights H_s and mean zero-crossing periods T_z for locations on earth including their frequency of occurrence. There are various standard spectra to choose from and it highly depends on the type of sea and severity that is analysed which spectrum is the most appropriate. The most common ones are the modified Pierson-Moskowitz (P-M) and Joint North Sea Wave Observation Project (JONSWAP) spectra, because they are easy in use and have proven their use in engineering applications. The P-M and JONSWAP spectra are discussed here briefly. [10]

The modified Pierson-Moskowitz spectrum The modified Pierson-Moskowitz or P-M spectrum is a two-parameter spectrum that is used for a fully developed, open sea such as the North Atlantic [27]. Mathematically, the spectrum is given by Eq. (2.9) [16] with significant wave height H_s , wave peak frequency ω_p and wave frequency ω .

$$S_{PM}(\omega) = \frac{5}{16} H_{1/3}^2 \omega_p^4 \omega^{-5} \exp\left(-\frac{5}{4} \left(\frac{\omega}{\omega_p}\right)^{-4}\right) \quad (2.9)$$

The wave peak frequency can be related to the wave peak period T_p with Eq. (2.5). There exist theoretical relations between the wave peak period T_p and other wave period definitions such as the zero-crossing wave period T_z as defined in Figure 2.5. This is useful, since the zero-crossing wave period is usually given in statistical records of wave heights. The relation between the wave peak period T_p and zero-crossing wave period T_z is given in Eq. (2.10) [16]. For the P-M spectrum, the non-dimensional peak shape parameter is taken as $\gamma=1.0$.

$$\frac{T_z}{T_p} = 0.6673 + 0.05037\gamma - 0.006230\gamma^2 + 0.00033341\gamma^3 \quad (2.10)$$

The JONSWAP spectrum The JONSWAP spectrum is a modification of the P-M spectrum to include fetch-limited or coastal seas, such as the North Sea [28], which are also areas where Feadships generally operate. This spectrum is given in a mathematical form in Eq. (2.11) with normalising factor $A_\gamma = 1 - 0.287 \cdot \ln \gamma$ and spectral width parameter σ as given in Eq. (2.12). For the JONSWAP spectrum, the non-dimensional peak shape parameter is taken as $\gamma = 3.3$. It can be seen that the JONSWAP spectrum reduces to the P-M spectrum for $\gamma = 1.0$.

$$S_J(\omega) = A_\gamma S_{PM}(\omega) \exp\left(-0.5 \left(\frac{\omega - \omega_p}{\sigma \omega_p}\right)^2\right) \quad (2.11)$$

$$\begin{cases} \sigma = 0.07 & \text{for } \omega \leq \omega_p \\ \sigma = 0.09 & \text{for } \omega > \omega_p \end{cases} \quad (2.12)$$

In Chapter 3 the JONSWAP spectrum is used to determine the internal load response spectra from which the design load distributions are derived that are used in this thesis.

2.3. Short term wave statistics

The creation of the wave spectrum allows us to determine the statistical characteristics of a wave record or standard spectrum. There is a distinction between short and long term statistical characteristics of a seaway. In the short term, i.e. a relatively short duration in time of around an hour, the sea state is such that its probability function of wave elevation does not change in time. This means that its statistical properties are *stationary*, i.e. the mean values of wave elevation or wave height do not change in time. For a longer duration in time, i.e. days or years, the statistical properties are *not stationary*, e.g. the mean values of wave elevation or wave height change in time, for example due to seasonal weather change. If statistical properties for a long time are regarded then it is referred to as long-term wave statistics. These are required for extreme design load analysis, e.g. the loading conditions in an extreme storm that happens once in 20 years. A long term analysis is not required to determine the deflections and rotations resulting from operating conditions. Evaluation of the short term wave statistics starts with the spectral moments of the wave spectrum, as defined in Eq. (2.13) [28].

$$m_{n\zeta} = \int_0^\infty \omega^n S_\zeta(\omega) d\omega \quad (2.13)$$

The zero order moment $m_{0\zeta}$, simply the area under the wave spectrum, corresponds to the variance squared or mean square wave elevation σ_ζ^2 of the surface elevation ζ [28]. This and other statistical characteristics are given in Eq. (2.14) - Eq. (2.17). [27].

$$\sigma_\zeta = \sqrt{m_{0\zeta}} \quad \text{Root Mean Square wave elevation} \quad (2.14)$$

$$\zeta_{as} = 2\sqrt{m_{0\zeta}} \quad \text{Significant wave amplitude} \quad (2.15)$$

$$H_s = 4\sqrt{m_{0\zeta}} \quad \text{Significant wave height} \quad (2.16)$$

$$T_z = 2\pi \sqrt{\frac{m_{0\zeta}}{m_{2\zeta}}} \quad \text{Mean zero-crossing period} \quad (2.17)$$

In design for operation, it can be useful to determine what the most probable maximum wave amplitude is in a sea state. It can be shown that this is the rather simple relation seen in Eq. (2.18) [27]. The number of cycles occurring in the duration of exposure to this sea state is given as N , which can be calculated with Eq. (2.19) with exposure time to the sea state of t_{exp} and mean zero-crossing period T_z .

$$\zeta_{max} = \sqrt{2m_0\zeta \ln N} \quad (2.18)$$

$$N = \frac{t_{exp}}{T_z} \quad (2.19)$$

Clearly, Eq. (2.18) shows that if the duration to the sea state increases, the probability that a wave with a higher wave amplitude is encountered is higher, hence the most probable maximum is also higher. It must be noted that there is a chance of 0.63 that the actual experienced maximum wave amplitude is higher than the most probable wave height ζ_{max} , though with a small increase in magnitude. This is because the maximum values have their own probability density function. [27]

2.4. Seakeeping analysis

Seakeeping analysis considers the seakeeping abilities or seaworthiness of a marine vessel. How well a ship behaves or what its performance is in a seaway can thus be determined by a seakeeping analysis. There are many aspects that can be considered in a seakeeping (performance) analysis and examples, as given by Tan [72], are as follows:

- Ship motions, like pitch and roll.
- Accelerations, in particular vertical and transverse directions.
- Course keeping.
- Increase in required power to attain the speed.
- Global hull girder loads.
- Local sea loads.
- Deck wetness and water ingress.
- Slamming (bow flare, bottom).

In the scope of structural analysis in the preliminary design, the global hull girder loads are the most relevant aspects as outcome from a seakeeping analysis. Therefore, a reference to seakeeping analysis in this document implies the determination of the global hull girder loads.

Tan [72] also mentions important ship characteristics that influence the seakeeping performance aspects, such as:

- Ship dimensions (length, beam and draft).
- Displacement and weight distribution
- Longitudinal position of the centre of buoyancy.
- Hull shape sections and bow flare.
- Ship speed.
- Bow type.
- Anti-rolling and anti-pitching devices.

These ship characteristics are input parameters for seakeeping software to calculate the ship performance in the aforementioned seakeeping aspects. The performance is essentially the *response* of the ship in a seaway. Many different seakeeping methods exist, which are generally classified according to the level of non-linearities they include [31]. The most common form of seakeeping analysis, especially in the preliminary design, is the linear response analysis, which is discussed in Section 2.4.1.

2.4.1. Linear response analysis

The linear response analysis is the most common type of seakeeping analysis, since it is relatively simple and rapid, making it a convenient tool for the preliminary design. A linear response analysis considers a linear ship-wave system, where the wave-induced loads and motions are proportional to the wave amplitude, advancing at a constant speed in regular, long-crested and small amplitude waves with small steepness. The ship motions of the ship are expressed in the 6 degree of freedom system as indicated in Figure 2.9.

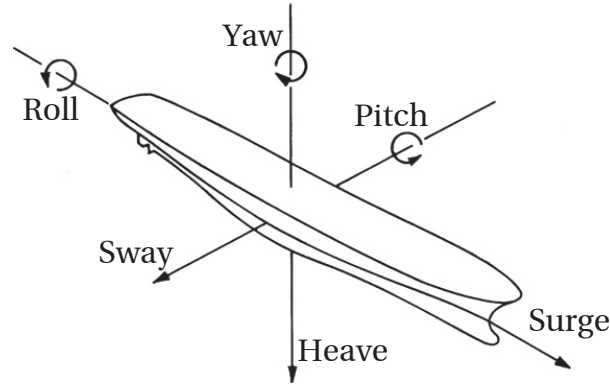


Figure 2.9: The six degree of freedom rigid body motion: surge, sway, heave, roll, pitch and yaw. Modified from [4]

In long-crested waves, a yacht can be advancing at a certain speed and have a heading angle with respect to the incoming waves. That means that the yacht experiences a different frequency than the wave frequency of the sea state. This is the encounter frequency ω_e , which is the frequency that is used in the hydrodynamic load calculations, since this is the wave frequency that results in the (increase of) pressure distribution on the hull. The encounter frequency can be calculated according to Eq. (2.20) with the sea state wave frequency ω , gravitational constant g , yacht speed V and heading angle with respect to the incoming waves β . This heading angle is defined in Figure 2.10 including common heading angle nomenclature.

$$\omega_e = \omega - \frac{\omega^2}{g} V \cos \beta \quad (2.20)$$

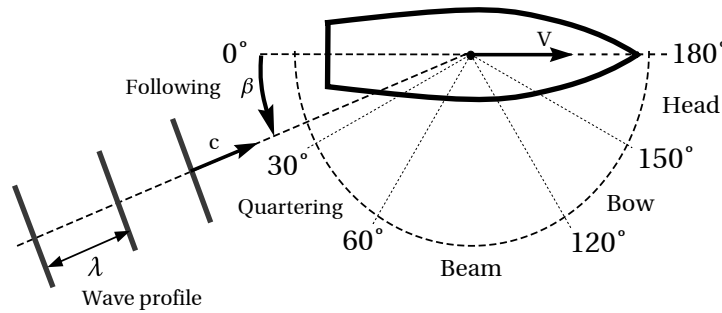


Figure 2.10: Incoming wave heading angle definition including common names for direction groups, such as head or following seas. Modified from [54]

The motions are calculated by solving the six coupled linear differential equations resulting from the general equations of motion as given in a concise form in Eq. (2.21). The components of this equations are on the left hand side: the mass matrix M which is defined by the ships mass (displacement), the added mass matrix A , which is due to the increase in inertia causes by displacement of water due to the moving ship, the damping matrix C , including damping terms from e.g. bilge keels, the stiffness matrix K , resulting from hydro-static buoyancy effects and the solution vector x containing the movements of the ship in the 6 degrees of freedom: heave, sway, surge, pitch roll and yaw. On the right hand side, the hydrodynamic force vector F contains the amplitudes of the excitation forces and/or moments. For an elaborate (mathematical) description of each of the components and how they are determined the reader is referred to Salvesen et al. [62].

$$(M + A)\ddot{x} + C\dot{x} + Kx = F \quad (2.21)$$

The determination of hydrodynamic forces works according to the following basic principle: solve the water flow velocity around the hull surface, calculate the resulting pressure distribution and integrate the pressure to get the exciting hydrodynamic forces. There are many flow analysis theories that can be applied to calculate these forces and the type mainly defines the amount of non-linearities that are taken into account and hence the accuracy of the response analysis. The most complete mathematical formulation to analyse water flow are the Navier-Stokes equations and the continuity equation. These equations are non-linear partial differential equations, assuming a viscous flow. Currently, only fundamental flow problems are solved using the full Navier-Stokes equations and for practical applications the theory becomes too computationally expensive. Simplifications can be made, such as an average flow computations, i.e. time-averaged, which results in the Reynolds-averaged Navier-Stokes (RANS) equations. Both Ma et al. [45] and Sun et al. [71] performed a seakeeping analysis in regular head seas with a RANS computation and, though close agreements with experiments are obtained, it is concluded that RANS computations cannot replace other methods yet in design, due to excessive computational costs. The approach that overcomes these computational costs is the potential flow method that assumes irrotational flow. Instead of the four coupled non-linear partial differential equations, one linear differential equation has to be solved. This potential flow method is widely used and they are divided in panel and strip methods. The panel methods are three dimensional methods that discretise the wetted ship hull into small panel elements for which the potential flow problem is solved. The accuracy of panel methods is generally found to be higher than strip methods, though an in-house validation study at Feadship showed little improvement of the panel method PRECAL (MARIN, Wageningen, the Netherlands) as compared to SHIPMO (MARIN, Wageningen, the Netherlands). This is also confirmed by Phelps [55]. In all cases, computational time is still significantly higher for panel methods than for strip methods. The strip method is therefore a good candidate for the research in this thesis and is described in more detail in Section 2.4.2.

2.4.2. Strip method

The strip method is a technique where the ship hull is divided in a series of strips. The potential flow problem is independently solved for these strips by regarding a strip as an infinitely long prismatic cylinder with the cross-section of the location of the strip, this is visualised in Figure 2.11. This essentially splits the three-dimensional problem in multiple two-dimensional problems to solve the potential flow. The resulting hydrodynamic forces are then integrated for the complete ship to use in the equations of motion. [55]

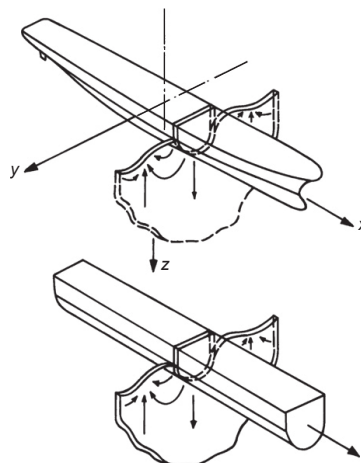


Figure 2.11: Strip theory principle: Two-dimensional flow around an infinite cylinder, corresponding to a cross-section of the ship. [4]

The strip method originated from different sources, such as Gerritsma and Beukelman [25], and a more complete method is given first by Salvesen et al. [62] on which many of the software programs are based today. Strip theories get more accurate, where first only linear strip theories existed (suitable for low sea states), extensions to include non-linearities are made by using quadratic strip theories by Jensen and Pedersen [34] (appropriate for moderate seas) and non-linear time domain methods as demonstrated by Xia et al. [79] (applicable in higher seas). Ma et al. [45] compared such a non-linear strip method in the time domain with a RANS computation, it is still less accurate than the RANS method, but computationally cheaper and hence of high practical value. Another example of the successful implementation of a non-linear strip method in

the time domain is given by Rajendran et al. [59] where excellent agreement with experiments is observed: maximum error in the estimation of the largest hogging and sagging peaks of only 13% and 8.5%, respectively. The linear strip method includes many assumptions and simplifications which makes it computationally the cheapest option to date and remarkably effective, especially in the preliminary design [35]. The assumptions and/or limitations for linear strip methods are summarised as follows: [4, 28, 34, 53, 55]:

- The ship hull is assumed to be slender with gradual lengthwise cross-sectional transitions, this means 3D effects (i.e. no direct hydrodynamic interaction between strips) are not taken into account.
- The hydrodynamic forces are assumed to be linear, thus only applicable in low to moderate seas ($H_s < 4$ m) This also means that the ship is supposed to have vertical ship sides, meaning no differentiation in hogging and sagging vertical bending moments. This is discussed in more detail in Section 2.4.6.
- Strip methods fail for waves shorter than one-third of the ship length, i.e. $\lambda < \frac{1}{3}L_{oa}$.
- Only applicable for ships with low Froude number, since no proper interaction is modelled between waves and oscillating ship.
- Decreased accuracy for following and quartering waves and at the extremities of the ship.

For this research, the mentioned limitations are not necessarily problematic. Feadships hulls are relatively slender with gradual cross-sectional transitions and since the Feadships operate normally in low to moderate seas at relatively low speed (at least for situations where the customer is on board and the discomfort due to structural flexibility is an issue) the assumption of hydrodynamic forces to be linear is allowable as well as the Froude number limitations. There is also a small differentiation between the hogging and sagging moments in operational conditions, since non-linear effects are less for low seas, as will be discussed in Section 2.4.6. Considering the wave length, the waves shorter than one-third of the ship length are not necessarily regarded, since the relevant extreme responses occur for wave lengths of approximately the ship length [28].

2.4.3. Response to an irregular seaway

The hydrodynamic loads due to the water pressure can be calculated with the strip method. It needs to be combined with the description of an irregular sea way to calculate the actual response of the ship. The response to an irregular seaway can be performed in the time and frequency domain. A time domain analysis means that the equations of motion in Eq. (2.21) are solved for an input wave record that is a function of time. As mentioned in Section 2.2.5, such a wave record is often not available or has to be generated with random phase data. There is, however, no guarantee that this wave record is representative for the sea state, because certain peak waves may or may not occur in this time record, leading to an high uncertainty in the accuracy of the response. This can be solved by using a time record of a sufficiently long time to make sure that the statistical properties match reality. In practice this means that very long or very many time records have to be analysed for the response, which is rather impractical and expensive, especially for the preliminary design. [37]

In the frequency domain, the solution of the equations of motion is obtained for a series of regular waves with unit amplitude, wave frequency, ship speed and heading. For one regular wave, a general response (motion or load) then has an amplitude r_a and a phase. In a linear response analysis, the response scales linearly with wave amplitude ζ_a , so by dividing the response amplitude by the unit wave amplitude, the transfer function for this wave-ship system is obtained, see Eq. (2.22).

$$\frac{r_a}{\zeta_a}(\omega) = H(\omega) \quad (2.22)$$

The transfer function is often called the Response Amplitude Operator² (RAO). For example, a heave RAO of 2 m m^{-1} means that the heave response amplitude $r_a = 2$ m for a regular wave of amplitude $\zeta_a = 1$ m.

The RAO's are only valid for one regular wave, but since the wave-ship system is assumed linear, the superposition concept to describe the irregular sea surface given in Section 2.2.1 can be used to determine the response to an irregular seaway. This so-called frequency response analysis, is illustrated in Figure 2.12.

From linear systems theory, the in-, and output spectra of linear systems are related by a frequency response function $H(\omega)$ (or RAO) by Eq. (2.23) as derived by Crandall and Mark [13].

$$S_r(\omega) = |H(\omega)|^2 S(\omega) = RAO^2 S(\omega) \quad (2.23)$$

²This definition is adopted in this work, though in literature, the definition of the RAO is sometimes taken as $H(\omega)^2$

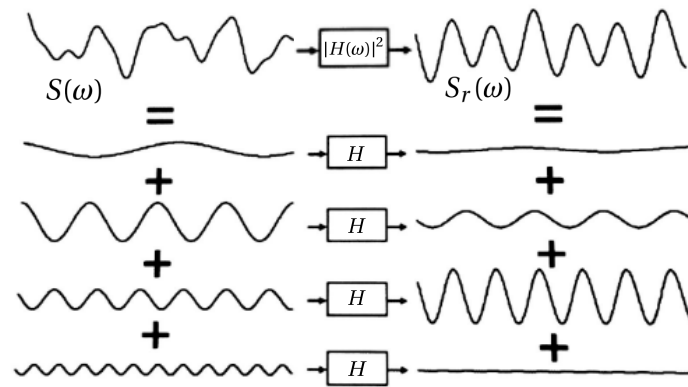


Figure 2.12: The ship response to an irregular seaway is constructed from the individual responses to the harmonic waves that define the irregular seaway. Modified from [9]

Spectral analysis similar to the short term spectral analysis from Section 2.3 can then be used to find extreme values of the response spectrum, as demonstrated by Ochi [49]. The Most Probable maximum Response *MPR* for a time duration can be obtained by replacing the wave amplitude ζ_a by response amplitude r_a and the zero order moment of the wave amplitude spectrum $m_{0\zeta}$ by the zero order moment of the response spectrum m_{0r} in Eq. (2.18), resulting in Eq. (2.24).

$$MPR = \sqrt{2m_{0r} \ln N} \quad (2.24)$$

2.4.4. Internal loads

The internal loads can be determined by the principle of a dynamic equilibrium with Newton's second law using the wave excitation forces and the inertia of the yacht (i.e. the masses and accelerations) calculated by solving the equations of motion (Eq. (2.21)). The ship is then regarded as a single beam along its longitudinal axis and the internal moments M and shear forces Q for a cross-section are given in Figure 2.13.

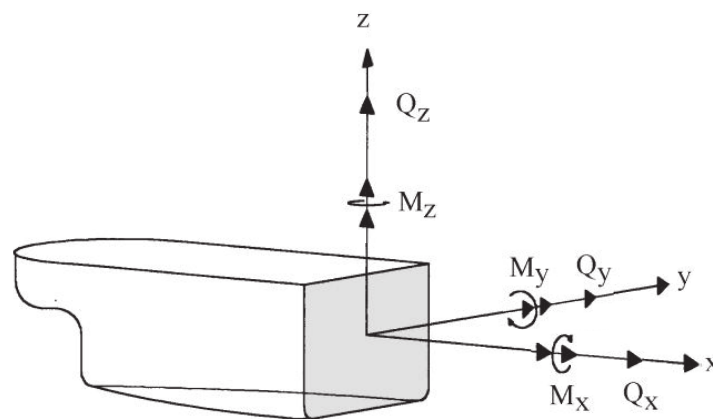


Figure 2.13: The internal loads evaluated at a cross-section of a ship. Modified from [37]

For example, the internal shear loads per cross section j are determined by Eq. (2.25) [62]. The components in the equation are the inertial forces F and the total exciting wave forces of the force vector F in equation 2.21: the hydro-static restoring force R , the Froude-Krylov force E and the hydrodynamic body motion force D . A similar equation can be set up for the dynamic moment equilibrium.

$$Q_j = I_j - R_j - E_j - D_j \quad (2.25)$$

Once the dynamic equilibrium is computed around a point, usually the c.g., then any point on the in the x-y-z space of the ship beam can be evaluated for the internal loads by evaluating the cross-product.

2.4.5. Equivalent Design Wave

In Section 2.4.4 the loads are determined at a point on a ships cross-section and at that particular point, mean or maximum values can be calculated for the internal loads by spectral analysis of the response spectra. These values, however, do not provide an actual set of concurrent load distributions. A load distribution containing all the maxima of the load responses is not valid, since these maxima do not necessarily occur simultaneously, which is mathematically indicated by a different phase angle of a response. The load distribution is thus time-dependent, for which a time domain analysis is required. This results in a large amount of load cases to be analysed and together with the long simulation time required for a time domain analysis to obtain long term response statistics, a more convenient approach is found to be the Equivalent Design Wave (EDW) concept. The EDW concept is used to reduce the number of load cases to check for extreme structural loads that result in e.g. buckling or yielding [73]. In this concept, a design wave that causes the maximum value of the response of interest at a chosen location, this is called the Target Response (TR). This can be a maximum response value calculated by hydrodynamic analysis, but also a maximum value (such as an internal bending moment) provided by classification societies. Once the target response is determined, the magnitude of the target response at other locations as well as other load components at other locations can be determined by including their phase difference with the target response. For example, a critical location is chosen, e.g. at 40% of the ship length, and the maximum long term response value of the vertical bending moment is calculated with Eq. (2.24). Then, an EDW is chosen with an amplitude, frequency, heading that causes that specific value of the vertical bending moment at that location. For a regular EDW, several approaches exist to determine these wave characteristics. E.g. Folso and Rizzuto [20] provided a trade-off analysis to determine a suitable method for a regular EDW characteristic determination. Note that the EDW concept does not try to represent the irregular waves themselves, but it just tries to approximate the concurrent load distribution on the ship in an extreme situation. In addition to a regular EDW, also other waves are possible: de Hauteclocque et al. [14] present in addition to a regular EDW also response conditioned waves and directional response conditioned waves, all illustrated in Figure 2.14. A more detailed analysis of irregular design wave is given by Fang et al. [19], which found that irregular design waves tend to result in more realistic and reliable loads. Despite the higher accuracy, a regular design wave is used in this work for simplicity and to demonstrate the possibilities an EDW has for determination of the load distributions. Future research can use this knowledge to increase the accuracy of the load distributions, if required.

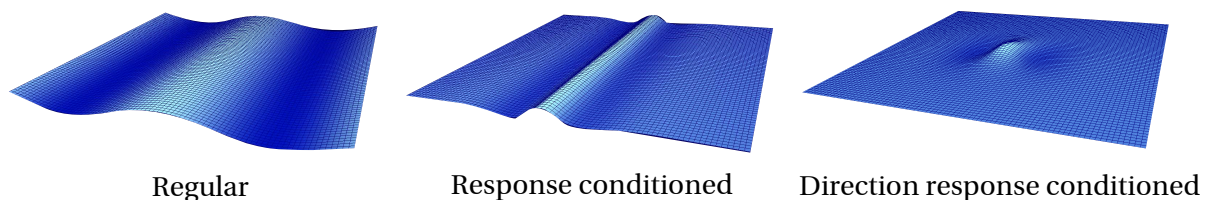


Figure 2.14: Visual of three different Equivalent Design Wave types: a regular wave, a response conditioned wave and a direction response conditioned wave. [14]

2.4.6. Non-linearity's in seakeeping analysis

Many types of non-linearity's exist in seakeeping analysis as indicated by Kring et al. [38] and Hughes et al. [28]. The first major contribution is the steepness of the incoming wave train, resulting in a non-linear relation between the amplitude of the ship motion response and the exciting wave. The second major contribution is attributed to the non-linear hydrostatic and Froude-Krylov forces from wave-hull interaction. This causes asymmetry in the vertical wave bending moment, i.e. a difference in hogging and sagging moments. Clauss et al. [11] found a significant increase in the asymmetry for increasing wave height and attribute this mainly due to relative wave steepness and bow geometry, i.e. large bow flare or non-vertical ship sides increase the asymmetry. Vertical ship sides translate into a high block coefficient (The block coefficient of a yacht is defined in Eq. (2.26) with displacement V , Lloyds rule length L_r , breadth B and draught T) and indeed Soares and Schellin [70] found that for large (above 200 m) tankers with mainly vertical sides (and a high block coefficient) there was no difference in the hogging and sagging moments. The other way around, Fonseca and Soares [21] concluded that a small block coefficient caused a large non-linear response in the hogging and sagging responses. Since (Feadship) superyachts usually have a small block coefficient, as mentioned by Roy et al. [61], the non-linear response in hogging and sagging can not be neglected for extreme sea states.

$$C_b = \frac{V}{L_r B T} \quad (2.26)$$

The above mentioned types of non-linearity's and others increase with wave amplitude, therefore a linear response analysis is not suitable for large amplitude waves. Some attempts are made, e.g. by Soares and Schellin [69], to apply non-linear corrections to linear responses to artificially transform it to a hogging and sagging response, only valid for certain wave amplitudes. The sea states analysed in this thesis regard operational conditions of Feadships, which generally operate in relatively calm waters. That means that the non-linearities are relatively small and for the preliminary design it is sufficient to perform a linear response analysis. Nevertheless, in the future, it can be interesting for Feadship to use methods that incorporate non-linearities to a larger extent to generate long term extreme load cases, also for strength assessment (currently, empirical rule design loads are used for this, which are generally conservative estimates).

2.5. Structural modelling

The structural modelling of the yacht structure can be done in many ways and it deals with the idealisation of the structure into structural models that calculate displacements, rotations and/or stresses, called the structural *response*, by application of a load. Iterations are performed on the structure until it meets the design requirements. This process is often performed manually, though optimisation methods and algorithms are of increasing interests to obtain the optimal solution within a given time frame. In commercial shipping, probabilistic load analysis is performed for strength and fatigue assessment, which is done to a lesser extent for superyachts. Certification requires strength assessment and the structural integrity of the yacht should be sufficient, but in addition to strength, stiffness of superyachts is also an important design driver. The structural models that are used for structural analysis mainly depend on the design phase and hence the time frame and level of detail that is available. For ships the models often start with simple analytical (beam bending) equations, such as given by Hughes et al. [28]. Then, more advanced methods that combine multiple structural element types can be used, such as a coupled-beam method described by Naar et al. [48]. At last, full 3D Finite Element (FE) models are analysed in the most detailed design phase.

The simple structural idealisation that is often used is regarding the yacht hull girder as a prismatic beam, for which classical linear beam theory can be used. The basics assumption in classical beam theory is that the cross-section orthogonal to the x-axis at any x location remains plane and keeps its shape during deformation, i.e. the cross-section translates and rotates as a rigid body. The equilibrium equations, derived by regarding the equilibrium on a beam element, in classical beam theory are according to Eq. (2.27) and Eq. (2.28) [24], with bending moment M , shear force V and applied load q .

$$\frac{dM(x)}{dx} = V(x) \quad (2.27)$$

$$\frac{dV(x)}{dx} = -q(x) \quad (2.28)$$

The determination of the deformations of a beam can be described according to different beam theories, of which the two well-known beam theories are the *Euler-Bernoulli* beam theory, which is simple in use, and the more complicated *Timoshenko* beam theory. The latter includes shear deformations, which is relevant for beams with a length over height ratio of $L/h < 10$ [51]. The length of height ratio of the hull of Feadship yachts is in the same order of magnitude and ranges from $L/h \approx 8-12$, hence shear deformation might be of importance for the global and local deformations that are of interest in this work. Naar et al. [48] demonstrates the influence of the shear deformations for a passenger ship ($L = 160$ m) with a ratio of $L/h = 5$. The deflections of the ship, modelled as a prismatic beam without hull side openings (window cut-outs etc.) are determined for beam theory with and without including shear deformations. The vertical displacement results for a hogging bending load case are compared to a FE model, which can be seen in Figure 2.15 for case A (prismatic beam without cut-outs). Including the shear deformation results in a maximum vertical displacement that is 30% larger, which results in a match with the FEM results.

The shear deformations in the material itself result in an increase in vertical displacement, but another effect is caused by cut-outs in the side of the hull, which lower the shear stiffness due to absence of material. This can not be captured by beam theory that includes shear deformations. Instead, Naar et al. [48] proposed a coupled beam method that combines multiple beams in vertical direction that are connected by distributed springs. In Figure 2.15 it can be seen that for case A this coupled beam method showed good agreement

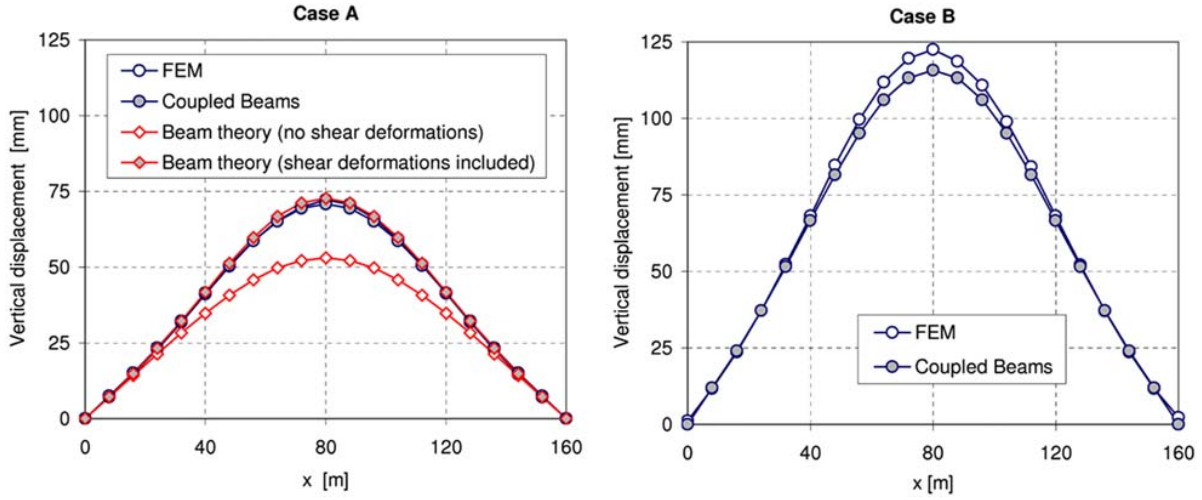


Figure 2.15: Vertical displacement of the main hull of a passenger ship for different beam theories, a coupled beam method and a FEM.[48]

and also for case B (prismatic beam with cut-outs) a close agreement is observed with the FEM. Another approach is given by Heder and Ulfvarson [26], where the decks are represented by rods and the side sections with cut-outs by orthotropic elements with an equivalent stiffness of the sections with cut-outs.

Feadships also have hull openings, hence a coupled-beam method will be required for a more accurate result. However, quick and flexible methods are desirable in the preliminary design due to the custom and frequent design cycle of Feadships, which makes a proper coupled-beams method difficult to realise in the scope and time frame of this thesis. A more suitable starting point is therefore using less extensive methods than the coupled beam method. An increasing trend, however, is larger openings for tender garages and beach clubs in Feadships and therefore coupled beam methods can be a suitable research option in the future, once simpler methods prove to be insufficient. The beam theory used in these methods that will be used in this thesis are the Euler-Bernoulli beam theory and the Timoshenko beam theory, which are shortly discussed in Section 2.5.1 and Section 2.5.2, respectively.

2.5.1. Euler-Bernoulli beam theory

In the Euler-Bernoulli beam theory, it is assumed that the displacements and rotations of the beam only occur due to the bending moment and the shear deformations can be neglected. The rotation of a cross-section is given as $\theta(x)$, which is related to the vertical displacement $w(x)$ according to Eq. (2.29) and remains perpendicular to the neutral axis [60].

$$\theta(x) = -\frac{dw(x)}{dx} \quad (2.29)$$

The relation between the moment and the vertical displacement is then given by the Ordinary Differential Equation (ODE) in Eq. (2.30)[77], with bending constant stiffness EI .

$$EI \frac{d^4 w(x)}{dx^4} = q(x) \quad (2.30)$$

2.5.2. Timoshenko beam theory

In the Timoshenko beam theory both bending and shear deformations are taken into account. The rotation ϕ of a Timoshenko beam is independent of the slope of the beam (as given in Eq. (2.29)). Instead of one ODE, now two ODE's are to be solved, given in Eq. (2.31) and Eq. (2.32), with shear stiffness GkA , where k is the *shear correction factor* to compensate for the assumption that the shear stress is constant over the cross-section, this is discussed in more detail in Section 2.5.3.

$$EI \frac{d^3 \theta(x)}{dx^3} = -q \quad (2.31)$$

$$\frac{dw(x)}{dx} = \frac{EI}{GkA} \frac{d^2\theta(x)}{dx^2} - \theta(x) \quad (2.32)$$

If the shear deformations are not taken into account, the Timoshenko beam theory should give the same result as the Euler-Bernoulli beam theory. Indeed this is true, because no shear deformation means an infinitely stiff behaviour in shear or $GkA \rightarrow \infty$, for which Eq. (2.32) results in Eq. (2.29) and the ODE in Eq. (2.31) can again be written as Eq. (2.30).

This effect is illustrated in Figure 2.16, where the rotation of the cross-section of a Timoshenko beam is given by angle ϕ . If the shear deformations γ_{xz} is taken zero, the rotation of the Timoshenko beam cross-section is the same as the rotation of the Euler-Bernoulli beam rotation given in Eq. (2.29).

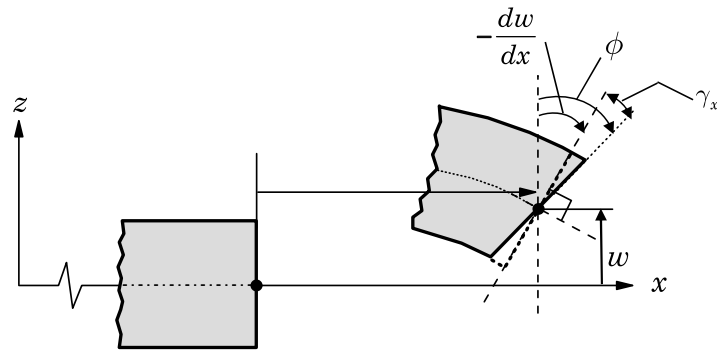


Figure 2.16: The effect of the shear deformation on the rotation of a cross-section for a Timoshenko beam. Modified from [60]

2.5.3. Shear correction factor

In Timoshenko beam theory a constant variation of the shear stress is assumed over a cross-section. In reality, this is not true (it should be zero at the boundaries) and a constant variation over an area A results in an overestimation of the stiffness against shear deformations [1]. The shear correction factor k is introduced to reduce the effective area of the cross-section to compensate for this assumption. For a rectangular beam, where the shear stress distribution is quadratic, it can be shown that the shear correction factor is 5/6 [60]. In other words, by analysing a rectangular beam with the Timoshenko beam theory that assumes a constant variation of shear stress over the cross-section, it is necessary to reduce the area in the calculations by a factor of 5/6. For more standard cross-sections, shear correction factors are derived and compared by e.g. Cowper [12] and Hutchinson [29]. For arbitrary cross-sectional shapes, such as the cross-section of a yacht hull, these derived factors are not applicable and other methods are required. Jensen [32] provides an overview of the shear coefficient determination for ship hulls where the simplest and most conservative estimation of the shear coefficient is mentioned to be the projected vertical area of the cross-section given in Eq. (2.33).

$$A_v = \int_A \cos^2 \theta dA \quad (2.33)$$

The shear coefficient then becomes as given in Eq. (2.34).

$$k_v = A_v / A \quad (2.34)$$

More accurate methods are numerical mesh-based methods, such as the Pilkey method [57], that are often used in commercial FEA software to determine the cross-sectional properties of arbitrary shapes.

2.6. Finite Element Analysis

In the previous sections, the yacht is modelled as a prismatic beam. For a non-prismatic beam, the bending and shear stiffness are a function of x and can *not* be taken outside the integration, e.g. Eq. (2.30) results in Eq. (2.35).

$$\frac{d^2}{dx^2} \left(EI_x \frac{d^2 w(x)}{dx^2} \right) = -q(x) \quad (2.35)$$

In theory, Eq. (2.35) can be solved analytically, but this is only practical for 2 or 3 discrete cross-section changes. More, or a continuous property distribution, result in variable coefficients of integration instead of constant and thus numerical solutions are required [24]. Such a numerical solution is the Finite Element Analysis (FEA). In FEA the structural element is discretised into smaller elements and the equilibrium equations at the nodes are solved to determine the behaviour of the whole structure.

The set-up of FE models in commercial software packages such as Abaqus/CAE (Dassault Systemes, Vélizy-Villacoublay, France) or FEMAP (Siemens, Berlin and Munich, Germany) generally requires a lot of time and is therefore mainly used in the detailed design stages. If the geometry of the structure is simplified such that the geometry of the elements is relatively simple (e.g. 1D or 2D), then the use of FEA with commercial software is also applicable to the preliminary design or even with self-made finite element codes. For example, the deflection of a non-prismatic beam, such as a yacht hull, can then be modelled with 1D beam elements that approximate the gradual change in cross-section. By increasing the number of elements, as seen in Figure 2.17 for a tapered (i.e. non-prismatic) beam, the varying cross-section is captured increasingly better.

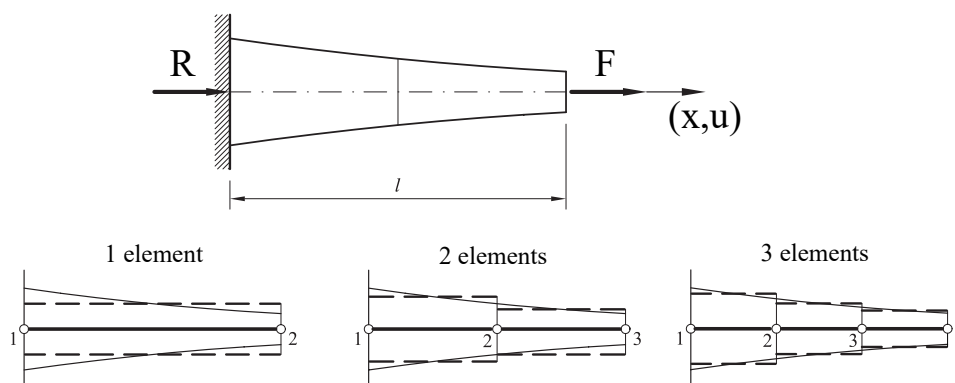


Figure 2.17: Finite element discretisation of a tapered beam with 1D beam elements. Modified from [50]

Each element has constant properties, such as Young's Modulus E , area A and/or moment of inertia I , these are defined by the actual characteristics of the structure that is modelled. Based on the location of the element the properties can be different, e.g. in Figure 2.17 the area of the elements changes the more elements are used. For each element a local (element) stiffness matrix $[K]^{(e)}$ and an element load vector $\{f\}^{(e)}$ calculated and these are assembled in the global stiffness matrix $[K]$ and force vector $\{F\}$, respectively. The static equilibrium equation Eq. (2.36) is then solved for the unknown displacements and rotations, in Figure 2.17 this is considers the axial displacement u . [50]

$$[K] \{u\} = \{F\} \quad (2.36)$$

The properties, loads and degrees of freedom in this approach are determined by the element type that is used. This element type is based on the structural element that is modelled (a beam, plate, rod etc.) and can be different according to the theories they are derived from. In the case of the beam theories discussed in Section 2.5.1 and Section 2.5.2, there is a difference between Euler-Bernoulli and Timoshenko beam elements and these elements have different properties, loads and degrees of freedom. [50]

2.7. Load transfer to structural model

Load application to a structural model seems straightforward, but in case of a yacht, direct application of pressures or hydrodynamic forces to a FE model results in rigid body motions, since there is a resultant acceleration of the yacht. In FEA this non-equilibrium state can be eliminated with methods such as 'inertial relief'. Inertial relief is a method that eliminates rigid body motion based on a new set of relative loads to analyse the elastic behaviour of a free-free body system [78]. A free-free body can be anything that is unconstrained, such as a flying aircraft or a floating yacht. Methods without inertial relief are also possible. Zhao et al. [81] provide a method to use the sectional internal moments calculated by a strip method to form an equivalent pressure distribution in 3D on a hull. By taking the internal moments, as calculated in Section 2.4.4, the inertia of the yacht is already taken into account and hence the pressure distribution is automatically in equilibrium. The FE model is then simply analysed by a static analysis, this process is visualised in Figure 2.18.

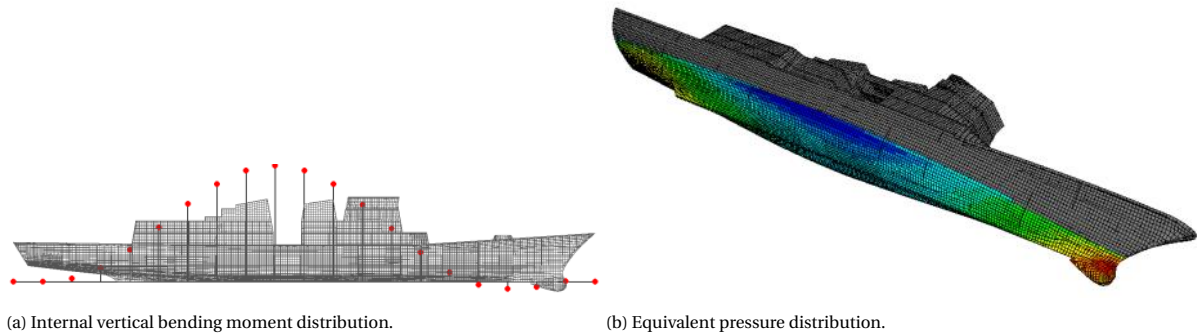


Figure 2.18: Translating the 2D internal vertical bending moment distribution generated by a strip method to an equivalent pressure distribution over the hull in a 3D FE model. [81]

The same authors, Ma et al. [44], successfully applied the same method for panel based seakeeping analysis, transferring the pressure distribution of the coarse seakeeping panel mesh to the finer structural mesh and they solved the resulting problems with imbalanced forces due to pressure integration. The classification societies also provide methods to apply loads that are in equilibrium to a yacht structure, e.g. the loads can be distributed over nodes at locations of the transverse frames/bulkheads below the waterline to prevent local stress concentrations [40].

2.8. Summary and discussion

The important load components on the hull girder of a ship are the vertical, horizontal and torsional bending moment, from which the vertical bending moment is the most important parameter.

The irregular and short-crested ocean surface can be described by the summation of a series of long-crested harmonic waves. This summation is represented in a wave spectrum that indicates the magnitude of the energy density for all wave frequencies present in a sea state. Time records of the sea state are usually not available for engineering applications and therefore standard spectra are developed that can generate a wave spectrum based on spectral parameters that are available. The most important parameters are the significant wave height H_s and the mean zero-crossing period T_z , which are normally given in a scatter diagrams for a chosen locations obtained from experimental measurements. The most common standard spectrum is the JONSWAP spectrum, which is applicable in areas where Feadships operate. If the duration of such a sea state is short, i.e. less than 60 minutes, spectral analysis can be applied to the (standard) wave spectrum to determine the so-called short term wave statistics.

A ship sailing in a seaway can be regarded as a linear system, where the ship is the system, the wave spectrum is the input and the response of the ship to the waves in the form of a response spectrum is the output. Linear systems provide convenient equations that relate the input and output spectrum with transfer functions, which are commonly referred to as Response Amplitude Operators (RAO's). This approach is called a linear response analysis and similar to the spectral analysis of the wave spectrum, the spectral analysis of the response spectrum results in spectral parameters such as the most probable maximum response for a duration of time the ship is exposed to the sea state. These spectral parameters can be used in the design to determine the most likely or maximum internal load response that is expected.

Part of a seakeeping analysis is the determination of the hydrodynamic loads that act on the ship due to waves. Computationally heavy methods to perform the flow analysis for the hydrodynamic loads are Reynold-Averaged Navier Stokes (RANS) methods. Less computationally heavy are the potential flow methods, that simplify the velocity field in of the incoming water flow by assuming irrotational flow. The most common potential flow methods can be divided in panel methods and strip methods. Panel methods discretise the wetten ship hull into small panels and solve the three-dimensional potential flow for each panel to obtain the incoming pressure. The strip methods discretise the ship hull in sections or 'strips' that are treated as infinitely long prismatic cylinders to solve the potential flow in two-dimensions. The resulting two dimensional pressure is then integrated along the length to obtain three-dimensional loads. All methods include non-linearities to a different (or no) degree, which defines in which situation they can be used. Strip methods are generally the least computationally heavy and with a reasonable accuracy for sea states with $H_s \leq 4$ m, hence are preferred for the preliminary design. The effect of the non-linearities increase with wave height, however, in the scope of this thesis, sea sates with relatively low wave heights are regarded, hence the strip methods is a suitable

method to use.

The loads that cause the bending and torsion of the yacht structure are the internal loads. These are obtained by solving the equations of motion in the linear response analysis and then regarding the dynamic equilibrium situation. In this situation, the internal loads at any location in the 3D ship hull can be determined by subtracting the hydrodynamic loads acting on a section from the inertia loads. The difference are the internal loads that are felt by the structure and causing in to deform globally.

Structural idealisation of the yacht structure can be done by modelling the hull as a non-prismatic beam using the Finite Element Method (FEM). The simple Euler-Bernoulli beam theory can be used for the beam that assumes that displacements and rotations are only caused by the applied bending moment. For yachts with a relatively low length over height ratio, the shear deformations can have a significant contribution to the global deformation. These shear deformations can be taken into account for beam elements by using the Timoshenko beam theory.

The load application to finite element models is relevant for the validation of the 1D beam model. This validation will be performed with available rule design load distributions, which are already in equilibrium, hence inertia relief methods are not required. The most suitable approach is then the application of discrete section forces by distributing the loads over the nodes below the waterline at locations of transverse bulkheads.

3

Operational wave-induced loads

In the marine industry, the structural design of ships is commonly performed by using rule design loads that are provided by classification societies, which is proven to be quick and effective for the longitudinal strength assessment of a ship hull based on its main particulars. These design rule loads are used for strength assessment of the yacht and do not reflect the wave-induced loads encountered in normal operating conditions of the yacht during which the structural deformations cause creaking interior. In this chapter, design load distributions are derived that represent the loading conditions on a yacht hull that are encountered in actual operating conditions to answer the first main research question of this thesis work.

The maritime (research) field that covers the determination of wave-induced loads is called seakeeping. It involves the analysis of the *seakeeping abilities* or *seaworthiness* of a marine vessel. The many different seakeeping methods work according to the following principle: 1) solve the water flow velocity around the hull surface, 2) calculate the resulting pressure distribution, 3) integrate the pressure to get the exciting hydrodynamic forces, 4) solve the ship equations of motion to obtain the ship motions and accelerations. In this solved state, the ship is in a dynamic equilibrium and the difference in inertial loads and applied wave forces at one location will result in the internal loads that acts on the structure. A proven and quick method to determine the hydrodynamic loads used in the preliminary seakeeping design is the strip method. An importance assumption here is that the ship is modelled as a rigid body, which means that the structural response does not influence the wave-induced loads, which is also the assumption that allows the division of structural model and loads in this thesis. For small elastic deflections compared to the rigid-body motions, this rigid body assumption is valid and seakeeping and structural analysis can be treated separately [34, 39]. For less stiff ships with e.g. aluminium hulls or ships with a low natural frequency ω_n this assumption should be adopted with more care [2].

In this research, the linear strip method SHIPMO [46] is used to derive an operational internal load distribution in the yacht that can be applied in the preliminary design phase. SHIPMO is implemented in the software suite Qship supplied and developed by the Maritime Research Institute (MARIN) in Wageningen, the Netherlands. The approach that is adopted in this work is represented schematically in Figure 3.1.

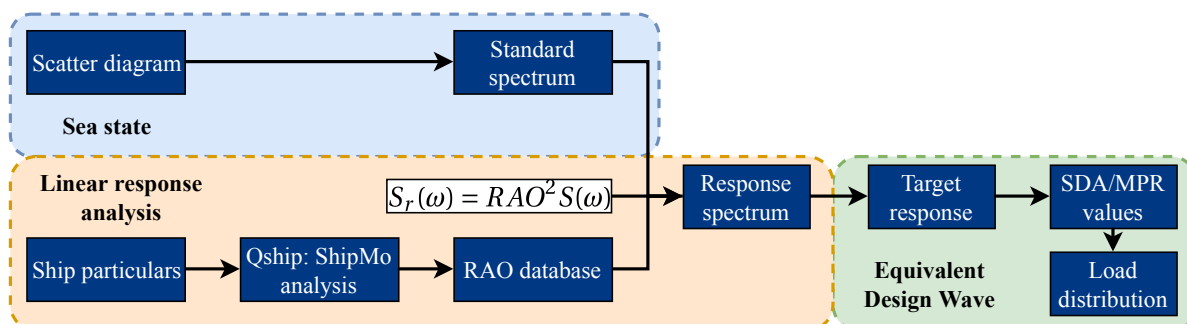


Figure 3.1: The approach for the determination of a wave load distribution with a linear response analysis, sea state definition and equivalent design wave.

The main part of the analysis consists of a linear response analysis, which is where SHIPMO is used. With

the necessary yacht particulars (such as hull shape, loading conditions and appendage size and location) a linear response analysis is performed by subjecting the hull to a series of unit amplitude sinusoidal waves of a chosen frequency range and a database of Response Amplitude Operators (RAO's) is obtained, which defines the motion and internal load responses to these waves. The response to an irregular ('actual') seaway is then obtained by regarding the wave-ship system as a linear system with the ship as system, the wave spectrum of the sea state as input and the resulting response spectrum as output of the system. Then, the load distributions are derived by combining the response spectral characteristics with an Equivalent Design Wave (EDW). The linear response analysis and sea state considerations are discussed in Section 3.2 and the EDW method is discussed in Section 3.3. At last, a summary of the results is given in Section 3.4.

3.1. Test case

The linear response analysis and the derivation of the load distributions are performed for one, recently designed, yacht. Consequently, also the structural model in Chapter 4 and the validation of the results are all performed for the same yacht. The main reason for that is that there is a complete overview of the yacht particulars available that is obtained through the most recent analysis methods, such as an weight distribution, full hull geometry design etc. Also, for the validation a three-dimensional detailed Finite Element (FE) model is used, which are only available for a limited amount of yachts, since a demonstration of the strength carrying capabilities with a 3D FE model for certification is only required for yachts above a rule length of $L = 75$ m [42] and not that many suitable FE models exist. The overall particulars of this test case yacht are given as reference in Table 3.1.

Table 3.1: Yacht particulars of the test case.

Particular	Value	Unit
L_{oa}	88	m
B	13	m
T	4.2	m
D	7 (aft)	m
	11 (wide body)	m
V_{cruise}	16	kts

3.2. Linear response analysis

The linear response analysis with the SHIPMO strip method starts with the definition of the appropriate ship particulars. The hull geometry is divided into the strips and appendage information can be included as illustrated in Figure 3.2. A chosen loading condition (e.g. empty or fully loaded) defines the mass distribution of the yacht, which is used to determine the total volume of the hull beneath the water surface the inertia properties of the mass elements the yacht is divided in.

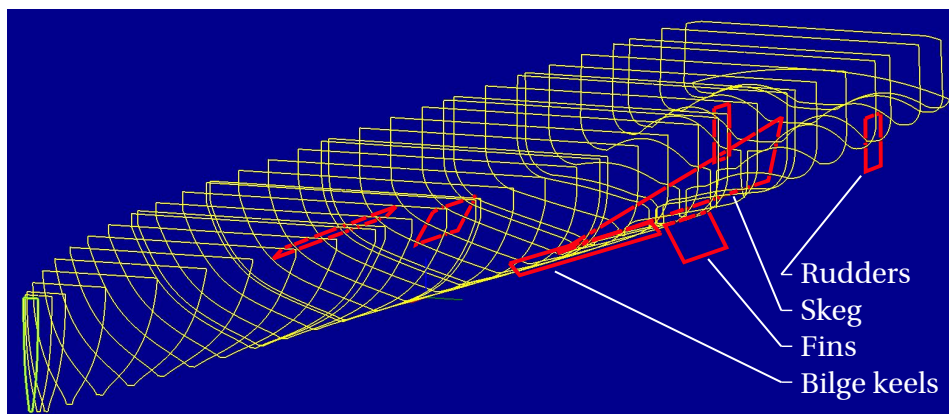


Figure 3.2: The hull geometry in strips including appendages.

The analysis is performed for set of unit amplitude regular waves with a range of frequencies that can be

chosen in agreement with the occurring frequencies in the sea states under consideration. Furthermore, a selection of headings can be chosen, ranging from 0° to 180° and different yacht speeds can be analysed. The next step considers the definition of the internal loads and at what location they are determined and is discussed in Section 3.2.1.

3.2.1. Internal loads

The starting point to determine the internal loads (or more precisely the internal load RAO's, which is the response amplitude divided by the wave amplitude of the incoming waves, see Eq. (2.22)) is regarding the ship in a dynamic equilibrium using Newton's second law, see equation 3.1. It states that the total inertia force on the yacht is sum of all forces acting on the yacht, which is equal to the total yacht mass times the acceleration of the centre of gravity.

$$m\ddot{x} = F_{inert} = F_{wave} + F_{rest} + F_{damp} + \dots \quad (3.1)$$

The internal loads are determined at chosen locations on a transverse cross-section of the yacht (or *cut*) that divides the ship in a front and aft section. The amount of cuts depends on the length of the yacht and one around every few meters is sufficient. The internal loads at the chosen location are then calculated as the difference between the total inertia *aft* of the cut and the total applied force *aft* of the cut as indicated in Eq. (3.2). Note that the same result is obtained by regarding only the loads in *front* of the cut, though with opposite sign.

$$F_{internal} = F_{inert_{aft}} - F_{total_{aft}} \quad (3.2)$$

The sign conventions used for the internal shear forces and bending moments are given in Figure 3.3 and are defined as follows:

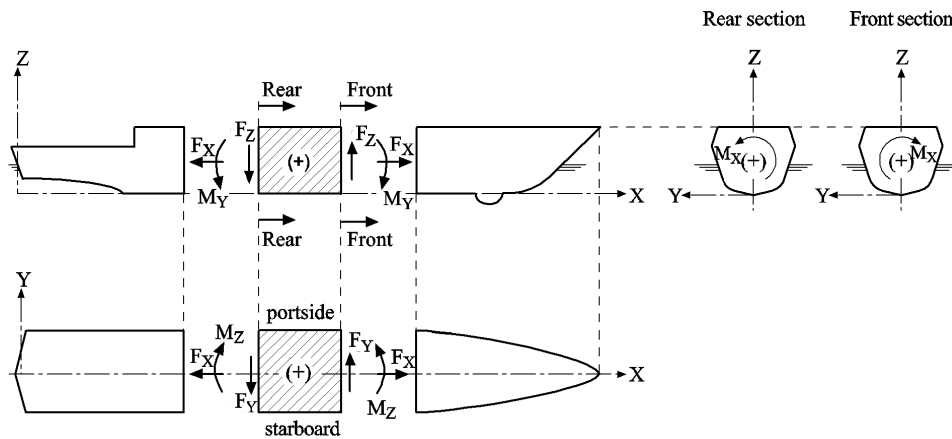


Figure 3.3: The sign conventions for the hull girder internal shear forces and bending moments. Modified from [15]

- The vertical bending moment M_y is positive if it induces tensile stresses in the strength/main deck (hogging bending moment) and negative if it induces tensile stresses in the bottom (sagging bending moment).
- The vertical shear forces F_z are positive if the resultant forces calculated with Eq. (3.2) act downward aft of the cut and upward in front of the cut.
- The horizontal bending moment M_z is positive if it induces tensile stresses in the starboard side and negative if it induces tensile stresses in the port side.
- The horizontal shear forces F_y are positive if the resultant forces calculated with Eq. (3.2) act to starboard and to portside in front the cut.
- The torque or moment of torsion M_x is positive if the resulting moment aft of the cut results in a negative rotation around the x-axis and in front of the cut in a positive rotation around the x-axis.
- The surge forces F_x are positive if the resultant forces calculated with Eq. (3.2) point backwards aft of the cut and frontwards in front of the cut.

The internal loads in Eq. (3.2) can be determined at any point on a transverse cross-section or cut. The vertical and horizontal shear forces and the surge forces result in a 3D force problem for the ship. Therefore there is always a contribution of two forces that cause a moment around an axis. The location of this point on a cut should therefore be chosen such that it represents the actual internal loading the structure experiences. This can be done by using some simplifications and assumptions.

First, the vertical location of the point on a cut defines the influence of the surge forces on the vertical bending moment M_y . It is demonstrated by Rajendran et al. [58] that the effect of the surge forces on the vertical bending moment are insignificant, which is confirmed by in-house validation of the SHIPMO strip method solver. Therefore, the height of the point can be chosen freely without concern for significant errors in the vertical bending moment.

Second, the transverse location on a cut defines the influence of the surge forces on the horizontal bending moment M_z . The horizontal shear forces are lower in magnitude than the vertical shear forces and therefore the surge forces have a non-negligible influence on the horizontal bending moment. The major part of the horizontal bending moment is still caused by the horizontal shear forces, since they are larger in magnitude, but have a similar moment arm. It will be demonstrated in Chapter 4 that the horizontal bending moment results in a small hull girder bending and is therefore not the most important load to look at. This means that, although there can be a significant error on the horizontal bending moment by a free choice of the transverse location on cross-section, the overall bending moment is still too small to result in a significant deformation.

Considering the bending moments, the point on a cut can thus be chosen freely, but that does not provide a guidance for the location choice. For that, the remaining internal torque is used. The torque is caused by the vertical and horizontal shear force, with similar moment arms. Though the horizontal shear force is smaller in magnitude, it has a non-negligible contribution to the torque. The location choice (vertical or transverse) hence has a large influence on the magnitude of the torque. A choice can be made by using a definition originating in the structural properties of a cross-section called the *shear centre*. A shear load with a line of action through this point on the cross-section produces no twisting of the cross-section [47]. Thus if this point is used for determination of the internal load RAO's, the torque at that point is actually the torque that is experienced by the structure. The shear centre can therefore be used as a reasonable choice for the location of the point on a cut to determine the internal load RAO's and it is also found to be done in literature e.g. by Iijima et al. [30]. For the test case yacht, the shear centre lies for the most part at the centre line through the middle width of the ship ($y = 0$). The height is varying slightly along the length of the ship and for this study the average height of the shear centre is chosen. This choice is considered a reasonable approximation for this study, since the height only influences the horizontal shear force contribution to the torque, which is smaller than the vertical shear force contribution, thus resulting in the least deviations in torque magnitude. In short, the internal load RAO's for the six load components in the linear response analysis are determined at transverse cross-sections at position $y = 0$ with respect to the centre line of the width at a height of the average shear centre location. An example of the results of the internal load analysis can be seen in Figure 3.4, where the vertical bending moment RAO at the amidships longitudinal transverse cut is given, including the phase angle. The RAO indicates the magnitude of the vertical bending moment per meter wave amplitude for each wave frequency. For example, a wave with amplitude 1 m and a frequency of 0.6 rad s^{-1} results in a vertical bending moment of $\approx 1.1 \times 10^4 \text{ kN}$ amidships. The phase indicates at what moment in time the amplitude of the response is reached with respect to the maximum amplitude of the sinusoidal wave hitting the location of the Center of Gravity (CoG). The phase information of the internal loads is used in Section 3.3 for the equivalent design wave. A database is created that stores the RAO and phase information at all longitudinal locations where the transverse cuts are made, for all six load components, all wave frequencies, all headings and all ship speeds.

3.2.2. The response spectrum

In a linear response analysis, the wave-ship system is regarded as linear, which means that the response spectrum $S_r(\omega)$ of the respective load of interest can be calculated with equation Eq. (3.3), as mentioned in Section 2.4.3. The wave spectrum $S(\omega)$ is the input spectrum of the linear wave-ship system and the RAO defines the response for each frequency as indicated in Figure 3.4.

$$S_r(\omega) = RAO(\omega)^2 S(\omega) \quad (3.3)$$

The RAO's for the load components are known, only the wave spectrum $S(\omega)$ in which the yacht operates is still unknown. The choice of the wave spectrum can be related to common areas of Feadship activity to

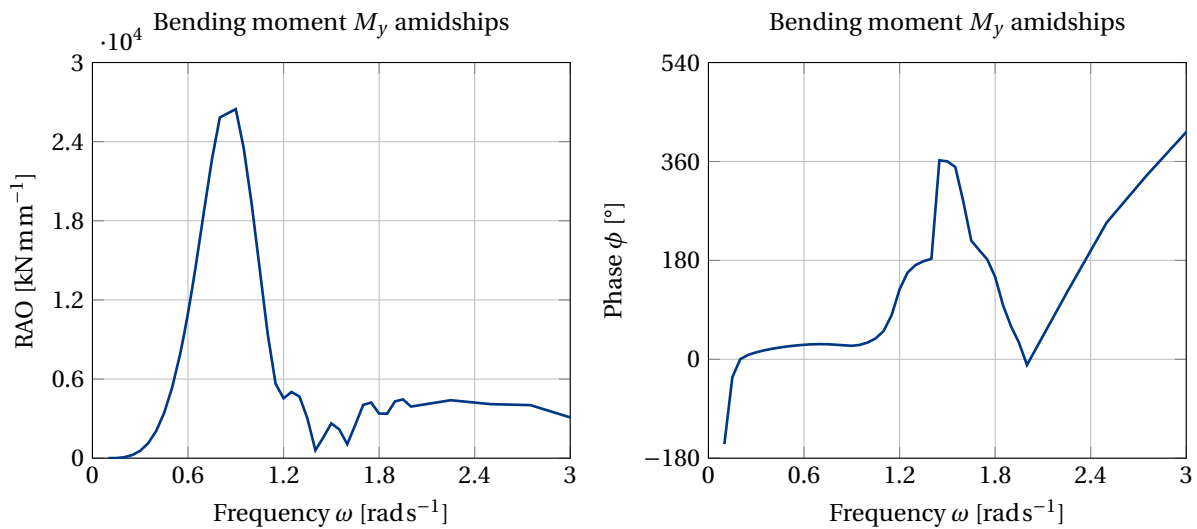


Figure 3.4: The Response Amplitude Operator (RAO) and the phase of the vertical bending moment M_y amidships for $V = 16$ kts and $\beta = 180^\circ$.

represent actual operation responses. In this work, the standard and widely used JONSWAP wave spectrum is taken as standard wave spectrum, given in Eq. (2.11), because it is applicable in fetch-limited¹ seas, which is true for the areas Feadships generally operate. The spectrum can be generated with the significant wave height and mean zero-crossing period that are present at a location, which are generally available in scatter diagrams. In Figure 3.5 the JONSWAP wave spectrum is calculated with Eq. (2.11) for $H_s = 2$ m and $T_z = 6.1$ s.

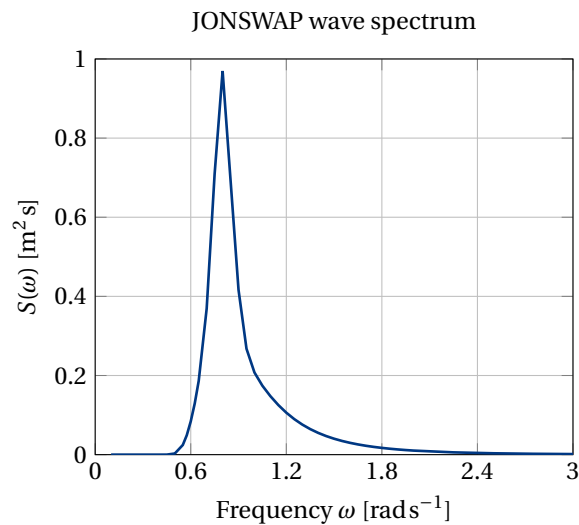


Figure 3.5: The JONSWAP wave spectrum for significant wave height $H_s = 2$ m and mean zero-crossing period $T_z = 6.1$ s.

As demonstration, the response spectrum of the vertical bending moment M_y is given in Figure 3.6, calculated with Eq. (3.3) with the RAO data given in Figure 3.4 and the wave spectrum given in Figure 3.5. The wave spectrum contains the most energy at frequencies where the RAO spectrum has a peak, hence the response is amplified. If the peaks do not overlap, then the response spectrum is low, meaning the yacht does not respond with a large magnitude for that specific load to the sea state.

From spectral analysis of the response spectrum, characteristics can be determined in a similar way as presented for the wave spectra in Section 2.3. The only difference is that the response spectrum is regarded instead of the wave spectrum.

It is thus possible to determine the maximum amplitude of the response, often called Significant Double

¹Fetch is the distance over which the wind acts to produce waves

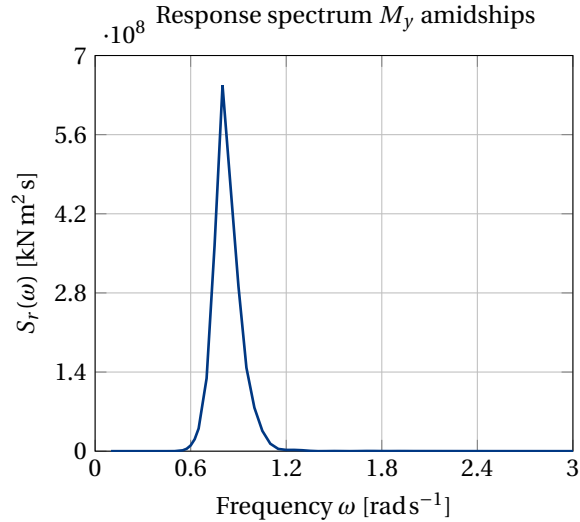


Figure 3.6: The response spectrum for the vertical wave bending moment M_y amidships in a sea state with $H_s = 2$ m, $T_z = 6.1$ s, $V = 16$ kts and $\beta = 180^\circ$.

Amplitude (SDA), by rewriting Eq. (2.15) as Eq. (3.4), by using the zeroth spectral moment of the response spectrum m_{0r} instead of the zeroth spectral moment of the wave spectrum $m_{0\zeta}$. Similarly, the Most Probable maximum Response (MPR) is repeated in Eq. (3.5) for convenience with exposure time to the sea state $t_{exp} = 30$ minutes (this time period can be at maximum hours, otherwise the statistical characteristics of the sea state can not be assumed to be stationary as described in Section 2.3).

$$SDA = 4\sqrt{m_{0r}} \quad (3.4)$$

$$MPR = \sqrt{2m_{0r} \ln N} \quad (3.5)$$

For the vertical bending response spectrum in Figure 3.6, the zeroth spectral moment m_{0r} is determined as 1.1×10^8 kNm. The SDA and MPR values are then calculated with Eq. (3.4) and Eq. (3.5) at each longitudinal location (transverse cut) and given in Figure 3.7. The longer the exposure to the sea state, the higher the probability that the response reaches the maximum SDA value, i.e. the MPR approaches the SDA values for increasing t_{exp} .

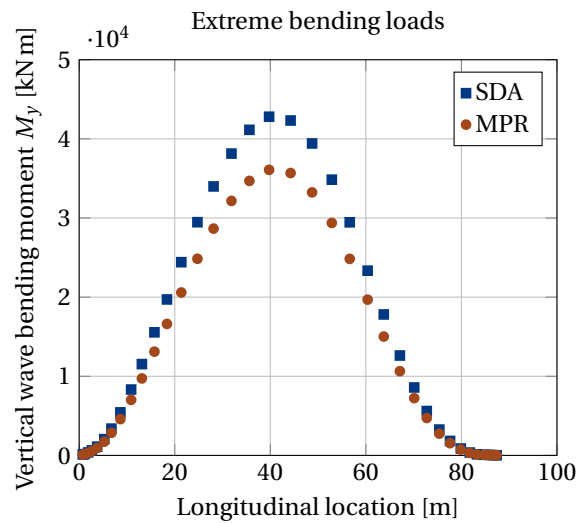


Figure 3.7: The longitudinal distribution of the Significant Double Amplitude (SDA) and the Most Probable maximum Response (MPR) of the vertical bending moment M_y for $\beta = 180^\circ$ and $V = 16$ kts.

The vertical bending moment amidships is taken as example in this section, but the same approach is used for the other internal load components that were indicated in Figure 3.3. This means that at any longitudinal location, the SDA and MPR values of the internal loads are known for the chosen sea state. The process is summarized in Figure 3.8: the RAO's of all internal loads are determined at a transverse cut location for unit sinusoidal waves with varying frequencies, Eq. (3.3) is used to calculate the response spectrum for all internal loads. Then, Eq. (3.4) and Eq. (3.5) are used to determine the SDA and MPR values of all internal loads. The results are six SDA and six MPR values, one for each internal load, at each transverse cut location.

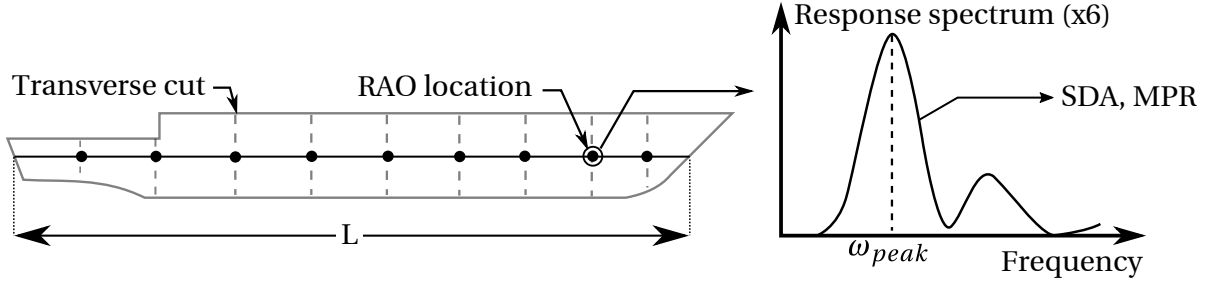


Figure 3.8: Most probable response determination at each transverse cut location.

The SDA and MPR values merely indicate what the (most probable) maximum response is at that location, not what the distribution is of the internal loads if at one location the most probable maximum response is reached. Directly obtaining a load distribution is not possible from these points, because these maxima do not necessarily occur simultaneously and the phase differences of the internal loads are to be taken into account. A commonly used method to derive a load distribution in succession to a spectral analysis is the Equivalent Design Wave (EDW), which includes the phase information (given in Figure 3.4) that is also calculated by the SHIPMO analysis. This approach is discussed in Section 3.3.

3.3. Equivalent Design Wave

In the structural analysis of ships, equivalent design waves are simple wave patterns that represent the extreme load situations on the structure that occur in its lifetime. This definition applied to this study means that the equivalent wave or waves should represent the most probable response or maximum response of a load on a location for a certain duration in a sea state. The equivalent wave is *not* to model the sea waves themselves or to model the resulting stress distribution caused by the waves, but it is a means to check response of the structure for an envelope of extreme lifetime responses or most probable extreme for a duration in a sea state. The latter concerns the loads encountered in operation that cause comfort problems, while the extreme lifetime responses are strength related, which is not part of this study.

A set of equivalent design waves can be used to create a set of load distributions to predict the most probable extreme deflections and rotations of the structure in a sea state for which comfort due to (excessive) local and global deflections should be avoided. The features of such equivalent waves and how they are selected are discussed in Section 3.3.1 and Section 3.3.2 and the resulting load distributions including a comparison to classification rule loads (Lloyd's register and Bureau Veritas) is given in Section 3.3.3.

3.3.1. Equivalent Design Wave features

The EDW adopted in this thesis is a regular sinusoidal wave that induces an internal load on a specific location. This internal load at a location is called the Target Response (TR) of the EDW, since the target of the EDW is to cause that response at that location. The EDW is characterised by an amplitude and a frequency, which are used to determine the internal loads at other locations than the chosen target response. There are multiple options available to determine these parameters that Folso and Rizzuto [20] investigated and the most effective selection criteria they found for the EDW parameters is adopted in this study.

The amplitude of the EDW can be chosen by dividing the target response, which can be for example a SDA or MPR value, by the RAO of that load component and the location of the target response, see Eq. (3.6). This means that the amplitude of the EDW is such that it always reaches the target response (SDA/MPR value) at that location at some point in time during the period of the EDW.

$$a_{EDW} = \frac{TR}{RAO_{TR}} \quad (3.6)$$

The EDW frequency ω_{EDW} is chosen as the frequency at which a peak in the response spectrum of the target response is observed, see Eq. (3.7) with ω_{peak} as seen in Figure 3.8, since this peak indicates the frequency of the maximum response energy.

$$\omega_{EDW} = \omega_{peak} \quad (3.7)$$

The EDW with amplitude a_{EDW} and frequency ω_{EDW} now causes the target response TR. The load components at other locations r_{other} can be determined by their phase difference with respect to the chosen target response according to Eq. (3.8). Where RAO_{other} is the RAO of the load component at another location or the RAO of another load component at the same or other locations, ϕ_{TR} the phase angle of the chosen target response and ϕ_{other} the phase angle of the other load component, which are both taken for the EDW frequency.

$$r_{other} = RAO_{other}(\omega_{EDW}) \cdot a_{EDW} \cdot \cos(\phi_{TR} - \phi_{other}) \quad (3.8)$$

Important to realise is that the choice for the target response, greatly influences the load distributions that are created. The target response can be chosen as any load component in the 6 degrees of freedom, at any longitudinal location x along the yacht, for every yacht speed V , for every wave heading angle β , for every mean zero-crossing period T_z and for all significant wave heights H_s . Or, mathematically, see Eq. (3.9).

$$\text{Target Response} = f(x, V, \beta, T_z, H_s) \quad (3.9)$$

This large range of possible target responses, means a large range of possible load distributions as input for the structural response analysis. In theory, the structural analysis can be performed for all these load cases, however, in the preliminary design quick and clear design tools are preferred. The amount of load cases decreases drastically, by recognising relations between the different dependent variables and their influence on the result. This is discussed in more detail in Section 3.3.2.

3.3.2. The target response

The goal of determining the load distributions with Eq. (3.8) is twofold: it can be used to compare the loads measured/derived in structural monitoring during operation with the calculated loads for validation purposes or it can be used as a design load distribution to test the stiffness of the yacht and determine the elastic deformations. For the first goal, the parameters of the sea state (H_s and T_z), the operation parameters (V and β) and the location of the measurements (x) are known and can be used directly to derive a load distribution that can be compared to the measurement results. For the second goal, a design envelope of load distributions is to be created that covers the operational profile of the yacht for which the deflecting of the structure is not allowed to cause discomforting problems. Essentially, this is a long-term probability analysis that combines the probability of occurrence of the operation parameters and the sea state. Such analysis is not in the scope of this thesis. However, assumptions can be made for all parameters that reflect the comfort standards set by Feadship itself, which can be used more directly without a long-term analysis. The process of selecting the parameters for the target response of the equivalent design wave is illustrated schematically in Figure 3.9.

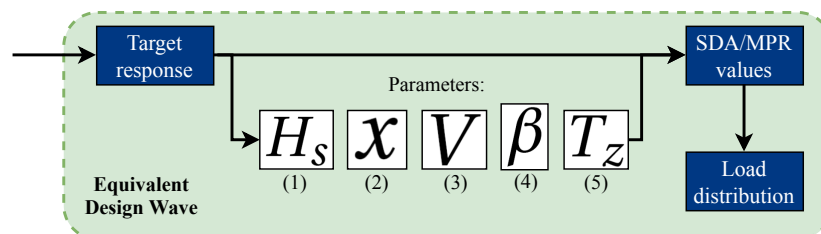


Figure 3.9: The 5 parameters that are chosen for the target response of the EDW to obtain load distributions.

The first step is assuming a comfort limit for the significant wave height by observing common wave heights for areas of Feadship activity. Sea state information provided by Det Norske Veritas - Germanischer Lloyd [16] can be used to determine this. A reasonable significant wave height can be $H_s = 2$ m, which indicates that for this sea state and wave heights below, no creaking is allowed. The results scale linearly with the wave height, hence this can be increased up to $H_s = 4$ m, for which the strip method is still sufficiently accurate.

The second step is to decide at what longitudinal location the target response should be achieved, because the SDA values at any longitudinal location seen in Figure 3.7 can be taken. Extreme and fatigue loads assessment is normally performed by regarding the bending moments amidships and the torsional moment at 25% of the length between perpendiculars L_{pp} from the aft perpendicular as described by Soares and Garbatov [66]. For now, these locations are used for the other steps and this assumption is validated shortly after.

Step three considers the speed, which is somewhat arbitrary, because it affects the response magnitude, but also the wave encounter frequency differently for different load components. In general, an increase in response magnitude of all target responses is observed for a speed increase, because a higher speed increases the pressure distribution and consequently the loads. Therefore, the choice of speed is unlikely to affect the conclusions of this chapter. For this study, the cruise speed of $V = 16$ kts is taken, meaning that for this speed and below no creaking is allowed in sea states of $H_s \leq 2$ m.

The fourth step is generating response spectra at the chosen locations, speed of $V = 16$ kts and significant wave height $H_s = 2$ m for all heading angles by using Eq. (3.3). The SDA values are then calculated with Eq. (3.4) and plotted for all wave frequencies and heading angles in polar plot form. These plots for the bending moments and torque can be seen in Figure 3.10. For the vertical bending moment it can be seen that the maximum response occurs at a wave peak frequency ω_p of 0.8 rad/s for a wave heading of 180° . The wave peak frequency can be related to the mean zero-crossing period T_z according to Eq. (2.5) and Eq. (2.10), resulting in $T_z = 6.1$ s. Note that the SDA response peak value of 4.2×10^4 kN m in Figure 3.10 for $\beta = 180^\circ$ is the same as the SDA peak value in Figure 3.7.

For the horizontal bending response, it is first noted that larger mean zero-crossing periods are more likely to occur (i.e. low peak frequencies) and below $T_z < 4$ s mostly low wave heights are observed [16], meaning that the choice of $H_s = 2$ m is probably conservative. Also, for wavelengths $\lambda < \frac{1}{3}L_{oa}$, strip methods are generally not accurate, which corresponds to frequencies of $\omega_p \approx 1.5$ rad/s for this yacht. Therefore the peak occurring at the lowest peak frequency is taken, which is at $\omega_p = 1.3$ rad/s, corresponding to $T_z = 3.8$ s for a heading of $\beta = 120^\circ$. For the torque, the SDA peak at the lowest peak frequency is also taken for the same reasons as for the horizontal bending moment, which is at $\omega_p = 1.1$ rad/s, corresponding to $T_z = 4.4$ s for a heading of $\beta = 60^\circ$. The heading angles determined from Figure 3.10 agree with the common heading angles that govern the response for the equivalent design waves according to literature [67, 68]. A summary of the results of the target response parameters for the three main loads is given in Table 3.2.

Table 3.2: The chosen parameters for the target responses for the test case yacht.

Target response	Location	V [kts]	β [°]	H_s [m]	T_z [s]
M_y	amidships	16	180	2	6.1
M_z	amidships	16	120	2	3.8
M_x	25% L_{pp}	16	60	2	4.4

The SDA and MPR values can now be calculated along the length of the yacht for the target response parameters given in Table 3.2 with Eq. (3.5) and Eq. (3.4), respectively. In Figure 3.11 the results for the three main loads can be seen for varying longitudinal locations. Note that the SDA and MPR values are absolute amplitude values of the loads and do not necessarily occur simultaneously in magnitude or have the same sign.

First, it can be seen that the assumption for the location of the maximum response is indeed amidships for the bending moments, with the peak of the horizontal bending moment slightly ahead of the vertical bending moment peak (this is in agreement with the bending moment graphs in the work of Soares and Garbatov [67]). The location of the maximum torque response is also approximately at the assumed maximum location of 25% of L_{pp} for the torque.

Second, at the aft end of the yacht for $L < 5$ m, the torque SDA/MPR values do not go to zero, but increase going aft. In the limit, all loads should converge to zero, however, for the torque, there can be immediately a moment arm to the (average) shear center if the width does not change gradually, hence a rather steep increase can still be expected. For this yacht, there is no gradual increase in width at the rear, while at the bow there is a gradual decrease in width towards the front (this can also be seen in the example hull geometry in Figure 3.2). In Figure 3.11, the SDA values are also plotted for a lower speed of 5 kts instead of 16 kts. A sudden change in slope at $x = 5$ m is not seen, which is also true for other lower speeds. The increase in SDA values is directly linked to large RAO values at aft end of the yacht, which are calculated by the strip method software SHIPMO in QSHIP. The Seakeeping Committee of the 16th ITTC [75] concluded that the torque calculated

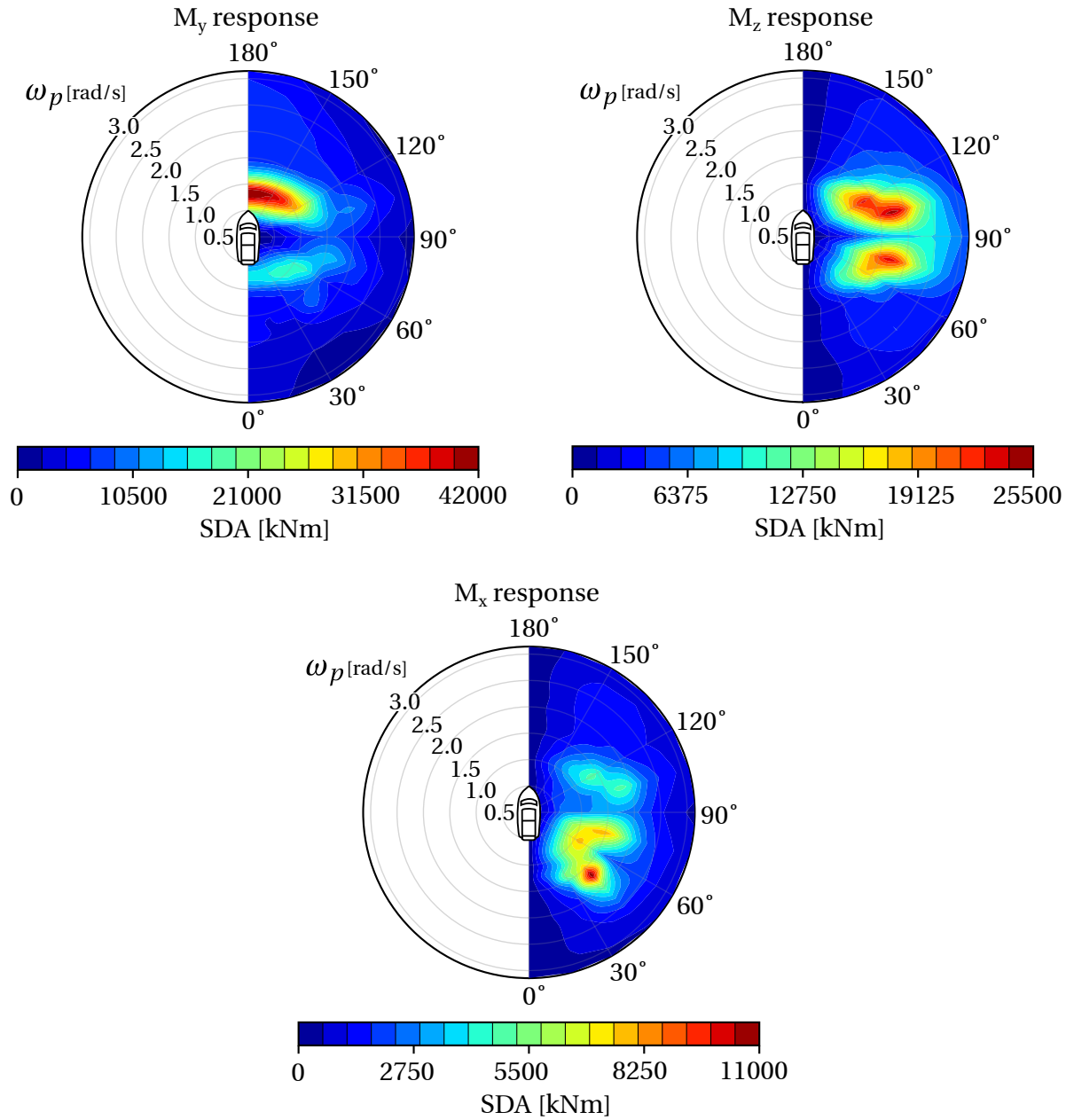


Figure 3.10: Polar plots the Significant Double Amplitude SDA of the bending moments amidships and the torque at 25% L_{pp} w.r.t aft perpendicular for different heading angles and wave peak frequency ω_p .

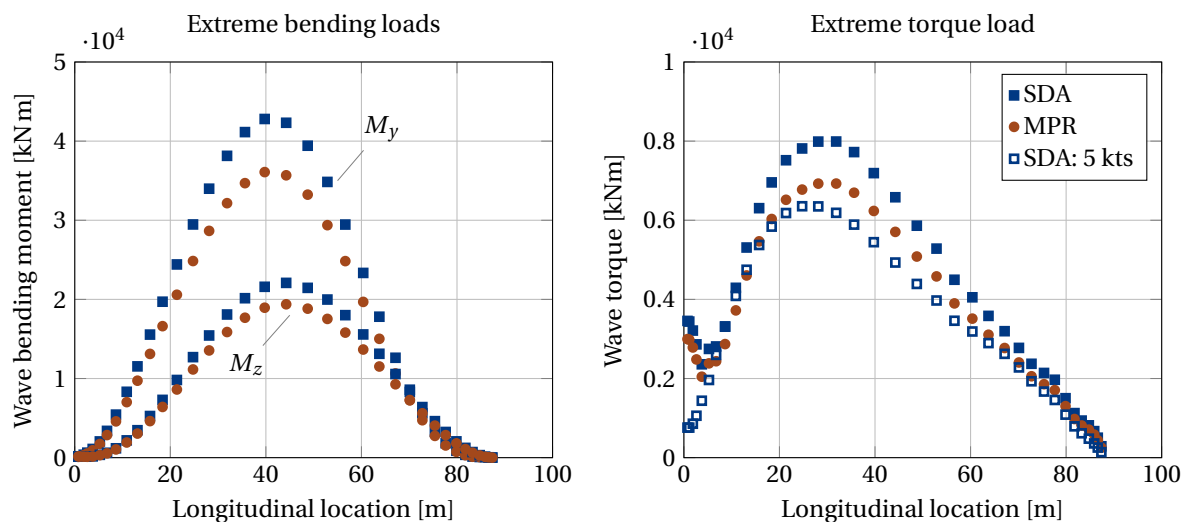


Figure 3.11: The longitudinal distribution of the most probable maximum response MPR for $t_{exp} = 0.5$ hours and Significant Double Amplitude SDA for the bending loads $M_{y/z}$ and torsional load M_x .

by several strip methods showed discrepancies among the methods and the experiments to compare them with. The exact source of the rather unrealistic behaviour at the extremities is therefore not easy to determine and since the torque should physically converge to zero, it is advised to not incorporate the locations if the SDA suddenly changes slope, in this case for $x < 5$ m. This means that the RAO values of those locations are not incorporated in the load distribution calculations with Eq. (3.8). In Section 4.6 the influence of omitting these values is discussed in relation to the global deformations and the influence is found to be only local and small.

3.3.3. Load distributions

The extreme responses along the length of the yacht are determined in Section 3.3.2 as MPR or SDA values. In this section, load distributions are derived based on these values as target response using the EDW method described in Section 3.3. The most conservative method or highest comfort level is achieved if the design load distributions are calculated with the SDA values of Figure 3.11 as target response. In Table 3.3 the EDW features are given that result in three load distributions for the three main loads with the largest SDA value in Figure 3.11 taken as target response. Thus, for the load component M_y , a regular EDW with amplitude $a_{EDW} = 1.6$ m and frequency $\omega_{EDW} = 0.8$ rad s⁻¹ results in the SDA response of 4.2×10^4 kNm amidships, i.e. the peak in Figure 3.11.

Table 3.3: The EDW features used for derivation of the design load distributions.

Feature	Symbol	M_y	M_z	M_x	Unit
Amplitude	a_{EDW}	1.6	1.5	1.6	[m]
Frequency	ω_{EDW}	0.8	1.25	1.1	[rad/s]
Wavelength	λ	96	39	51	[m]

The wavelength corresponding to the equivalent design waves is calculated using Eq. (2.6). It is known that in general the vertical bending moment is maximum for wavelengths in the same order of the length of the yacht [28], hence this is an additional check for the validity of the EDW. The wavelength for M_y is indeed in range with the length: yacht length of 88 m and a wavelength of 96 m.

In Figure 3.12, the three load distributions resulting from the Equivalent Design Waves are given including the SDA responses. Also, a comparison is given with rule load distributions, for the hogging vertical load, the Lloyds rule load is used and for the torque the Bureau Veritas rule load is used, these are discussed in more detail in Section 4.4.1.

First, it can be noted that the curve for the bending moments seems to go through all the SDA values and the same is to a lesser extent seen for the torque distribution (note that the curves are derived for the maximum SDA value and not created by connecting the SDA values). This means that if the maximum bending or torque

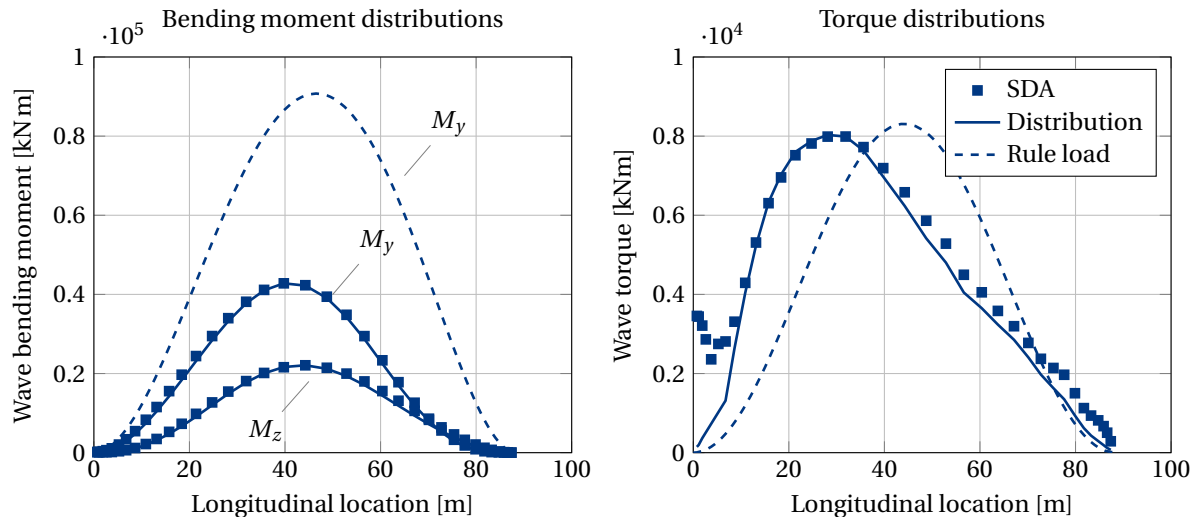


Figure 3.12: The longitudinal load distributions determined by Equivalent Design Waves EDW's with the maximum SDA as target response.

is achieved, all other locations also experience maximum bending or torque. The sudden slope change in the torque load distribution curve at $x = 5$ m is because the locations more aft than that had unrealistic SDA values and the RAO values were left out. The curve is forced through zero by not using the RAO values at those locations in Eq. (3.8) and linearly interpolating between the last realistic location at $x = 5$ m and $x = 0$ m. It will be demonstrated in Section 4.6 that this has a rather small effect on the torsion response, only affecting that particular longitudinal aft location. Since a mentioned limitation of the strip method in Section 2.4.2 is that the accuracy decreases towards the extremities, it is not advisable anyway to expect accurate results for the local deformations.

Secondly, comparison with the design rule load for the vertical bending moment shows that the design rule load has a larger magnitude than the derived load distributions for this sea state, which makes sense, since the design rules are meant for strength assessment and reflect the most extreme load case. The design rule load and the derived load distribution do have a similar shape, which means the regular EDW can be considered a sufficiently realistic method for the preliminary design. Furthermore, if the SWBM of Figure 4.8 is added to the derived wave bending moment in Figure 3.12 it can be calculated that the horizontal bending moment peak is approximately 40% of the vertical bending moment, which is in agreement with the statement made by Tupper [74] that horizontal bending moment peaks are typically only 40% of the vertical ones.

Thirdly, it can be seen that the torque distribution has a similar magnitude as the rule design torque for this sea state instead of the being lower as was the case for the vertical bending response. Also, instead of amidships, the peak is shifted more towards 25% of L_{pp} and as mentioned in Section 3.9, the latter is in agreement with literature. The torque rule load is a check for the order of magnitude and shape, however direct comparison is not advised, because its applicability to Feadships is questionable, which is discussed in Section 4.4.1.

3.3.4. Applicability for structural response

In Figure 3.12 the load distributions that result in the maximum SDA response of the chosen target response were given. For the vertical bending moment this happens for an EDW with heading angle of $\beta = 180^\circ$, for which the horizontal bending and torque are zero (this is visualized in Figure 3.10 as M_z and M_x show a zero SDA value for $\beta = 180^\circ$). The EDW's that cause the horizontal bending and torque distributions in Figure 3.12 also result in load distributions for other load components than that of the target response. Else said, for heading angles other than 180° , progressively beam seas on, the vertical bending decreases and concurrently horizontal and torque loads increase. These concurrent load distributions can also be calculated with Eq. (3.8). For example, if the vertical bending moment M_y is used as target response, the torque M_x load distribution can be calculated with Eq. (3.8). Vice versa, if the torque M_x is used as target response, the concurrent vertical bending moment M_y can be calculated. This is illustrated for the sea state of $H_s = 2$ m and $T_z = 4.4$ s in Figure 3.13.

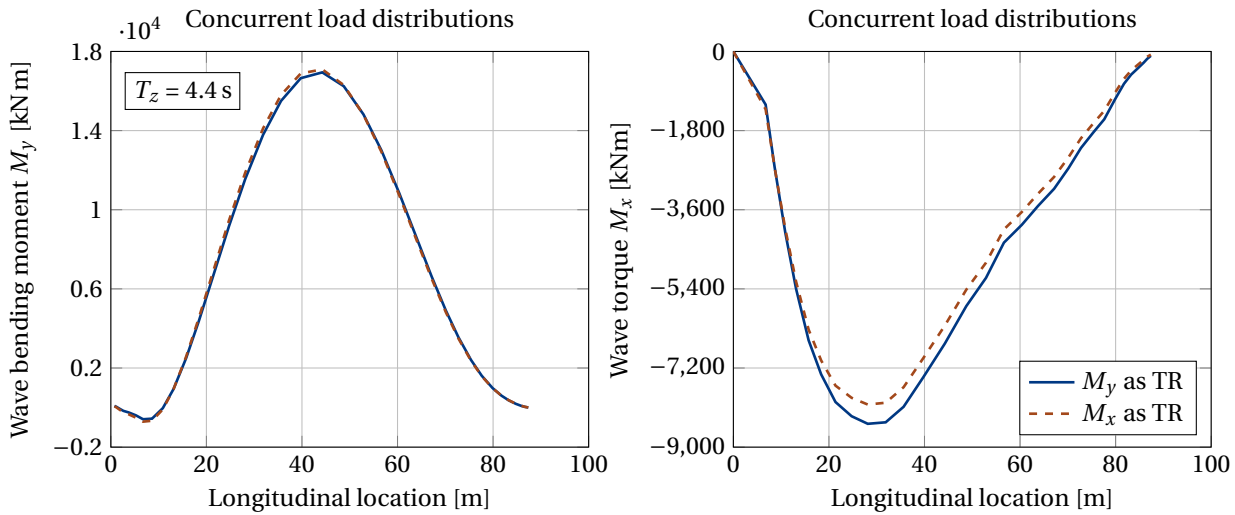


Figure 3.13: Concurrent load distributions obtained with a regular EDW, for $\beta = 60^\circ$, $H_s = 2$ m, $T_z = 4.4$ s and $V = 16$ kts. Comparison for target response TR taken as M_y or M_x

Four curves are given of which two concurrent curves: one set of curves by using M_y as target response and the other set by using M_x as target response. In this sea state, it is to a large extent irrelevant which load is taken as target response, i.e. the concurrent curves are similar irrespective of the target response choice. If M_y is taken as target response, the load distribution causing the maximum SDA value of M_y also results in a torque load distribution that causes the maximum torque SDA. This example is not true for all cases, however, as can be seen by using a sea state with $T_z = 6.1$ s instead of $T_z = 4.4$ s as illustrated in Figure 3.14.

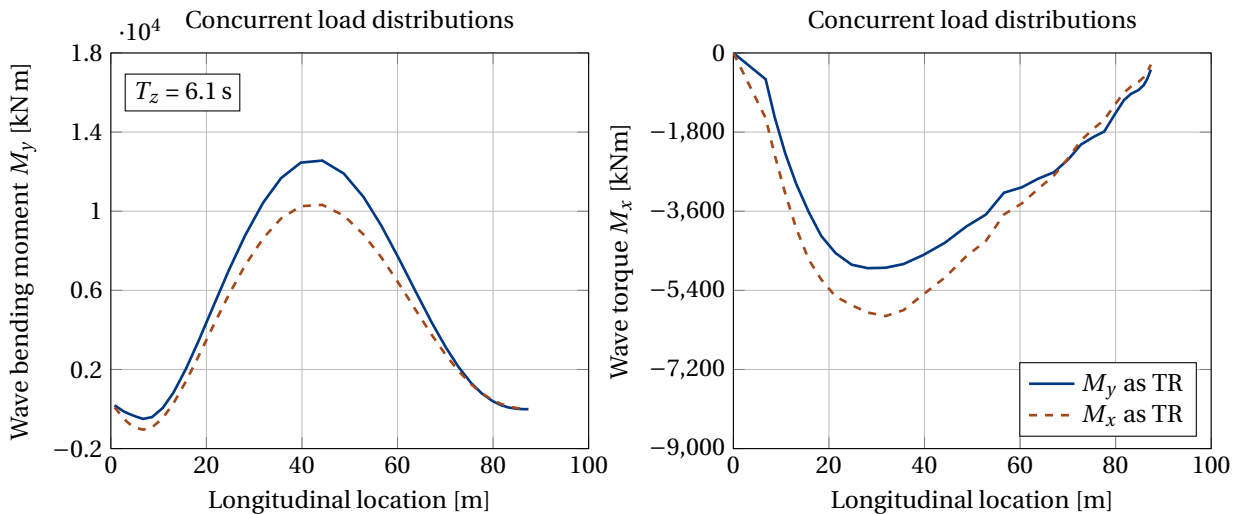


Figure 3.14: Concurrent load distributions obtained with a regular EDW, for $\beta = 60^\circ$, $H_s = 2$ m, $T_z = 6.1$ s and $V = 16$ kts. Comparison for target response TR taken as M_y or M_x

In the case in Figure 3.14, using M_y as target response, the concurrent torque distribution is lower in magnitude than if M_x is used as target response. Similar the other way around. There can be several causes of the discrepancies in the curves in Figure 3.14, which can be discussed by looking at Eq. (3.8). The discrepancies can be a result of the RAO's, the EDW features a_{EDW} and ω_{EDW} or the phase differences. In Table 3.4 the EDW features are given to generate the figures in Figure 3.13 and Figure 3.14, respectively.

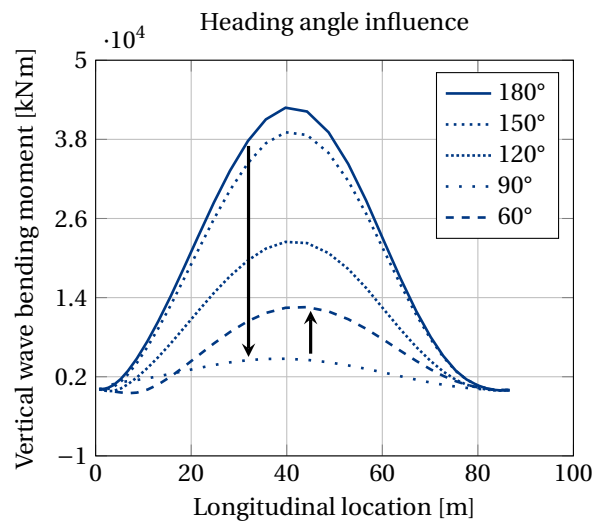
What can be concluded from Table 3.4 is that the same EDW causes the maximum response for M_y and M_x , because the amplitude and frequency to cause the response are similar for one sea state. That the curves do not overlap for a sea state with $T_z = 6.1$ s thus means that for that sea state the maximum responses do not occur simultaneously. For the sea state of $T_z = 4.4$ s, the moment at which the M_y response reaches its maximum

Table 3.4: EDW features to calculate the load distributions of M_y and M_x for different target responses.

Feature	Symbol	$T_z = 4.4$ s		$T_z = 6.1$ s		Unit
		M_y as TR	M_x as TR	M_y as TR	M_x as TR	
Amplitude	a_{EDW}	1.6	1.6	2.7	2.7	[m]
Frequency	ω_{EDW}	1.1	1.1	0.8	0.8	[rad/s]

is approximately similar to the moment at which M_x reaches its maximum. The regular EDW approach can thus be used to approximate concurrent load distributions, however in the scope of the structural response in Chapter 4, the addition of deformations caused by the waves is not straightforward and is dependent on the sea state. Therefore, it is advised for a complete overview of the load distribution envelope to perform a long term analysis that calculates load distributions for all sea states and determine the structural response for all of them if the combination of loads is deemed important. As mentioned before, this is outside the scope of this thesis, however, for current application of the methods in this work a suitable option is to select the load as target response that is expected (based on experience) to result in the worst (local) deformations (which are treated in Chapter 4) and use the concurrent load distributions for the other load components. If the curves such as presented in Figure 3.14 are not deviating too much, this can be an acceptable result for the preliminary design. Otherwise, the analysis can be performed two times, one for the target response as M_y and one with the target response as M_x . The case that results in the worst local deformations should then be adopted.

A last note that can help to make a decision which target response results in the worst (local) deformations is that the vertical bending moment, that can be seen as the most important hull girder load, decreases significantly in magnitude for heading angles that are important for the torsion. In Figure 3.15 the influence of the heading angle β on the vertical bending moment distributions is given. The heading angles for which a large torsion response is expected are 60° (and also 120° to a lesser extent), for which the peak of the bending moment decreases to 30-50% of the magnitude at $\beta = 180^\circ$. The local deformations will also decrease by a similar percentage, since the structural modelling considers only linear elastic behavior.

Figure 3.15: Heading angle influence on the vertical wave bending moment with $H_s = 2$ m, $T_z = 6.1$ s and $V = 16$ kts.

3.4. Summary

In Section 3.2, a linear response analysis is performed on a test case yacht with a length overall of $L_{oa} = 88$ m to generate a database of Response Amplitude Operators (RAO's) and phases for the internal load components of the six load components for each longitudinal location, all wave frequencies, all headings and all yacht speeds. For the sea state a JONSWAP spectrum is used and together with the RAO's response spectra are generated. Spectral analysis is performed in Section 3.2.2 to determine the Most Probable maximum Response (MPR) and the Significant Double Amplitude (SDA), indicating what the most extreme value of the load com-

ponents is. A polar plot of the results indicates for what heading the load component has a maximum and for what peak frequency T_p corresponding to a mean zero-crossing period T_z of the sea state. The longitudinal location of the maximum SDA/MPRA values is amidships for the vertical and horizontal bending moment and approximately at 25% of the length between perpendiculars L_{pp} , which corresponds to the locations given in literature.

The magnitude of the peaks are defined by the chosen comfort level that is set by Feadship by an appropriate choice of significant wave height H_s and yacht speed V for which no discomforting effects of an elastic deforming structure is allowed. The higher these values, the larger the load magnitudes and the more the yacht has to account for these loads to be as comforting as set by the Feadship standard. The chosen wave height affects the SDA/MPR values linearly, since it is a linear response analysis. For the torque it can be seen that an increase in speed leads to unrealistically high values at the aft extremity of the yacht, these points can be omitted for the derivation of the load distributions with only small effects on the global response as will be demonstrated in Section 4.6.

In Section 3.3, a regular Equivalent Design Wave EDW approach is used to derive a design load distribution from the MPR or SDA values by choosing a target response that the EDW has to cause. The magnitude of the load at longitudinal locations other than the target response or other load components is determined with the phase difference of the target response and the respective other component. In total, three different EDW's are used to determine the design load distributions of the vertical bending moment, the horizontal bending moment and the torque. The bending moments match in shape and the vertical bending moment is lower than the Lloyds hogging design rule load distribution for the taken sea state, which is as expected since the design rule loads are extreme load cases used for strength assessment. The torque distribution has a shape that matches literature and is in the same order of magnitude as the Bureau Veritas torque load distribution. In Section 3.3.4, the applicability of the equivalent design wave for concurrent load distributions is discussed with regard to the global and local deformations. The EDW's do not always lead to concurrent load distributions that reach their maximum response at the same time. The effect is different for different sea states and no general conclusions can be drawn at this moment. To do this, a long term analysis is required taking into account all possible combinations of sea states and operation parameters. In relation to the global and local deformations the load distributions can still be used as approximation as it is known that the vertical bending moment decreases significantly to 30-50% of the peak value for $\beta = 180^\circ$ for heading angles for which the torque reaches its maximum.

4

Structural response

In the previous chapter, design load distributions were derived from a linear response analysis and compared to the rule design loads from the classification societies Lloyd's Register and Bureau Veritas. These loads act on the yacht hull, which results in an elastic response of the structure that can come into contact with the interior and cause creaking noises or damage. The yacht structure itself consists of many different structural elements that result in a complicated structural behaviour. The study of this behaviour is the field of structural analysis and involves the simplification of the real structure in a structural model that can be analysed with mathematical equations and numerical methods. In this chapter, simplifications are made for the yacht structure to study the response and form conclusions on the longitudinal stiffness of the yacht that can be used for risk analysis in the preliminary design phase of new yachts. Additionally, insight in required interior clearances are obtained.

In the preliminary design a structural model should meet a certain accuracy, while being simple enough to allow for easy change in inputs and quick analysis. A simple structural model often used in the preliminary design of a yacht is the yacht hull modelled as a prismatic beam (i.e. constant cross-sectional properties along its length) that can be analysed by analytical equations, as described in detail by Hughes et al. [28]. This approach is not sufficiently accurate enough for global and/or local structural response, since the cross-sectional properties of a hull change significantly along its length. A non-prismatic beam is thus desirable, however, analytical methods to analyse such a beam are limited. As indicated by Gere and Goodno [24], analytical methods are only practical if there are only 2 or 3 discrete cross-sectional changes along the length of the beam, more changes or continuously changing properties (as is the case for a hull) requires numerical solutions. A suitable numerical solution is the Finite Element Method (FEM) that discretise the model in small elements with constant properties. The 'actual' varying cross-sectional property distribution can then be approached by increasing the number of elements. The structural modelling approach of the yacht structure is visualized in Figure 4.1.

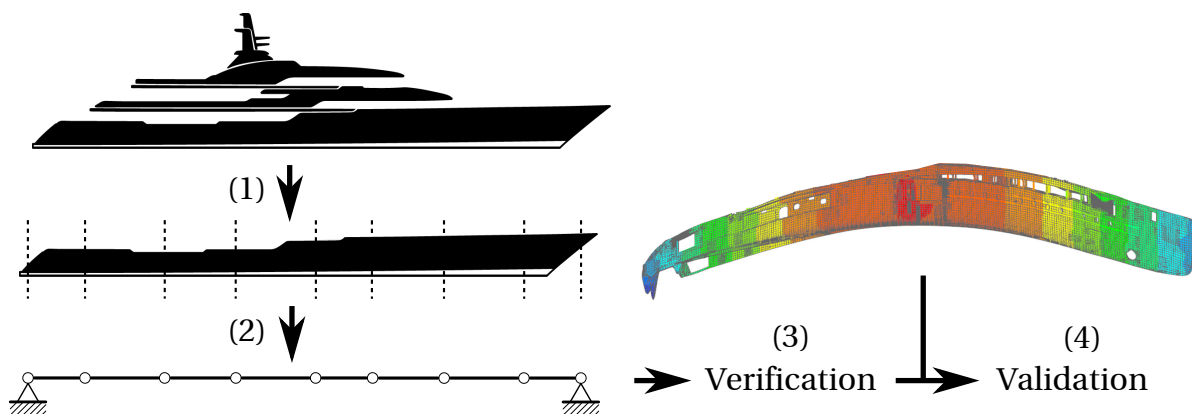


Figure 4.1: The structural modelling approach including verification and validation of the results.

The first step is the simplification of the real complicated yacht structure by regarding only the yacht hull

without a superstructure. This is done because most of the yacht stiffness comes from the hull and the shape of the hull is a rather constant factor along Feadships, while the superstructure can differ among yachts. If the results for the hull only agree, more complicated models can be developed as mentioned in the literature study in Section 2.5 that include the superstructure influence.

The second step is modelling the yacht hull as a beam with 1D finite elements that have constant properties along the length of the element that correspond to the longitudinal section of the real yacht structure. The real cross-sectional property distribution is approximated by increasing the used number of elements. The description of this model is given in Section 4.1.

The third step is verification of the beam model, since it is created in the Python programming language and it must be checked if the code routine is implemented correctly. The verification is done by creating a model with the same beam elements and properties in a commercial finite element software package. The verification study is given in Section 4.2.

The fourth step is the validation of the response, which can be divided in a global response and the local deformations derived from the global response. The beam model requires cross-sectional properties of the yacht hull, which are determined in Section 4.3. The results of the beam model global response are compared to the response of a detailed 3D Finite Element (FE) model of the test case yacht in Section 4.4 to determine the accuracy of beam model and the same is done for the local response in Section 4.5. The load distributions of Chapter 3 are then combined with the beam model in Section 4.6 to create the global response to an actual sea state and the subsequent local deformations to use for risk and clearance analysis. At last, a summary of the chapter is given in Section 4.8.

4.1. Finite Element model

The beam model consists of 1D beam elements and each element has constant structural properties that correspond to the (average) cross-sectional properties at that location of the yacht as illustrated in Figure 4.1. The actual property distribution is more accurately represented if the number of beam elements is increased. Mathematically, the properties of a beam element are contained in a so-called 'stiffness matrix'. The type of properties and the size of the stiffness matrix are dependent on the beam theory from which the stiffness matrix is derived and in what directions the beam is allowed to move which are called the degrees of freedom of an element. Note that the term 1D beam element refers to the apparent geometry of an element, which is a line (1D), but each element has twelve degrees of freedom, six at each node, that allow the element to move in three-dimensional space as seen in Figure 4.2. In this study the stiffness matrix of the beam elements is derived from the Timoshenko beam theory (see Section 2.5.2) that incorporates transverse shear deformation, which is generally applicable for 'thick' beams with a length over height ratio $L/h < 10$ [51]. In the literature study in Section 2.5 it was demonstrated that shear deformations are significant for passenger ships and because the length of height ratio of the hull of Feadship yachts ranges from $L/h \approx 8-12$, shear deformation might be of importance for the global and local deformations that are of interest in this chapter. In Section 4.4 a check is performed to see whether these shear deformations indeed result in a different structural response or that a more simple beam theory, such as the Euler-Bernoulli beam theory is sufficient.

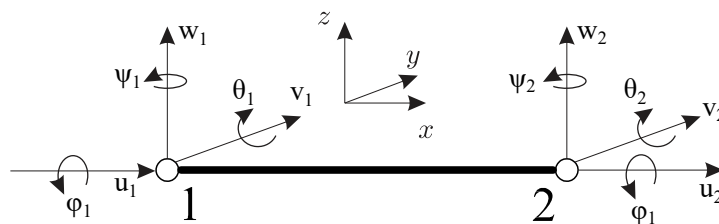


Figure 4.2: A 1D beam element with twelve degrees of freedom, six at each node.

In Appendix A, the stiffness matrix, element loading vector and directions can be found that are used in the beam model. The actual yacht structure is non-prismatic, which means that it has a variable cross-section and that neutral axis is not a straight line. In this beam model, the neutral axis is assumed to be a straight line across the length of the beam. According to Balduzzi et al. [3], this is a common practice by researchers and practitioners for modelling simplicity.

The element loading in the beam model is completely decoupled by assuming that the axial load is applied at the neutral point of the cross-section to decouple the axial and bending deformations, the moments are taken

along the principle axis to decouple the bending deformations themselves (i.e. M_y only causes displacement w_z and rotation θ_y and M_z only causes displacement w_z and rotation θ_z) and the shear forces are applied at the shear centre to decouple the flexural and torsional deformations. The moment distributions that are applied to the yacht are translated to a distributed load that is applied to each element.

Only St. Venant (or *homogeneous*) torsion is taken into account, since predictions using only St. Venant torsion are sufficiently accurate for hull sections that mainly consists of closed cross-sections or cellular parts, which is normally the case for Feadships [76]. Also, if the cross-section consists of combined open and closed cells, the major torsional stiffness and consequently rotation comes from the closed-cells [47]. The properties that define the behaviour of the Timoshenko 1D beam element which are stored in the element stiffness matrix of the element are given in Table 4.1.

Table 4.1: The stiffness matrix properties of a 1D Timoshenko beam element with twelve degrees of freedom.

Name	Symbol
Young's modulus	E
Shear modulus	G
Element length	l
Area	A
Shear areas	A_y, A_z
Principle moments of inertia	I_{yy}, I_{zz}
Torsional constant	J

For the most part, the cross-sectional properties are available for Feadships for the hull, because those properties are used for the longitudinal strength assessment required for certification of the yacht, for which only the longitudinal strength of the hull is regarded. The properties are obtained by manually entering ≈ 10 cross-sections in software provided by classification societies, e.g. Special Service Craft SSC software [43] provided by Lloyds Register, that aids the design and simultaneously checks for rule compliance. Only longitudinal strength is assessed in this software, hence all parameters in Table 4.1 are calculated except for the horizontal shear area (A_z) and the torsional constant (J). The latter is especially of importance, since the torque is desirable to analyse in the scope of this thesis. Therefore, a different approach is adopted to determine these properties, which is described in Section 4.3. The new approach also calculates the other properties that are already available and can therefore be used to compare with the results from the SSC software.

4.2. Beam model verification

The beam model is made in the Python programming language and to check whether the routine is implemented correctly, a verification study is performed by comparison with a beam consisting of 1D beam elements with the exact same properties and loading conditions in Siemens NX 11 [65].

It is highly inconvenient to incorporate varying cross-sectional properties of 1D beam elements in Siemens NX, because only linearly tapered properties can be used, which is also one of the reasons for development of a FE code instead of using NX directly. For this reason, the beam is modelled with constant cross-sectional properties along its length, which are given in Table 4.2 and are chosen approximately in order of magnitude as known for Feadships.

Table 4.2: Constant cross-sectional properties for the beam model verification study.

Property	Magnitude	Unit
E	200	GPa
G	79.0	GPa
I_{yy}	6.70	m ⁴
I_{zz}	11.0	m ⁴
A	0.60	m ²
$A_z = A_y$	0.45	m ²
J	10.6	m ⁴

As loading condition, the approximated load distribution for the hogging load case $P_{hog}(x)$ in Eq. (4.1) as defined by Lloyd's Register is adopted, which is normally applied to full 3D FE models [42]. This load distribution approximates the load case of a yacht and it is in equilibrium, which means that the reaction forces at

the boundary conditions should converge to zero with increasing number of elements. For the latter reason, this load distribution is also in the x-, and y-direction and as a distributed torsional load for the purpose of code verification, not to demonstrate actual structural response behaviour of a yacht. The definition of the coefficient M_w in Eq. (4.1) can be found in the Rules and Regulations for the Classification of Special Service Craft [41], the coefficients a_i are given in the SDA for Primary Structure of Passenger Ships [42] and x is defined as a percentage of the (rule) length of the yacht.

$$P_{hog}(x) = \frac{M_w}{L^2} (20a_1x^3 + 12a_2x^2 + 6a_3x + 2a_4) \quad (4.1)$$

A perfect agreement is observed for all displacements and rotations for the converged models (in both cases for a number of elements $n = 500$), in Figure 4.3 the vertical displacement and corresponding nodal rotations are given as example, all other degrees of freedom show the same exact agreement, hence the beam model is implemented correctly in Python.

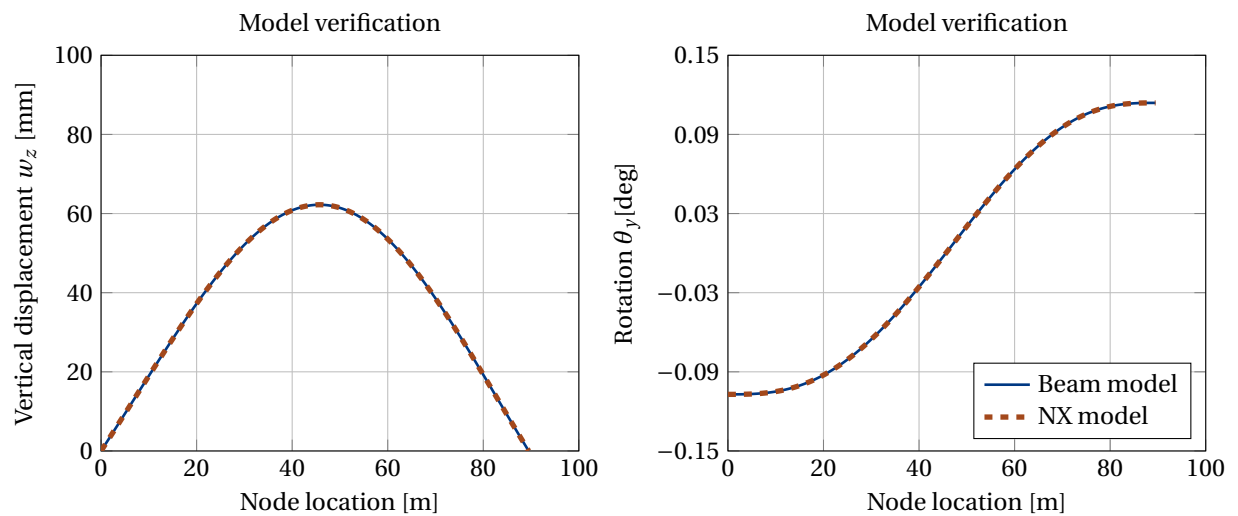


Figure 4.3: Verification of the beam model with an NX beam model with 1D beam elements for the vertical displacement and rotation, number of elements $n = 500$.

4.3. Property determination

The 1D beam model requires a cross-sectional property distribution of some parameters for which no analysis method is available at Feadship. Most are available, though, and currently calculated by the Special Service Craft (SSC) software provided by Lloyd's Register. A new method is proposed in this section and the properties determined by the SSC software are used as a reference to indicate the accuracy of the new method. The geometry information that is used as input in SSC, originates from 3D models created in Siemens NX 11. It is also possible, to obtain cross-sectional information 'directly' in Siemens NX from the 3D models by creating a cross-sectional outline of a cross-section as seen in Figure 4.4. This is possible if the model is a solid, which is generally not the case. Instead, shell models are used with colours (or comparable indicators) indicating the thickness. The generation of cross-section outlines can still be done by thickening of the shells with the thickening in such a way that the created solids of the individual components overlap each other. Normally, this means that the shells should be extruded to both sides, which is not entirely accurate, since the shell positioning of the structural components takes into account a certain thickening direction, which is either outward or inward. Nevertheless, thickening to both sides is assumed to influence the cross-sectional properties by a negligible magnitude, because the parts are shifted only one or two millimetres with respect to the neutral axis of the cross-section in contrast to the global dimensions which are in meters. Once the overlapping solids are created, cross-sections can be made such as given in Figure 4.4.

This cross-sectional outline can be used as an input for a user defined 1D beam element section that can be used in Finite Element Analysis (FEA) in Siemens NX. For standard cross-sections, hard-coded equations are used to determine the properties, but for arbitrary cross-sections, such as seen in Figure 4.4, numerical mesh-based methods are used (the Pilkey method [57]). The new method for determination of the cross-

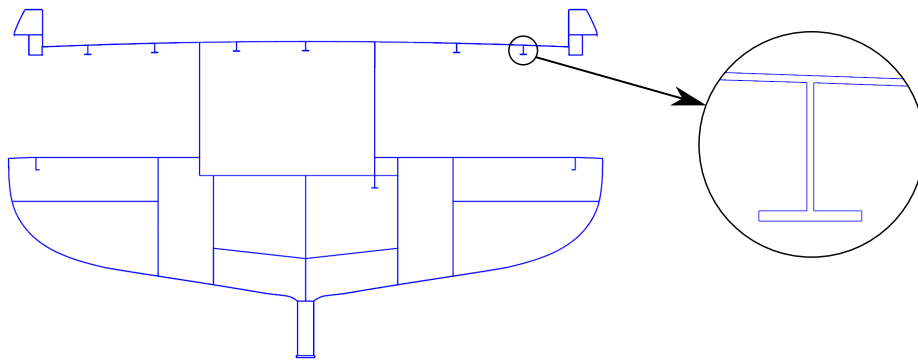


Figure 4.4: A cross-section obtained from a 3D model in Siemens NX with thickened shells to create overlapping solids.

sectional properties using NX is referred to as the 'NX section method' from now on. A performance test for standard cross-sections of the properties that are determined by this approach can be found in Appendix B. The sampling of the cross-sections of the yacht NX model is chosen at locations where rapid cross-sectional property changes are seen, such as at cut-outs or at additional decks. Also, structurally inefficient parts, e.g. of a longitudinal bulkhead, are left out of the cross-section and regarded as 'shadow areas' as described by Jensen [33].

For the comparison of the beam model with a 3D FE model, the same test case yacht as mentioned in Section 3.1 is taken, for which the cross-sectional properties are taken from the SSC software and calculated with the NX section method. In case of different materials (e.g. a steel hull with aluminium decks), the thickness of the geometry is adjusted according to the ratio of the stiffness's of the different materials (referred to in literature as the 'transformed-section' method [24]). A comparison of the properties of both the SSC and the NX section method is performed to check if the properties are similar in magnitude. The SSC software is meant for the longitudinal strength assessment, which is governed by the vertical moment of inertia I_{yy} and shear area in upward direction A_z . This means that the structural parts influencing these parameters are chosen with the most care and these calculated parameters can hence be considered to be the most accurate and close to reality (i.e. the horizontal moment of inertia I_{zz} is calculated, but structural parts that only or mostly influence this parameter and not the vertical moment of inertia, are not used as input in SSC, hence these results are less conform reality). A comparison of two cross-sectional property parameters are given in Figure 4.5.

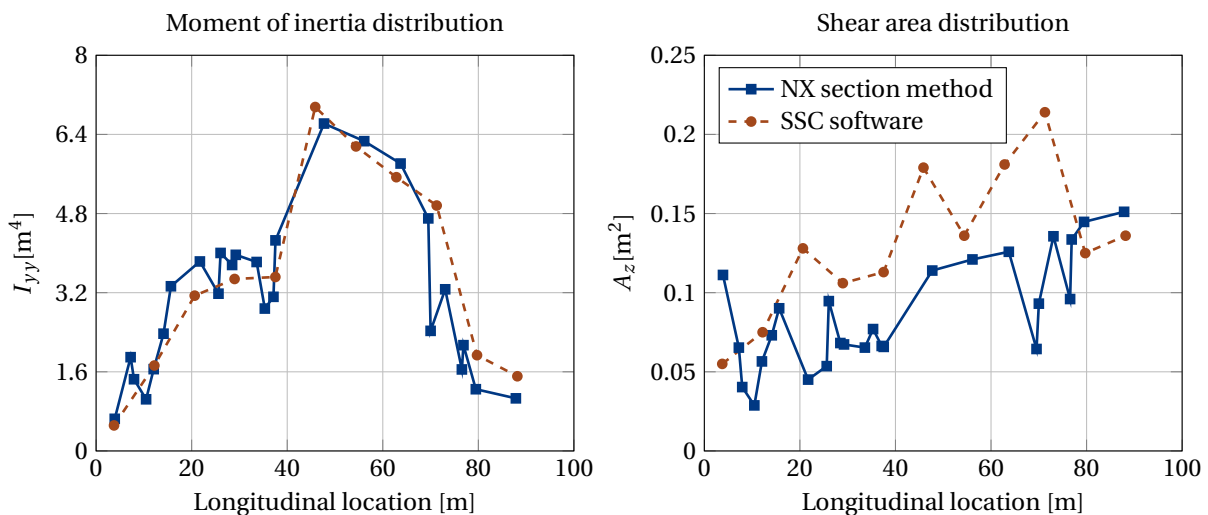


Figure 4.5: Comparison of the moment of inertia I_{yy} and shear area A_z distribution determined by the NX section method and by the SSC software values.

A good agreement is observed for the vertical moment of inertia, however, small deviations exist for multiple reasons: First, in the NX section method, secondary stiffeners are not taken into account, since experience

shows that they have a small contribution to the the global response. Second, more details are kept in the NX section method, while the geometry in SSC is simplified. Thirdly, in SSC only structural elements that contribute to the longitudinal strength are taken into account, while the NX section method can take into account more local elements that contribute only over a few meters, because the cross-sections are sampled more frequently. This more frequent sampling also explains the peaks at some locations where the structure has openings or other weakening of the structure. The shear area is for the most part higher for the SSC method, effectively resulting in a larger stiffness to shear deformations and hence a stiffer hull girder. In contrast with the moment of inertia determination, which is rather straightforward and common, the shear area determination is more arbitrary and can be performed in multiple ways. In SSC, the projected area of the structure to the respective axis (z -axis for A_z) is taken, as explained in Section 2.5.3, which is considered the most conservative method for ship hulls as indicated by Jensen [32] and therefore results in a higher shear area.

The result for the torsional constant J distribution can be seen in Figure 4.6, it is not possible to compare this, since it is not calculated by SSC and no other means of torsional stiffness parameter definitions is used possible at Feadship.

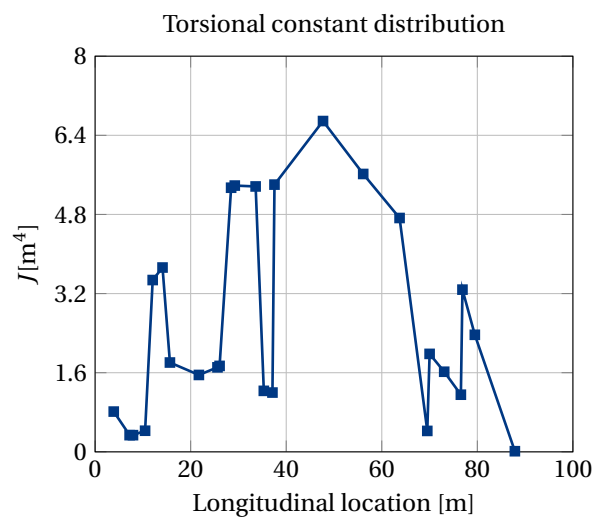


Figure 4.6: Torsional constant J distribution determined by the NX section method.

The cross-section corresponding to the relatively low torsion constant plateau in Figure 4.6 at a location of 15-25 m is given in Figure 4.4. The openings at the port side and starboard side effectively reduce the size of the largest closed-cell of the cross-section, reducing the torsional constant.

The horizontal moment of inertia is shows slightly more deviating results from the SSC values, but as mentioned before, these are not determined conform the actual present structure and the nature of these deviations can lie in either of the methods. Also, it will be demonstrated in Section 4.4 that horizontal bending response is not (the most) relevant to look at, hence these deviations in horizontal moment of inertia are not relevant in the scope of this thesis.

4.4. Global response

In Section 4.1, the finite element 1D beam model was introduced with the six degrees of freedom at each node. These degrees of freedom are the six deformation components of the neutral axis of the hull girder beam, which was assumed to be a straight line. This straight line deforms in three-dimensional space with the three deformations stored in the deformation component vector \mathbf{w} given in Eq. (4.2) and the rotations of the nodes that correspond to these displacements are stored in the rotation component vector $\boldsymbol{\theta}$ given in Eq. (4.3).

$$\mathbf{w} = \begin{bmatrix} w_x \\ w_y \\ w_z \end{bmatrix} \quad (4.2)$$

$$\boldsymbol{\theta} = \begin{bmatrix} \theta_x \\ \theta_y \\ \theta_z \end{bmatrix} \quad (4.3)$$

The deformation and rotation component vectors in Eq. (4.2) and Eq. (4.3) are called the global response of the beam model. In Figure 4.7 these individual components are visualized.

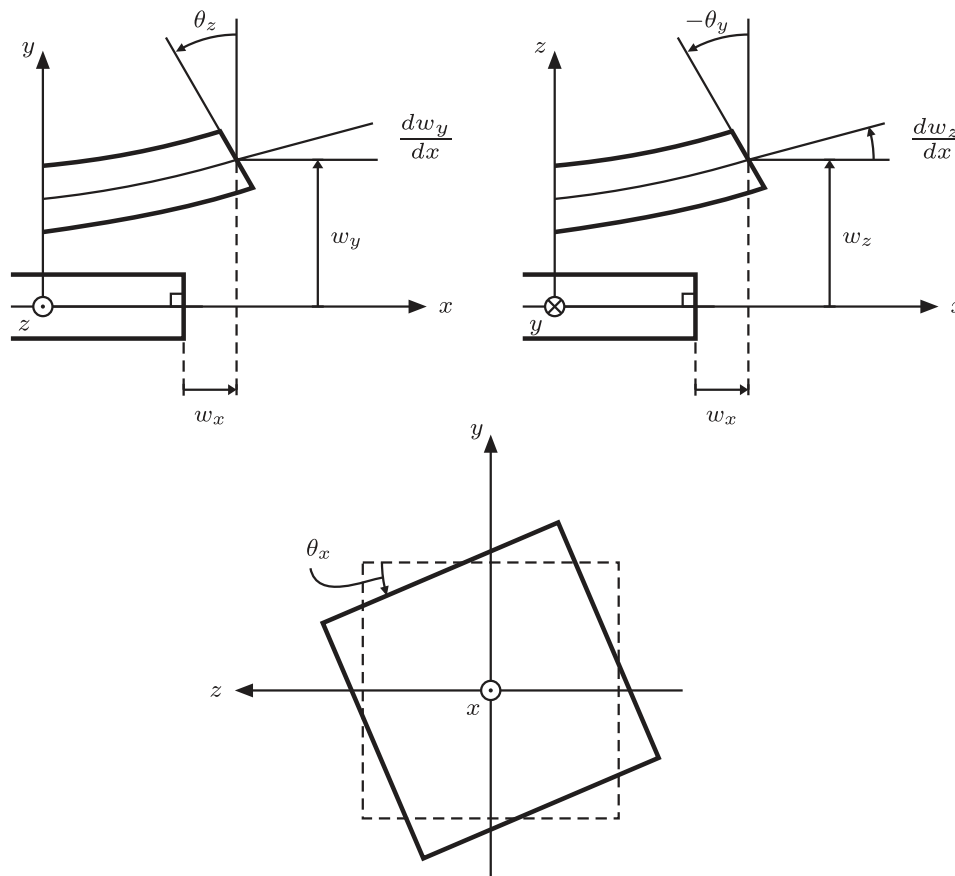


Figure 4.7: Deformation components in beam theory. [1]

Indicated in Figure 4.7 are the horizontal bending (top left), vertical bending (top right) and torsion (bottom). The bending components indicate the deformation of the neutral axis of the beam and the rotation components define the rotation of a cross-section of the beam. In the classical beam theory, which is used in this work as mentioned in Section 2.5, the main assumption is that the cross-section of the beam translates and rotates at coordinate x as a rigid body (i.e. it keeps its shape during deformation). Also, only linear beam theory is used, which means that the displacement components w_x , w_y and w_z are small compared to the beam length and that all rotation components θ_x , θ_y and θ_z are also small, which means that the small angles approximation in Eq. (4.4) holds.

$$\sin\theta \approx \tan\theta \approx \theta \quad (4.4)$$

The global deformation components at each node are compared to the response of a complete detailed 3D FE model of the test case yacht to draw conclusions on the accuracy of the beam model global response and the available information in the preliminary design. The loads applied to the beam model are decoupled, hence the validation can be performed by regarding the loads acting in the six degrees of freedom separately. The load cases that are used are discussed in Section 4.4.1.

4.4.1. Load cases

Classification societies provide load cases for strength assessment of ships that are commonly used and thoroughly validated for a wide range of ships and sea states. Therefore, using these rules design loads is good

method to use as load cases for the validation of the beam model.

First, the total vertical bending moment is considered, which is the sum of the the Still Water Bending Moment (SWBM) and the vertical Wave Bending Moment (WBM), see Eq. (2.1). The SWBM depends on the loading condition of the yacht, e.g. full/empty fuel tanks or amount of fresh water on board. In this study, one constant loading condition (half loaded) is chosen, as the variation in magnitude affects the beam model and the 3D FE model to the same extent. The WBM is taken as the hogging and sagging rule wave bending moments for hull girder strength assessment of passenger ships as provided by Lloyds Register [41], for which the hogging equation was given in Eq. (4.1). In Figure 4.8 the SWBM and the WBM for the hogging load case are given. The sagging load distribution is slightly larger in magnitude, but is opposite in sign with respect to the hogging bending moment. Also, it is a linear Finite Element Analysis (FEA) with linear material properties in tension and compression, thus the performance is not affected by the sign of the load. The global response validation results are given for the hogging state of the hull girder for the remainder of this chapter as the sagging state showed similar results.

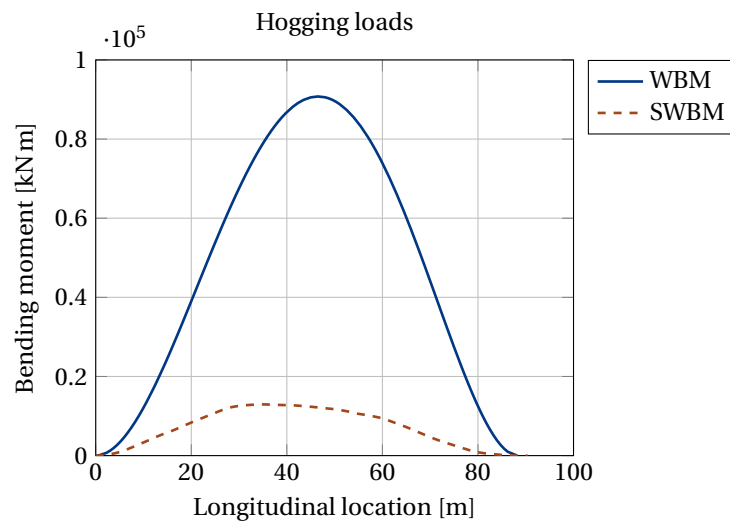


Figure 4.8: The bending moments for the hogging validation load case.

For the horizontal bending moment, strength assessment is normally *not* performed at Feadship and Lloyds does not provide any load distribution for the horizontal loads as it is not deemed relevant for yachts. This suggests that horizontal deformations might also be insignificant in operating conditions, however with the increasing size of yachts, this might become relevant in the future. Therefore, the possibility of analysing the horizontal loads is kept implemented in the beam model and an estimation is made for the horizontal loads from literature. In Section 3.3.3 the horizontal bending peaks were mentioned to be approximately 40% of the vertical ones, while Soares and Garbatov [67] showed that the average ratio of the total vertical hogging bending moment and horizontal bending moment $VBM/HBM \approx 30\%$ for a container ship. It is expected that the horizontal loads Feadships encounter are more conform the latter magnitude and therefore the horizontal bending is taken as 30% of the hogging validation loads as given in Figure 4.8 for the validation study.

Similar to the horizontal bending moment, the torsion is *not* regarded for strength assessment at Feadship and Lloyds Register provides no torsional load cases. A similar ratio as for the horizontal bending moment is not found in literature and therefore the wave torque load case is adopted from a different classification society: Bureau Veritas. The NR 600 regulations [7] cover the definition of the test case yacht in this work: a non cargo ship less than 90 m, however they do not provide a rule torque load distribution, just like Lloyds Register. Therefore the more general regulations of Bureau Veritas for the design of steel ships [8] is used, which gives a rule torque distribution for the test case yacht that is given in Figure 4.9.

The vertical, horizontal bending and the torque cover five degrees of freedom of the beam model, the remaining degree of freedom is the in-plane normal force. More than thousand kN of force is required to compress a normal yacht hull even a millimetre, hence this is not deemed important for this study.

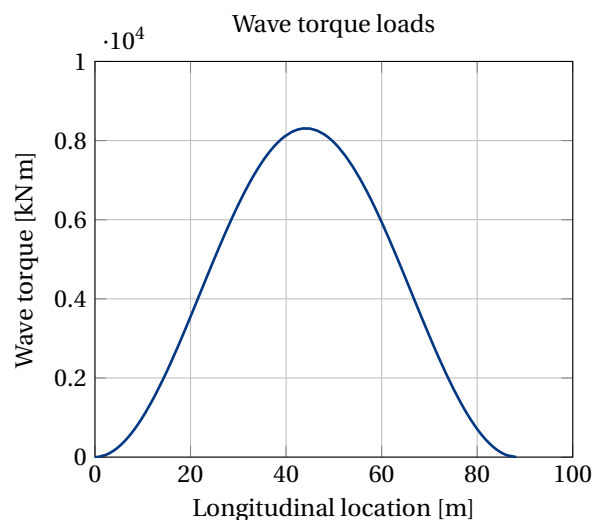


Figure 4.9: The torque load distribution for the torsion validation load case.

4.4.2. 3D FE model description

The detailed 3D FE model that is used for comparison of the beam model response is created for the structural design assessment for certification. This model normally includes a superstructure, which is omitted for comparison as mentioned in Section 4.1.

The model consists of 2D shell elements for the decks, hull plating and bulkheads and 1D beam elements for the primary and secondary stiffeners. The load application is performed by discrete forces and/or moments on multi-point constrained 'spider' or RBE3 elements that distribute the applied loads over nodes at locations of the transverse frames/bulkheads below the waterline as specified by Lloyds [40]. More information on how the elements distribute the loads and moments can be found in the Siemens Element Reference Library [64]. The internal load distributions as specified in Section 4.4.1 are obtained in the structure with this load application method, which is illustrated in Figure 4.10 for the hogging load case.

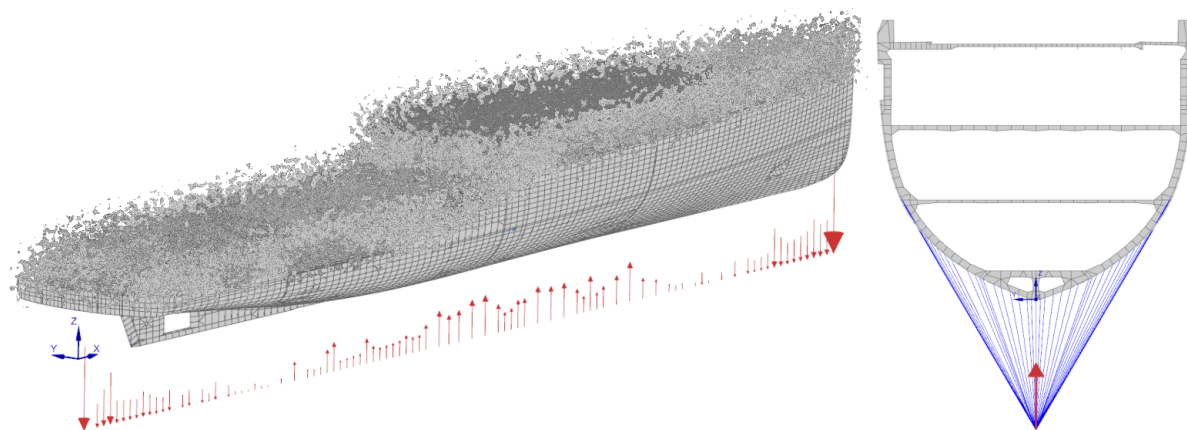


Figure 4.10: The load application by discrete forces and the distribution over nodes with a RBE3 spider element.

The desired internal bending moment load distribution is in equilibrium, but by discrete approximation of this distribution, the actual achieved internal bending moment distribution is not exactly the same as desired distribution and can be slightly off from the equilibrium situation. This could cause (large) reaction forces at the boundary conditions. This is solved by distributing the difference in load over the first and the last RBE3 element location such that there is shear force *and* moment equilibrium ¹.

The boundary conditions of the model are to prevent rigid body motion and there should be zero reaction forces (or a negligible magnitude compared to the total applied load), because the loads are in equilibrium.

¹Only applicable if the load difference is not too large, otherwise an unrealistic local response can be expected.

The location of the boundary conditions is indicated in Figure 4.11 and the same longitudinal locations are adopted for the 1D beam model.

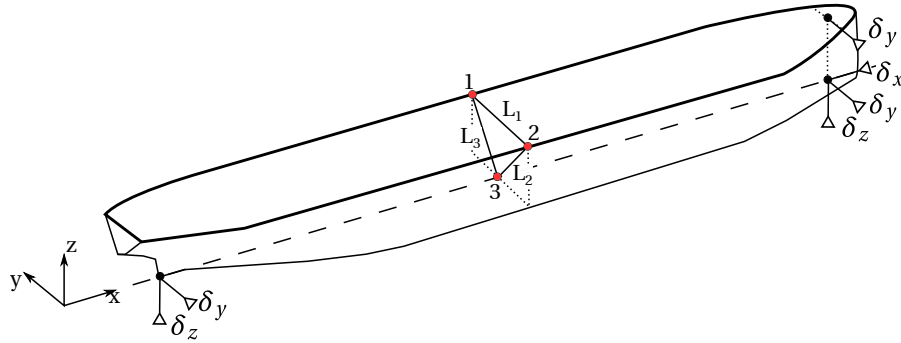


Figure 4.11: The boundary conditions δ applied to the detailed 3D FE model to prevent rigid body motion and cross-section corner nodes for response comparison.

For the 1D beam model, the nodal displacements and rotations can be directly used for comparison, but for the 3D FE model picking nodes on a cross-section for comparison is highly sensitive to the location and therefore can not be selected at random. Instead, the deflections are taken for the corner nodes of a cross-section and the rotation of the plane that goes through these nodes (points 1, 2 and 3 in Figure 4.11). Additionally, for the rotation around the longitudinal axis θ_x , the rotation of the triangle that is formed by connecting these points is calculated. This is only possible if the cross-section does not deform too much, which is true if the distances L_1 - L_3 are approximately equal before and after deformation. The maximum observed deviation in length is <0.5 mm, thus this assumption is reasonable. In the global response comparison in Section 4.4.3 the rotation of all three distances L_1 - L_3 are used to check if the deviations are not too large.

4.4.3. Validation results and discussion

The loads given in Section 4.4.1 are applied to 3D FE model as described in Section 4.4.2 and to the 1D beam model and the global response results are compared to validate the beam model. In Figure 4.12, the bending response for both vertical and horizontal bending is compared with the 1D beam model properties determined by the NX section method.

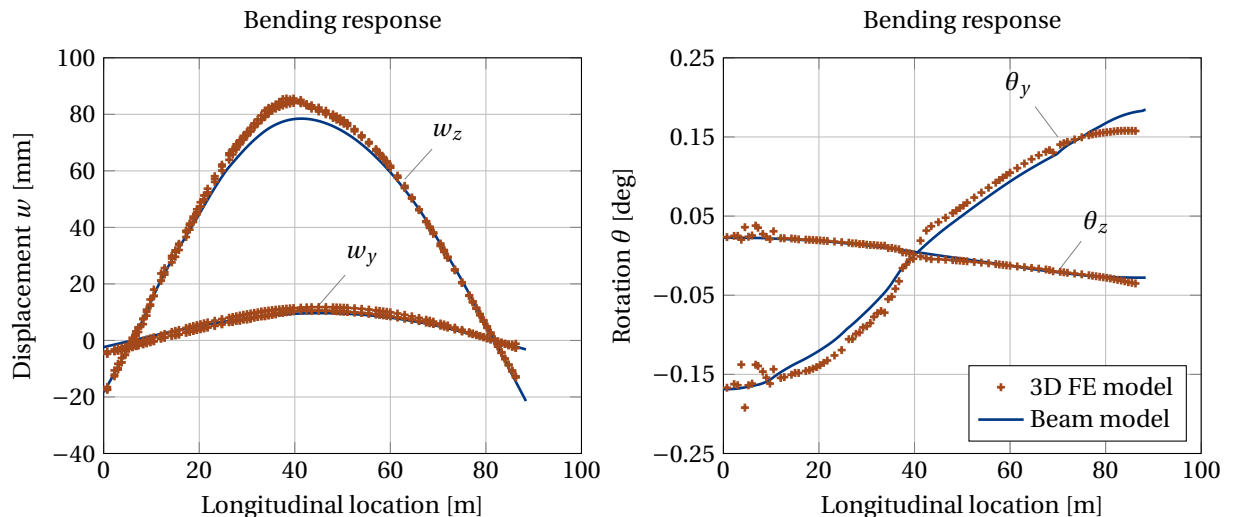


Figure 4.12: Bending response comparison of the 1D beam model with a full 3D FE model for the vertical and horizontal displacements and corresponding rotations.

A good agreement for the displacements and rotations is observed for both the vertical and horizontal bending response. The slightly larger rotation θ_y at the front extremity can be attributed to the smaller moment of inertia I_{yy} determined by the NX section method, as seen in Figure 4.5. The vertical bending displacements

and rotations are much larger than the horizontal response, which is expected, since the vertical bending moment is the most important hull girder load component [52]. The maximum horizontal displacement is low, only 14% of the maximum vertical displacement for this extreme load case for strength assessment and since load cases in operating conditions are expected to be much lower, the horizontal bending response is considered to be subordinate with respect to the vertical bending response in relation to structural deformations that cause creaking noises. In Chapter 3 the wave-induced load distribution for the horizontal bending moment had a peak magnitude of 40% of the vertical bending moment, larger than the 30% assumed used for this validation, however, this will still result in small global response.

The last global response is the torsion response, for which the comparison can be seen in Figure 4.13.

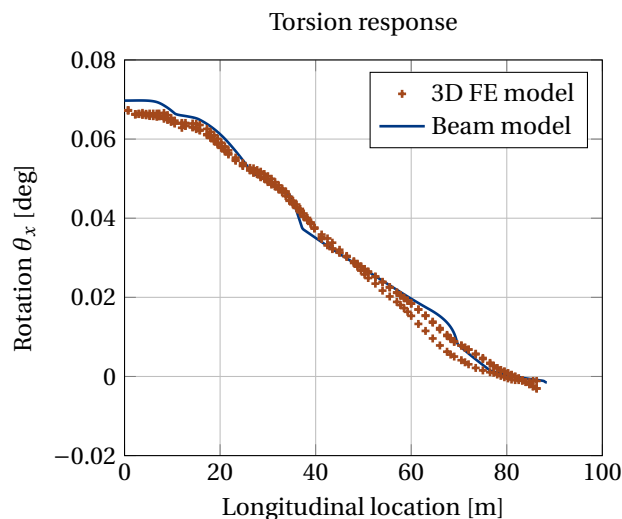


Figure 4.13: The torsion response comparison of the beam model with the full 3D FE model for the longitudinal rotation of the cross-section.

Again a good agreement is observed. This means that the rotation of the cross-section due to torsional loads is mainly caused by St. Venant torsion (or homogeneous torsion), since the beam model only includes the torsional constant for St. Venant torsion. This is also expected, since the yacht hull normally consists of closed cross-sections, for which the St. Venant torsional stiffness is dominant [33]. The magnitude of the angle of rotation is relatively small, which is in-line with the fact that torsional strength assessment is normally insignificant for yachts below 75 meters [42]. The test case yacht is larger, but it is not expected that the rotation increases significantly compared to a 75 m yacht. This small rotation can still result in relative movements of room corners in the order of millimetres, thus, it might be relevant to include the torsional response for the local deformations. The kinks in the beam model results in Figure 4.13 can be related to the locations where a sudden in-, or decrease is seen in the torsional constant in Figure 4.6. In the 3D FE model, these transitions are more gradual, since the stress field flows around the sudden openings that cause the torsional constant to decrease.

It is interesting to perform the same analysis for the properties determined by the SSC software to see if the accuracy increases or decreases with the NX section method. In Figure 4.14 the results of this comparison can be seen.

It can be seen that by using the properties determined by the SSC software, less agreement is obtained with the 3D FE model results. The difference in results can, to the largest extent, be attributed to the different shear area that is calculated by the methods. This was found performing multiple analyses using the NX section method properties and substituting only one of the property parameters determined by the SSC software in each analysis. It was found that none of the parameters showed a (significant) deviation in response, except for the shear area, for which the displacement curve is also given in Figure 4.14. The difference in shear area calculated by the two methods was already indicated in Figure 4.5. The NX section method thus results in a better agreement and if the SSC properties are used for the vertical bending response it should be taken into account the actual response is larger due to shear deformations since the vertical shear area is determined too conservative.

In the derivation of the stiffness matrices for the beam model elements, the Timoshenko beam theory is used, which includes the shear deformations. In Figure 4.15, it can be seen that if these shear deformations

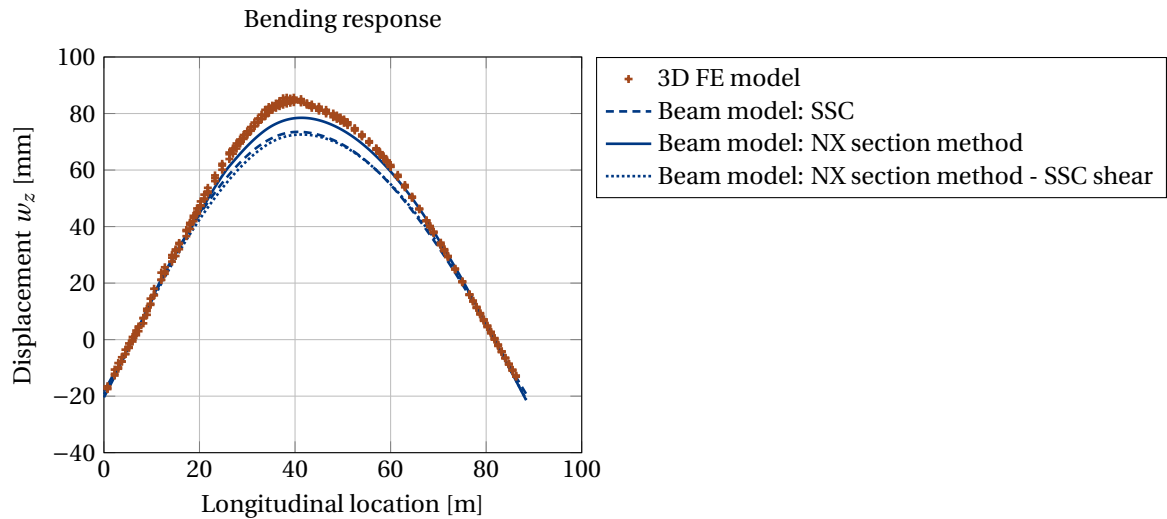


Figure 4.14: Influence of the property determination method

are excluded (which is done by letting the shear stiffness approach infinity, see Section 2.5.2), the maximum displacements decreases by 20% and the yacht hull appears stiffer. This is a rather significant amount, which was already demonstrated in Section 2.5 for a passenger ship of 160 m, hence for more accurate results the shear deformations should be taken into account for the yacht hull modelled as an 1D beam.

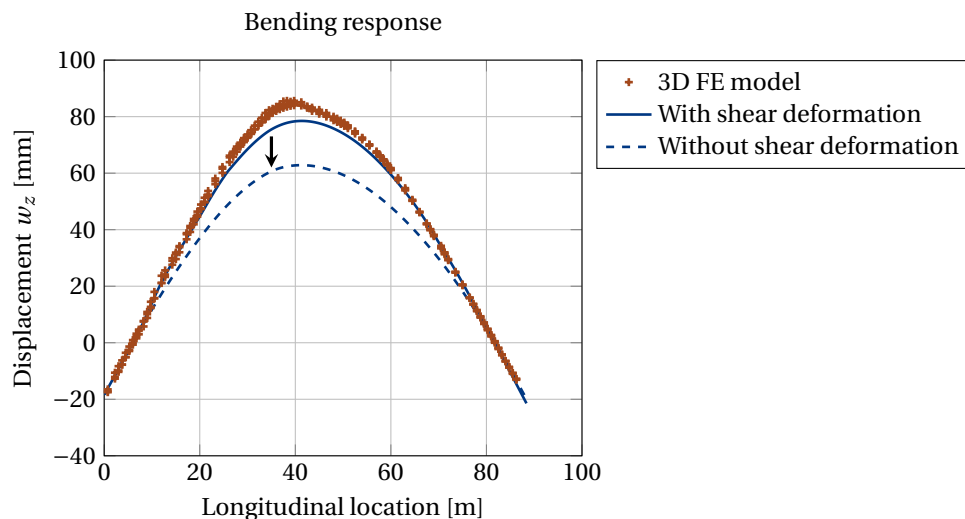


Figure 4.15: Influence of the shear deformations on the bending displacement.

Worth noting is that this analysis only regards the shear area of the structure that is present. Locations that have large cut-outs in the hull (e.g. windows) and where there is no connection between decks for a cross-section also result in the relative movement of the upper deck with respect to the lower deck (this is not the case in the cross-section of Figure 4.4, since there is still a connection to the upper deck). Effectively, the shear stiffness in between the deck is locally small or not present, this effect is not taken into account by regarding the hull as a one beam as discussed in Section 2.5.

4.5. Local response

The global response is a measure of the overall stiffness of the hull, but it does not give a detailed insight in the local deformation of the structure that can directly result in the problems mentioned in Chapter 1 that should be minimised to improve the (perceived) comfort level on board of Feadships. In this section an attempt is made to extract local deformation components from the global response using the displacement field provide

by linear beam theory. This simplified approach is not suitable to take into account local stress fields caused by structural elements or discontinuities, since it is derived from a global response. It can, however, provide initial estimates on the magnitude of required clearances or it can indicate risks with regard to excessive deflections.

The linear beam theory from which the beam elements are derived provides a displacement field for bending and torsion that describes a point on the beam in three dimensions as seen in Eq. (4.5) [5]. In Figure 4.7 this is any point on the rotated cross-section with the coordinates given with reference to the neutral point on that cross-section.

$$\mathbf{u}(x, y, z) = \begin{Bmatrix} u_x(x, y, z) \\ u_y(x, y, z) \\ u_z(x, y, z) \end{Bmatrix} = \begin{Bmatrix} w_x(x) + z\theta_y(x) - y\theta_z(x) + \omega(y, z) \frac{d\theta_x}{dx} \\ w_y(x) - z\theta_x(x) \\ w_z(x) + y\theta_x(x) \end{Bmatrix} \quad (4.5)$$

As mentioned before, the in-plane loads, causing deformation $w_x(x)$ are not taken into account, hence it can be left out Eq. (4.5). Also, an applied torque causes the non-planar displacement in the x-axis called the warping displacement $\omega(y, z) \frac{d\theta_x}{dx}$. From the 3D FE model it is found that these displacements are insignificant with respect to the displacements caused by the bending components. For model simplicity it is therefore decided to omit the warping displacements due to torsion from the analysis. The displacement field is then simplified from Eq. (4.5) to the displacement field in Eq. (4.6).

$$\mathbf{u}(x, y, z) = \begin{Bmatrix} u_x(x, y, z) \\ u_y(x, y, z) \\ u_z(x, y, z) \end{Bmatrix} = \begin{Bmatrix} z\theta_y(x) - y\theta_z(x) \\ w_y(x) - z\theta_x(x) \\ w_z(x) + y\theta_x(x) \end{Bmatrix} \quad (4.6)$$

The deformed coordinates of a point on a cross-section of the beam can thus be described if the displacement and rotation components in Eq. (4.2) and Eq. (4.3) are known at beam coordinate x . In Section 4.4 it is shown that these components can be calculated with good accuracy. For the local deformation analysis, the vertical bending response and the torsional response are treated separately and are discussed in Section 4.5.1 and Section 4.5.2, respectively. The horizontal bending response is omitted from now on, due to its small global response, however if analysis is required for future yachts, the approach is similar to that of the vertical bending response.

4.5.1. Vertical bending response

The vertical bending response happens in the xz -plane of the beam and it is treated separately from the torsion response. Therefore, the displacement field in Eq. (4.5) is simplified to Eq. (4.7).

$$\mathbf{u}(x, z) = \begin{Bmatrix} u_x(x, z) \\ u_z(x) \end{Bmatrix} = \begin{Bmatrix} z\theta_y(x) \\ w_z(x) \end{Bmatrix} \quad (4.7)$$

In relation to stiffness problems that possibly can occur such as creaking of interior, the local deformations in a specific room are sought after. In Figure 4.16 a room contour ABCD on an undeformed beam that represents the yacht hull can be seen. The z -coordinate of the points are given with respect to the neutral points on the corresponding cross-section. For each room with length ΔL the height of the neutral axis is taken constant as the average vertical height of the neutral axis in that section. After deformation, the deformed room coordinates are A'B'C'D', which can be calculated according to the displacement field in Eq. (4.7).

Not only the corners of the room can be calculated with Eq. (4.7), but the whole deformed room contour. A complete deformation profile is then obtained for a room, from which clearances or solutions can be sought for flexible connections of interior that allow for the deformations. In Figure 4.17 a deformed room contour is seen with the sampling of a discrete number of data points.

Several properties of the deformed room can be used, depending on the purpose of the room and the installed interior or technical systems. The expansion of the floor and/or ceiling Δx can be determined, as well as the magnitude of the bulging Δz . The deformed room coordinates are calculated in the global reference system, hence to determine the local components coordinates first all coordinates are calculated w.r.t. a reference point (i.e. the coordinates of the reference point are subtracted from the global coordinates). The deformation components Δx and Δz can be more easily extracted from the data if the cross-section is rotated by angle θ as seen in Figure 4.17. This can be done by multiplying all deformed room contour coordinates x and z with the rotation matrix in Eq. (4.8) to get the rotated coordinates x' and z' .

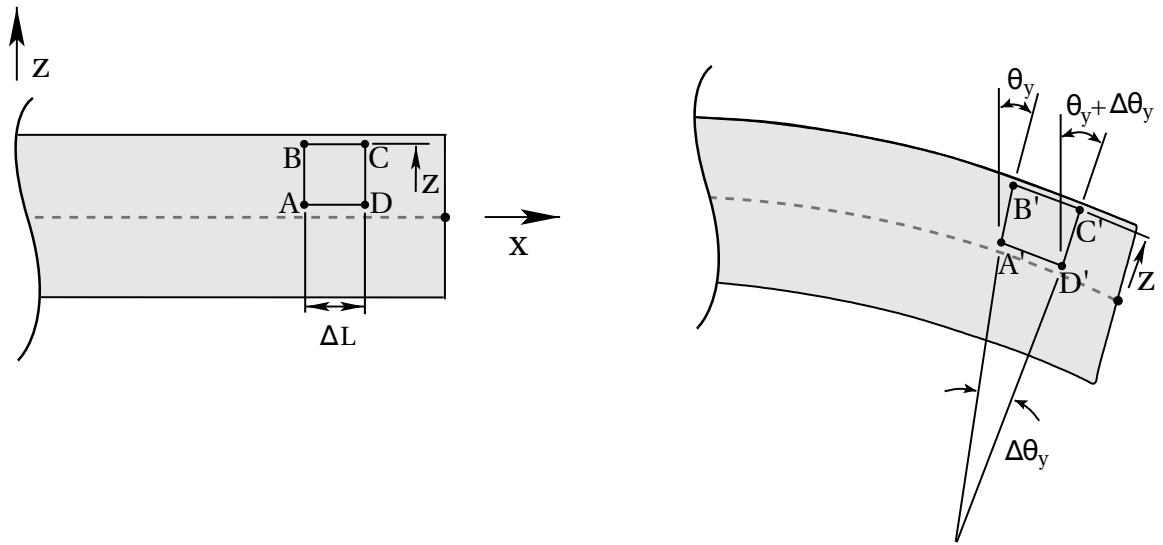


Figure 4.16: Room contour ABCD and A'B'C'D' on an undeformed and deformed beam, respectively. Modified from [5].

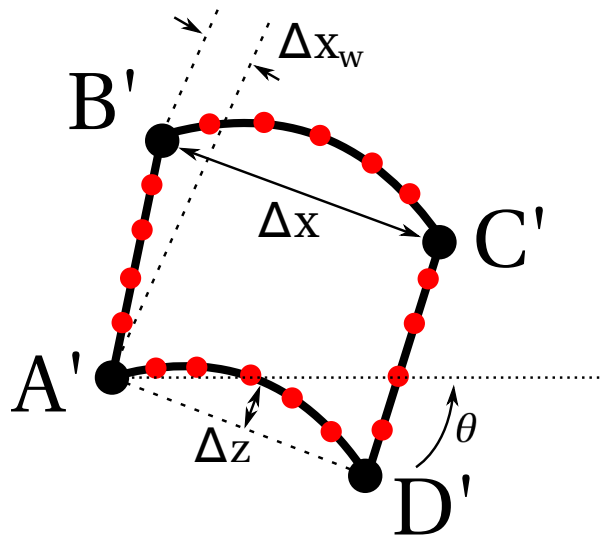


Figure 4.17: The deformed room contour A'B'C'D' sampled by discrete data points. Indicated are possible deformation properties.

$$\begin{bmatrix} x' \\ z' \end{bmatrix} = \begin{bmatrix} \cos\theta & -\sin\theta \\ \sin\theta & \cos\theta \end{bmatrix} \begin{bmatrix} x \\ z \end{bmatrix} \quad (4.8)$$

Visual inspection of the 3D FE model showed that locally the rotation of the walls is not equal to the rotation of the cross-section θ_y . This is especially true for locations where large differences exist between the amount of vertical connections in a cross-section between decks. This variation is not incorporated in the beam model as only one average shear stiffness (or actually shear area A_z) for the whole cross-section is used. For example, for the cross-section in Figure 4.4 there is less material to transfer shear forces to the upper deck compared to the amount of material that connects the lower decks. This means that the vertical walls connecting the decks have a rotation that is schematically indicated in Figure 4.18 and the walls between the lower decks have a different sign of rotation as the upper wall.

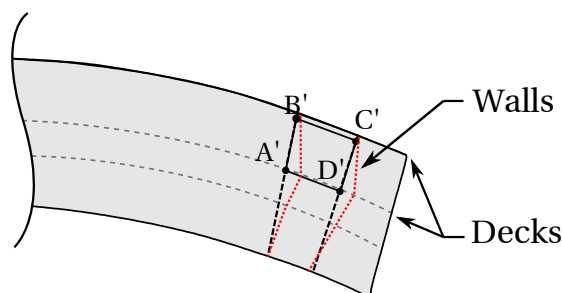


Figure 4.18: Schematic view of the observed wall rotations in the 3D FE model as compared to the assumed constant rigid rotation of a cross-section.

This shows that the assumption of a rigid rotation of a cross-section is not valid at locations where locally (in between decks) relatively less material is present to transfer the shear forces and the local rotation of the walls can not be determined accurately. Thus, also the deformation component Δx_w in Figure 4.17 can not be determined. However, the effect shown in Figure 4.18 is also present at a (not too large) longitudinal distance away from the cross-section, thus from wall A'B' to wall C'D'. This means that for the horizontal structural parts (decks) the coordinates in the global reference system are different, but the relative deformed properties Δx and Δz are still expected to agree with the 3D FE model.

The same 3D FE model used for the global response is used as comparison for the local response. Longitudinal sections are taken with a length of $\Delta L = 10$ m, to indicate the variation of the local deformations along the length of the yacht. Ideally for a good comparison, one horizontal line across the whole length is taken, however, due to the variation in geometry and an unstructured mesh this is not possible. The closest structural feature for this criteria is the main deck at the middle nodes of its width. The line along those nodes is largely continuous and has largely a constant height along the length of the yacht. If the line is not continuous (e.g. due to height variation), a shorter section is taken or completely omitted in between the segments of length $\Delta L = 10$ m.

The deformed coordinates of the main deck are obtained directly from the 3D FE model nodes in the middle width of the main deck and the deformed coordinates of the beam model are calculated by Eq. (4.7). The deformed coordinates and the undeformed coordinates as a reference are given in Figure 4.19.

From the deformed coordinates in Figure 4.19, the deformation components Δx and Δz as indicated in Figure 4.17 are calculated for the 3D FE model and the beam model for each longitudinal section of $\Delta L = 10$ m. The comparison between the deformation components Δx and Δz is given in Figure 4.20 and Figure 4.21, respectively.

The deformation components show a reasonable to good agreement at all sections. An exact match is not expected, since there are already two sources of deviation known: the displacement and rotation components \mathbf{w} and $\boldsymbol{\theta}$ used in Eq. (4.5) did not exactly agree and the neutral axis location is not necessarily at a constant height at the room longitudinal location. The largest observed deviation is 1.4 mm for Δx in section 40-50 and 0.8 mm for Δz in section 50-60. The deviation in Δx can be explained by local stress fields near the nodes affecting the results of the nodal displacements. For example, the deviation of 1.4 mm for Δx is rather large compared to the second largest, which is only 0.4 mm. Inspection of the 3D FE model shows that apart from the fact that in section 40-50 a higher deck is introduced in the hull (called a wide body), possibly resulting in a local stress concentration, there is also a stairs opening in the main deck close to the nodes where the

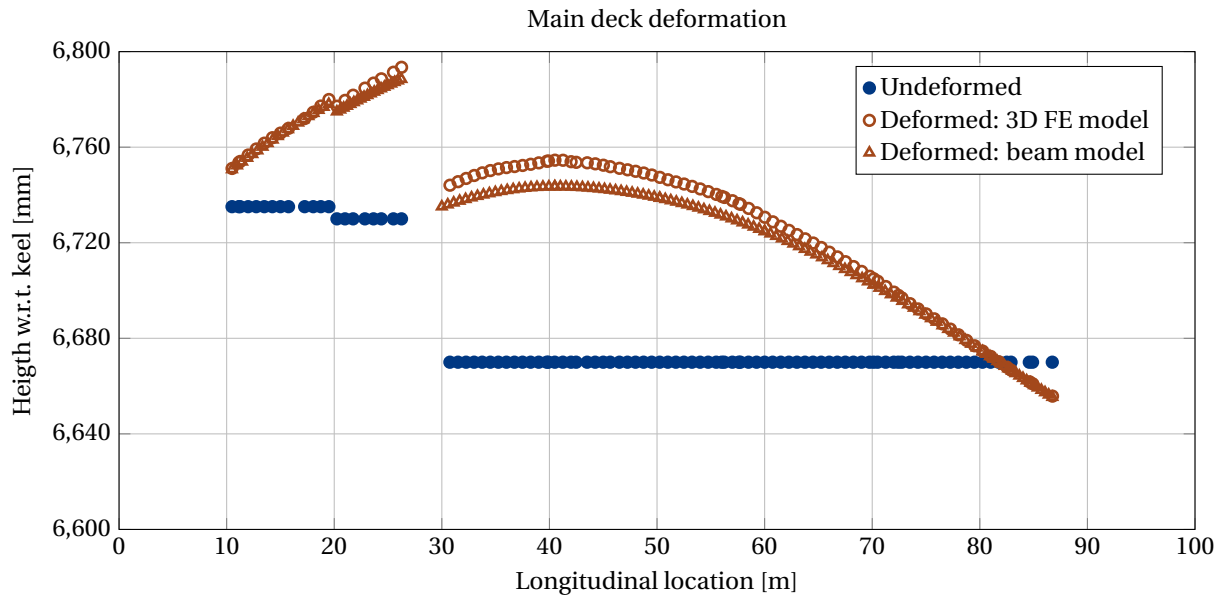


Figure 4.19: Undeformed and deformed location of the main deck due to vertical bending.

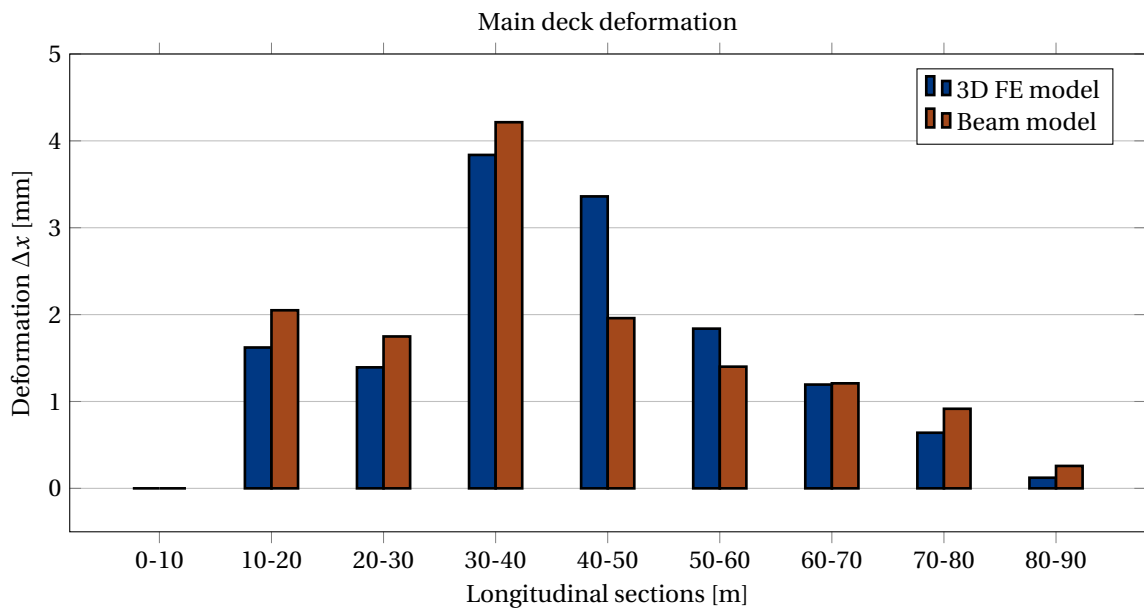


Figure 4.20: Magnitude of the deformation component Δx of the main deck for longitudinal intervals of 10 m.

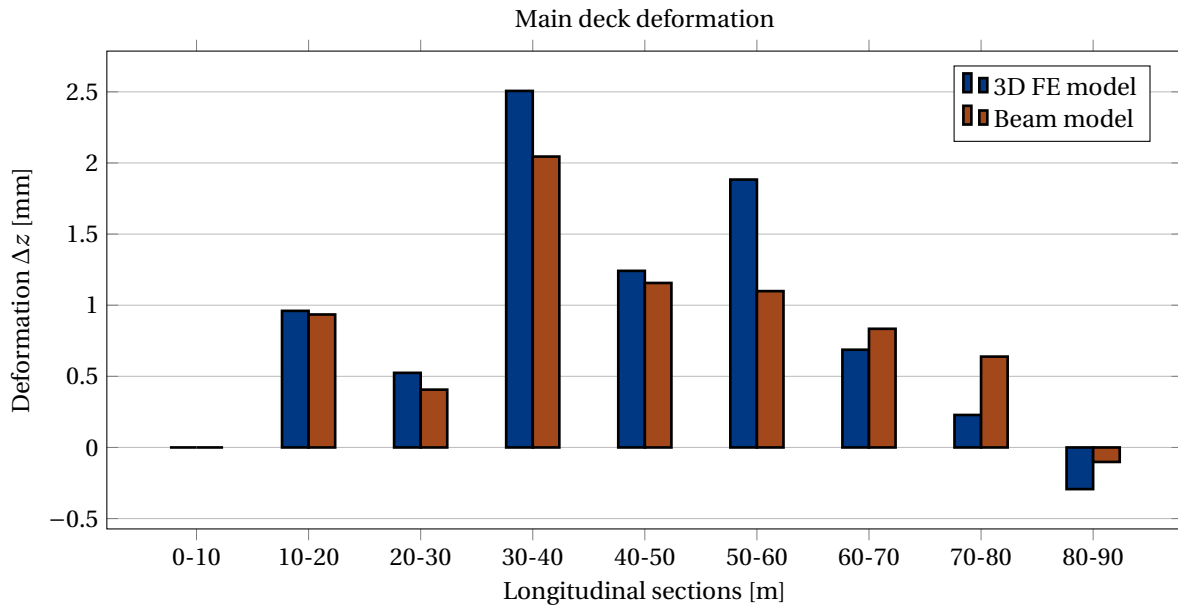


Figure 4.21: Magnitude of the deformation component Δz of the main deck for longitudinal intervals of 10 m.

results are obtained. The stress fields introduced by these discontinuities may cause the local deformations to deviate in the 3D FE model results for section 50-60.

Therefore, an additional check is performed at the height extremities of the yacht hull where no discontinuities are observed to see if the magnitude difference of the deformation components stays constant at other locations and further away from the neutral axis. Again, horizontal lines are taken of section length $\Delta L = 10$ m or smaller if the height is not constant along the section. For the aft part of this yacht ($L < 40$ m), the main deck is already located almost at the height extremity and the keel does not have a proper horizontal line, hence the deformation components are determined for $L > 40$ m at the locations at the minimum and maximum height of $z = 0$ m and 10.7 m, respectively, w.r.t. the keel. The deformation results for the minimum and maximum heights are given in Figure 4.22 and Figure 4.23.

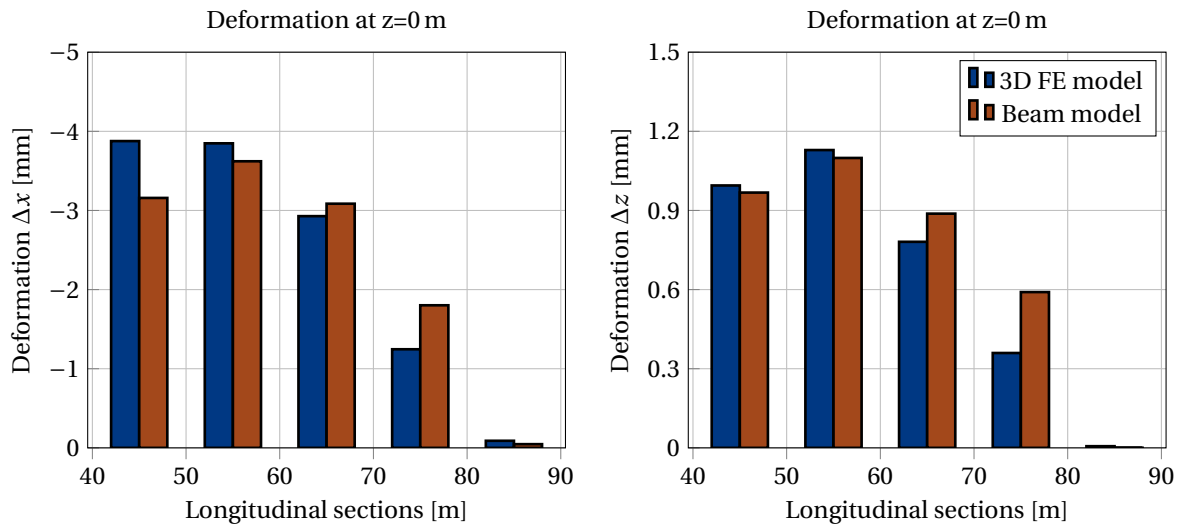


Figure 4.22: Magnitude of the deformation components of the minimum extremity of the yacht hull height at $z = 0$ m for longitudinal intervals of 10 m

A good agreement can be seen for the deformation components at both the minimum and maximum extremity of the yacht hull height. The largest deviation at the extremity's of the yacht hull height are for Δx 0.7 mm at section 40-50 and for Δz 0.25 mm at section 60-70. This suggest that the earlier observed largest

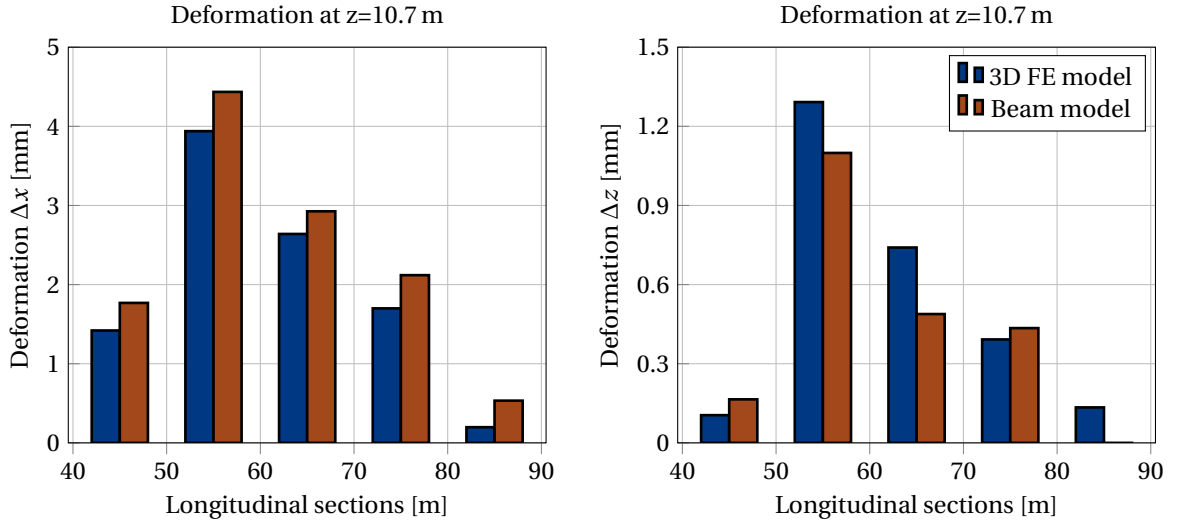


Figure 4.23: Magnitude of the deformation components of the maximum extremity of the yacht hull height at $z = 10.7$ m for longitudinal intervals of 10 m

deviation of $\Delta x = 1.4$ mm at the main deck is a result of a local discontinuities affecting the stress field in the 3D FE model rather than that the local deformations derived from the beam model are inaccurate.

4.5.2. Torsional response

The torsional response considers the rotation around the longitudinal x-axis (rotation in the yz-plane). Therefore, the displacement field in Eq. (4.5) is simplified to Eq. (4.9).

$$\mathbf{u}(x, y, z) = \begin{Bmatrix} u_y(x, z) \\ u_z(x, y) \end{Bmatrix} = \begin{Bmatrix} -z\theta_x(x) \\ y\theta_x(x) \end{Bmatrix} \quad (4.9)$$

In Figure 4.24 the rotation of a point P on a cross-section is illustrated with its rotated coordinates the coordinates calculated in by Eq. (4.9).

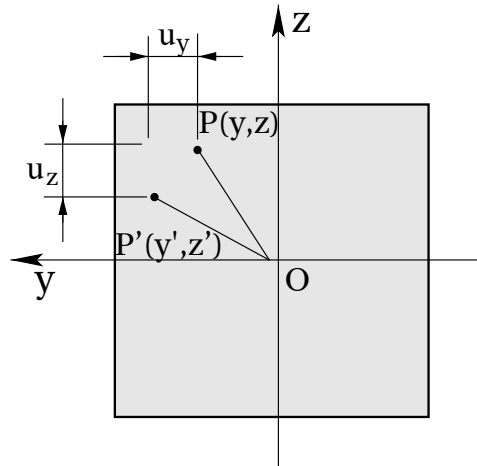


Figure 4.24: Displacement components of point P on the torsion of a cross-section. Modified from [5]

A result of the small angles approximation in the beam theory is that the deformed coordinate u_y is not dependent on the y-coordinate of the undeformed point and the deformed coordinate u_z is not dependent on the z-coordinate of the undeformed point [5]. Thus, the u_y deformation should be constant for a line of constant z-coordinate on a cross-section, i.e. a horizontal line. Similar, the u_z deformation should be constant for a line of constant y-coordinate on a cross-section, i.e. a vertical line. This can be clearly seen in the deformation contours for u_y and u_z of the 3D FE model given in Figure 4.25.

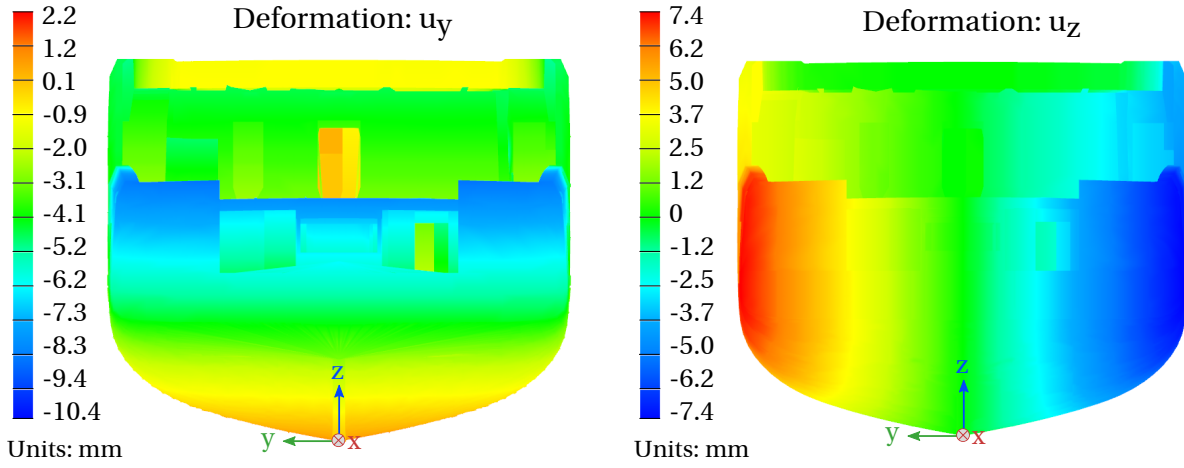


Figure 4.25: Rear view of the deformation contours of components u_y and u_z for a pure torque load case.

According to the beam theory, the coordinates y and z in the displacement field in Eq. (4.9) need to be given with respect to the neutral point of a cross-section, thus the neutral point remains stationary when a torque is applied at that cross-section, which is also the definition of the *center of twist* [23]. For a straight prismatic cylindrical beam, the neutral point and the center of twist coincide as demonstrated by Duncan et al. [17] and the displacement field in Eq. (4.9) is valid. However, the yacht hull is non-prismatic and it can be clearly seen in on the visible rear cross-section in Figure 4.25 that the point with no deflections (i.e. the stationary point or center of twist) is located approximately at the keel ($u_y = u_z = 0$ mm) at the rear and increasing to approximately 5.5 m at the front of the yacht, while it is known that the neutral point of any cross-section of the yacht at least lies above $z = 3$ m. This means that it if the displacement field given in Eq. (4.9) with the y -, and z -coordinates given with respect to the neutral point on a cross-section, the deformation components can not agree accurately with the 3D FE model results and consequently no correct local deformations in a room can be determined. That said, this does not mean that the displacement field in Eq. (4.9) can not be used at all. By inspection of the 3D FE model and looking at Figure 4.25, it could be seen that the u_z deformation is always zero at the y -coordinate $y \approx 0$. This means that the y -coordinate of the center of twist is always approximately zero, regardless of where the u_y deformation is zero. The latter is also true for the neutral point of a cross-section, since this point must lie on an axis of symmetry [1] and the xz -plane of a yacht ($y = 0$) can be considered a symmetry plane for most yachts. Therefore, the y -coordinate as used in the displacement field is known and is simply the y -coordinate of the point under consideration, enabling the determination of the deformation component u_z . In short, only the displacement field component u_z due to an applied torque can be expected to yield acceptable results and Eq. (4.9) is changed to Eq. (4.10).

$$\mathbf{u}(x, y, z) = u_z(x, y) = y\theta_x(x) \quad (4.10)$$

As for the vertical bending response, the local deformation of a room is of interest for the torsion, which means regarding the two end cross-sections at the room ends that rotate with respect to each other. In Figure 4.26, a room ABCD - EFGH is regarded of which the cross-section side EFGH rotates with respect to side ABCD by angle $\Delta\theta_x$.

The rotation is relative, hence the rotation of side EFGH with respect to side ABCD $\Delta\theta_x$ is given by the difference of the rotation components at those cross sections, see Eq. (4.11), with n indicating the number of an arbitrary cross-section (with side ABCD in Figure 4.26) and $n + 1$ the cross-section ΔL further in x -direction (with side EFGH in Figure 4.26).

$$\Delta\theta_x = \theta_x(x_{n+1}) - \theta_x(x_n) \quad (4.11)$$

Since the only deformation component that can be regarded with accuracy is u_z , only the deformation in z -direction as seen in the right side of Figure 4.26 is of importance. The relative vertical displacement of corner E with respect to A due to an applied torque can then be calculated as seen in Eq. (4.12) as given as Δu_z , with the y -coordinate with respect to the neutral point. The deformation Δu_z can thus be an indicator for the magnitude of the rotation and consequently if the torsional stiffness is sufficient. If the torsional stiffness

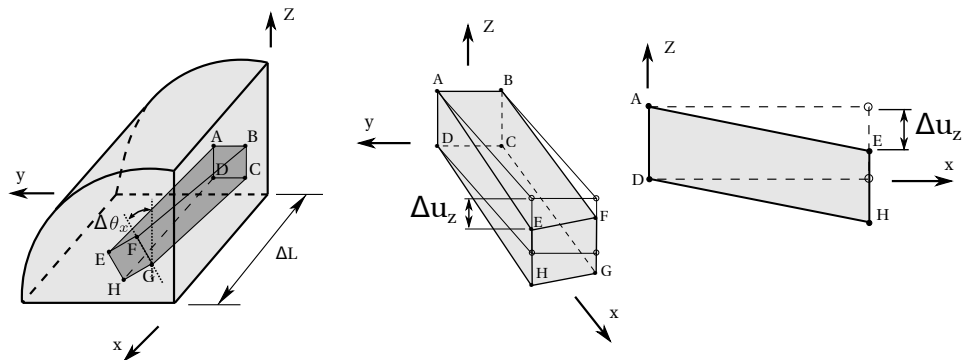


Figure 4.26: The rotation of room ABCD - EFGH by angle $\Delta\theta_x$ and the deformation component Δu_z .

is not enough, and the Δu_z is too large according to comfort standards for the deflection, then this room, or section, forms a risk in the design.

$$\Delta u_z = y\Delta\theta_x \quad (4.12)$$

An additional note is that it is not expected that the horizontal corner lines show a similar bulging behaviour as the horizontal lines in the vertical bending response, since the relation between the longitudinal x coordinate and the rotation θ_x is approximately linear as can be seen in Figure 4.13.

Now, a comparison can be made with the 3D FE model for the deformation in z -direction. Again, longitudinal sections are taken with a length of $\Delta L = 10$ m to indicate the deformation variation along the length of the yacht. Deformation u_z is largest at the largest y -coordinate (which is visible in Figure 4.25), so to indicate the most extreme deformation, the sections are taken at the outside of the hull at the starboard and port side on the waterline. The hull does not have a constant beam (width) and narrows towards the bow, i.e. the y -coordinate is not constant at the maximum width for a section $\Delta L = 10$ m and therefore, Eq. (4.12) is changed to Eq. (4.13).

$$\Delta u_z = y_{n+1}\theta_x(x_{n+1}) - y_n\theta_x(x_n) \quad (4.13)$$

The (un)deformed coordinates of starboard and port side on the waterline are obtained directly from the 3D FE model nodes and deformed coordinates of the beam model are calculated by Eq. (4.10). The nodes do not have a constant height along the length of the yacht, due to a non-structured mesh, but this is not a problem, since the z -coordinate does not influence the deformed coordinate u_z as discussed before. The results can be seen in Figure 4.27 and note that the port side deforms in positive z -direction, while starboard moves in negative z -direction, which is also visible in the deformation contours at the right graph of Figure 4.25.

The results in Figure 4.27 show good agreement except a small deviation between 60 and 70 m. The calculated deformation with the beam model is larger, which is expected since it could already be seen in Figure 4.13 that the rotation component θ_x is larger at those sections compared to the 3D FE model.

The relative displacements Δu_z for each section of ΔL can be calculated with Eq. (4.13) and the results are given in Figure 4.28 for port side (starboard is omitted, because it is similar in magnitude, only mirrored).

4.6. Local deformations with design loads

In the previous sections, it was shown that the global and local response showed good agreement with the 3D FE model of the test case yacht. In Chapter 3, operational loads were determined that represent actual load cases to a sea state. In this section, the loads and the beam model are combined to determine the global and local response for the test case yacht for the assumed sea state. This way, possibilities are created for risk identification in the preliminary design with regard to excessive deflections and initial estimates of required clearances can be made. The two major loading distributions of importance are the vertical bending response (EDW with heading 180°) and the torsional response (EDW with heading 60°) derived in Section 3.3.3.

For the vertical bending response, both the hogging and sagging state of the hull girder are regarded. The loading distribution for the hogging state is obtained by adding the wave bending moment M_y in Figure 3.12 to the SWBM given in Figure 4.8 and the sagging state by adding the negative of the bending moment M_y in Figure 3.12 to the SWBM given in Figure 4.8. Since the SWBM is always positive, a different magnitude of the

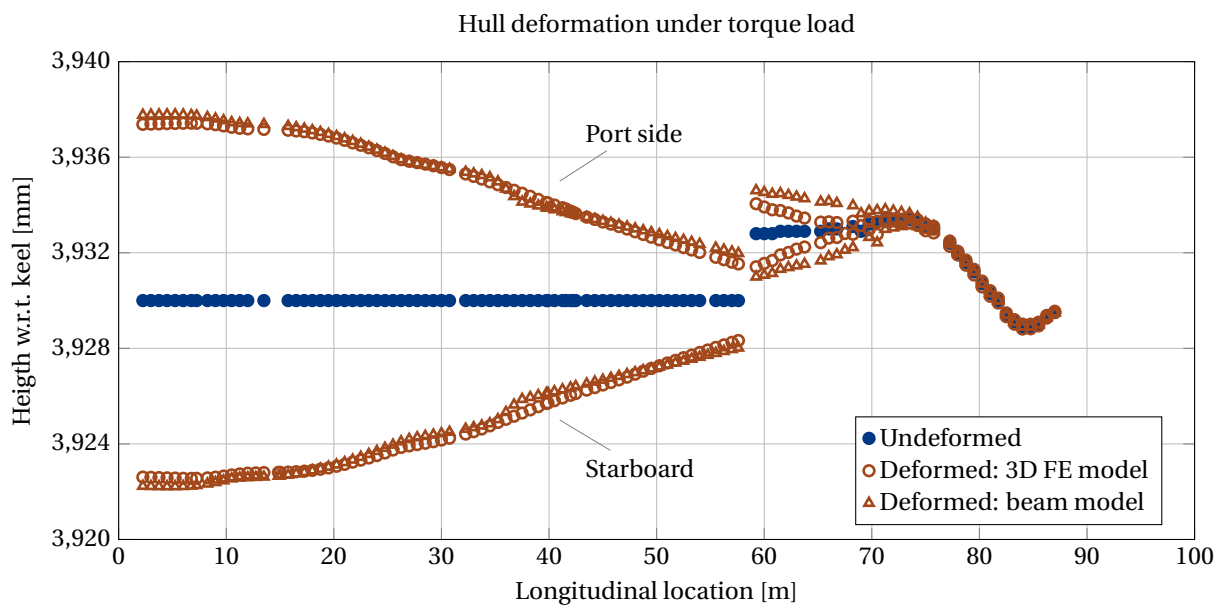


Figure 4.27: Undeformed and deformed location of port side and starboard of the hull at approximately the height of the waterline due to a wave-induced torque load.

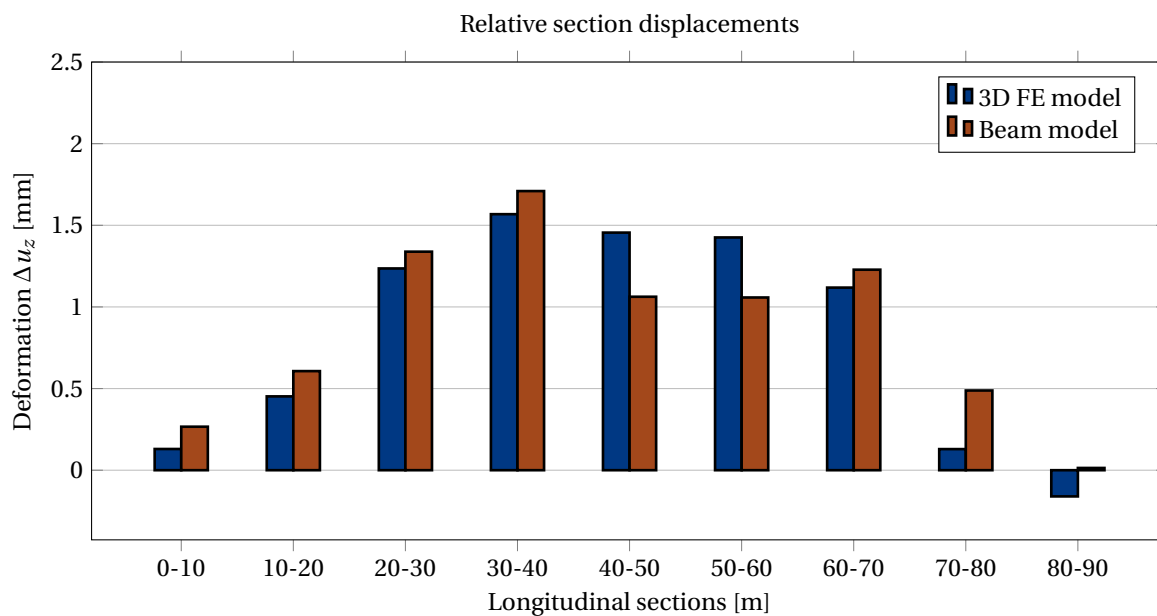


Figure 4.28: Magnitude of the deformation component Δu_z of port side of the hull at approximately the height of the waterline for longitudinal intervals of 10m due to a wave-induced torque load.

response is obtained for the hogging and sagging states. The global response of the 1D beam model for the hogging and sagging states is given in Figure 4.29. Note that for the EDW with heading 180° the horizontal bending moment and torque distributions are zero and no other displacements or rotations are present.

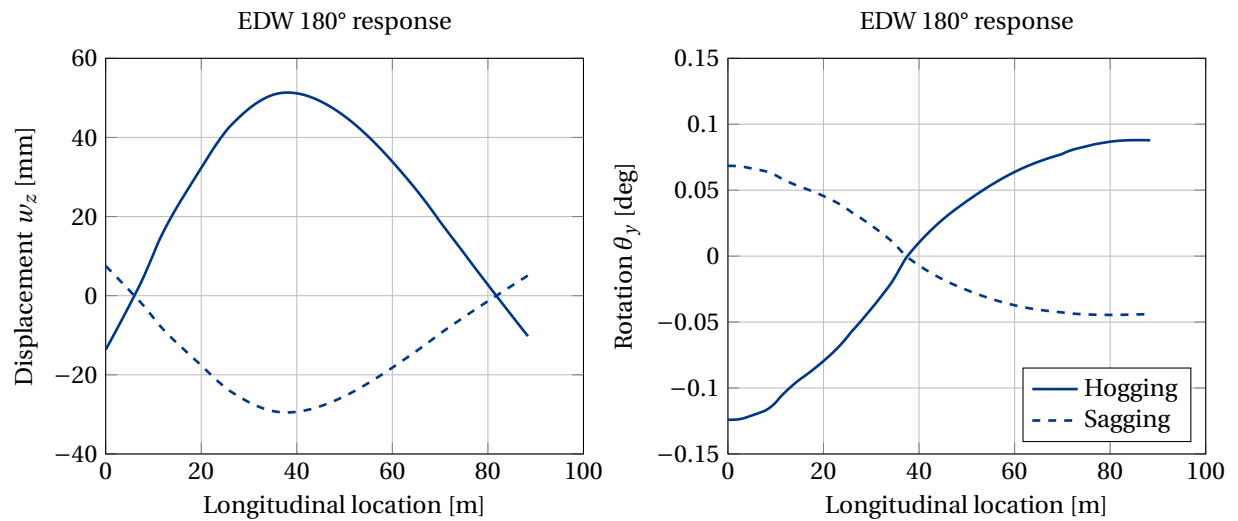


Figure 4.29: Response comparison of the 1D beam model for the 180° EDW in the hogging and sagging situation.

The peak magnitude of the hogging response displacement w_z is 51 mm, smaller than the peak for the hogging response for the Lloyd's hogging load case, which was 78 mm as seen in Figure 4.12. This decrease in magnitude of 35% is expected as mentioned before because the LLOYD's hogging load case is a load case for extreme strength assessment and not for an actual sea state. The sagging response is a bit smaller in magnitude at -30 mm, but opposite in sign as explained by the addition of the SWBM. The rotation θ_y is therefore also opposite in sign and smaller in magnitude for the sagging case. Note that the displacements are taken with respect to the boundary conditions, which are location at the intersections of the two displacement curves in Figure 4.29. This is not visible in the rotation curves, because the boundary conditions are simply supported, thus rotation is allowed.

The EDW with 60° heading angle results in the torque given in Figure 3.12, but also in a vertical bending moment² as indicated in Section 3.3.4. Similar to the hogging and sagging for the 180° EDW, the torsion the torque distribution also varies between positive (+) and negative (-) values. The results of positive and negative torque loads including the resulting vertical displacements are given in Figure 4.30. There are also rotations θ_y corresponding to the vertical displacements w_z similar to the rotations seen in Figure 4.29, but they are omitted for clarity.

For the positive torque, the vertical bending displacement w_z is small, which can be explained by the phase differences for which the torque occurs and the vertical bending moment. At the moment the maximum positive torque occurs, the yacht is located between two wave crests (see illustration in Figure 2.4), resulting in a negative (sagging) wave bending moment WBM. The positive SWBM is added to that, resulting in a small overall bending moment and a small vertical displacement. The summation of bending moments is illustrated in Figure 4.31 and a small bending moment as compared to the vertical bending moment distribution derived in Figure 3.12.

For the longitudinal rotation θ_x in Figure 4.30, two things can be noticed: first the introduction of the wide body (i.e. an additional deck) at approximately 40 m can be seen by a decrease in slope of θ_x . This is because the torsional constant of the cross-sections increases by the additional deck, which increases the size of the closed-cross section. Second, the magnitude of the rotation is larger at the rear end compared to the response seen in Figure 4.13. This is because the peak of the torque distribution is shifted to the rear half of the yacht (25% of L_{pp}) as seen in Figure 3.12, which is where the torsional constant is low compared to the front half.

In Figure 4.30 an additional curve is given labelled as the unadjusted torque. This curve is generated by using the torque load distribution that is obtained by not omitting the RAO data points at the aft extremity of the yacht where unrealistic SDA values were obtained (see Section 3.3.2). This results in a non-zero negative torque at the aft end, which rotates the end in opposite direction. It can be seen that the corrected values

²and horizontal, which is omitted as mentioned in Section 4.5.

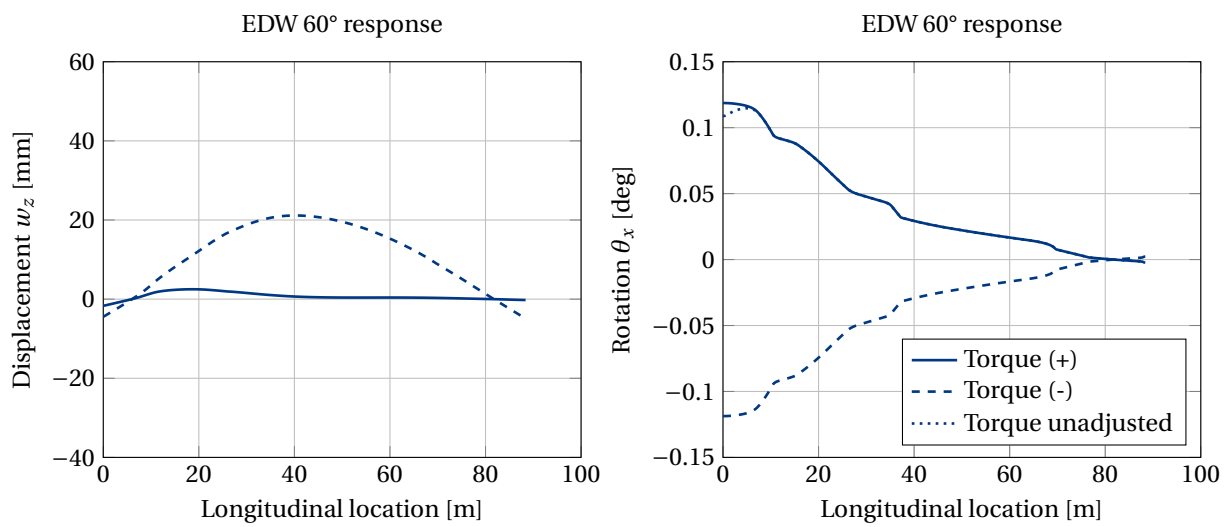


Figure 4.30: Torsional response comparison of the 1D beam model for the 60° EDW.

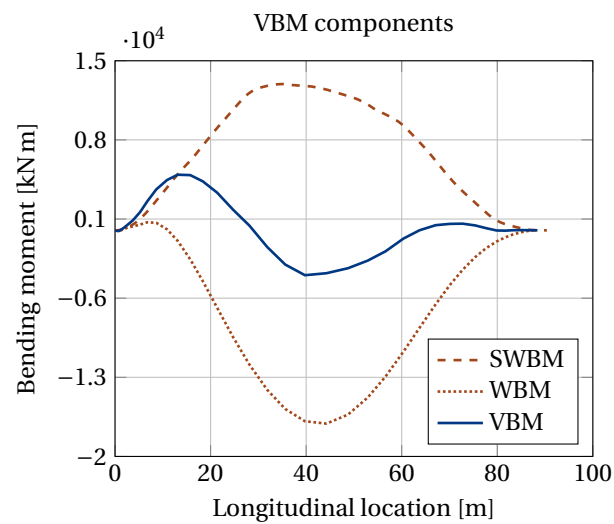


Figure 4.31: Addition of the Wave Bending Moment WBM and the Still Water Bending Moment SWBM for the 60° EDW for positive torque.

have only a small effect on the rotation and is limited to those longitudinal locations. A constant rotation is more realistic at the rear end, so neglecting the RAO data points is more accurate, however, its effect is small. The global response displacement and rotation components \mathbf{w} and $\boldsymbol{\theta}$ are now known for the design loads and the local response can be determined similar to described in Section 4.5. In Section 4.6.1 it is described how this local response can serve as a risk analysis method for new yachts and in Section 4.6.2 an example is given how the local response can be used for initial estimates of the clearances of interior instalment.

4.6.1. Risk analysis

The current information on problems caused by creaking interior is for the most part based on experienced discomfort during operation and not necessarily direct (documented) experiments. This experienced discomfort is linked by structural engineers at Feadship to the empirical relations that include the moment of inertia of the hull and geometry parameters (as mentioned in Chapter 1) to decide whether a new design is sufficiently stiff, however a direct link to the the experienced discomfort is not present. In this section, an attempt is made to increase the capacity to link experienced discomfort on part of the ship to deformation parameters that are a possibly a direct cause of it. As demonstrated in Section 4.5, locations can be chosen for which the deformation components Δx and Δz for e.g. decks can be determined with reasonable accuracy. The analysis can be performed for previous yachts where discomfort was experienced that can be related to the expansion of structure at specific locations and yachts that did not experience discomfort to formulate absolute limit criteria of the deformation components Δx and/or Δz . This way, an unambiguous limit is obtained to which the local deformation components of new yachts can be compared. It also provided more guidance on the required improvement on the structure if the limits are exceeded.

For the risk analysis to the deformation components due to vertical bending and torsion, a generic yacht hull is divided in segments of $\Delta L = 10$ m as seen in Figure 4.32. The length of these segments can be adjusted if needed and the 10 m is based on the general room length on board of Feadships.

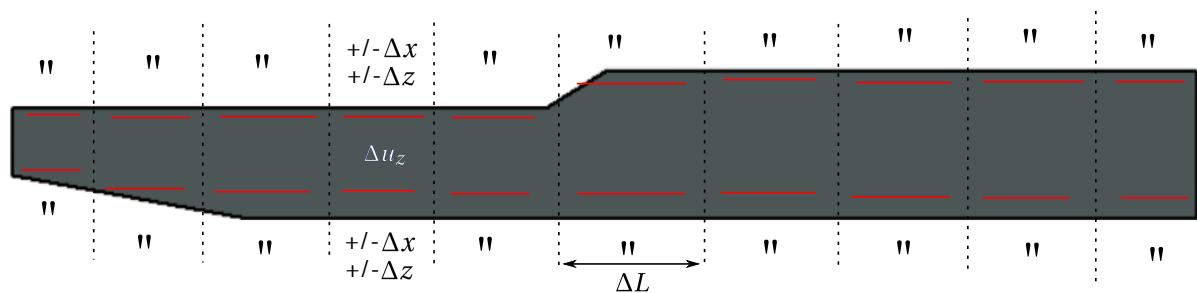


Figure 4.32: Yacht hull divided in segments of ΔL with top and bottom outer locations with deformation components Δx , Δz due to vertical bending and Δu_z due to torsion.

The outer locations in the z -direction (top and bottom) are the furthest away from the neutral axis and hence have the largest deformations in vertical bending. Each outer location (horizontal lines in Figure 4.32, two in each section) contains a positive (maximum) value for the deformation components and a negative (minimum) value, which correspond to the hogging and sagging states of the hull girder. For each of the sections, the resulting deformations for the design hogging and sagging states of the hull girder can be determined with the global response displacements and rotations given in Figure 4.29 according to the approach in Section 4.5.1. For the test case yacht, this is performed for the outer top and bottom locations (the decks) of the hull and the results can be seen in Figure 4.33 and Figure 4.34, respectively. Indicated is an example of a limit that can be set according to the desired level of comfort that is required for the yacht. The layout of a yacht (room locations and purpose) can differ between yachts and therefore a comparison of a section irrespective of the longitudinal location is important.

First, it can be noted that the hogging deformations are larger than the sagging deformations, which is expected, since the hogging global response is larger as seen in Figure 4.29. Second, the Δx deformation for hogging is positive on the upper decks (Figure 4.33) and negative for the keel (Figure 4.34), which makes sense since they are above and below the neutral axis, corresponding to tension or compression, respectively. The Δz has a non-noticeable change in magnitude for the upper decks or keel and it does not change sign, the latter meaning that the horizontal parts above and below the neutral axis follow the curvature of the hull (which is the curvature given by the displacement w_z in Figure 4.29). The indicated limits are just given as example and are currently fictitious in Figure 4.33 and Figure 4.34. Note that the limits do not necessarily

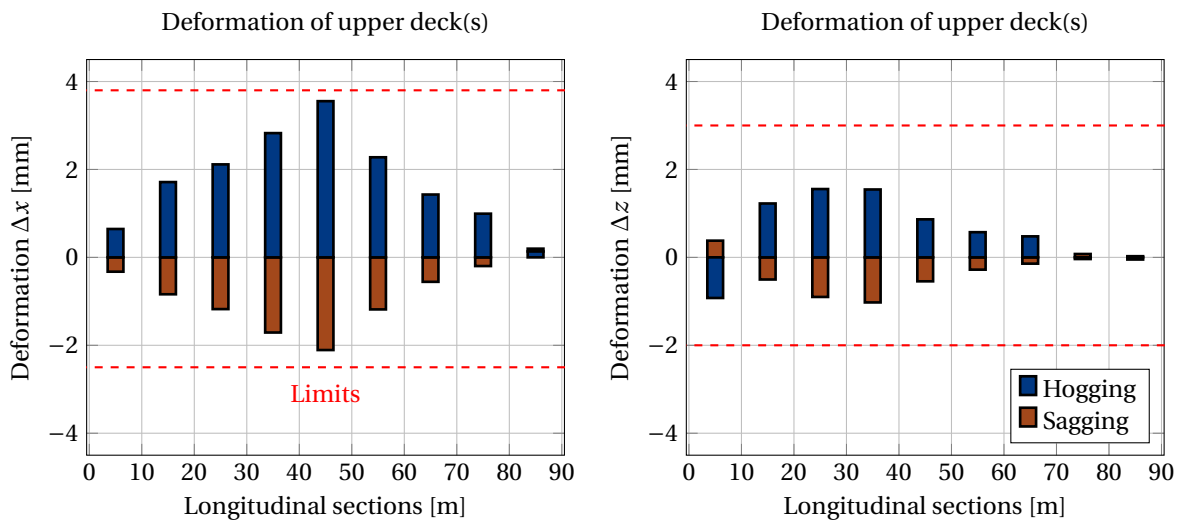


Figure 4.33: Magnitude of the deformation components Δx and Δz of the upper decks for longitudinal intervals of 10 m

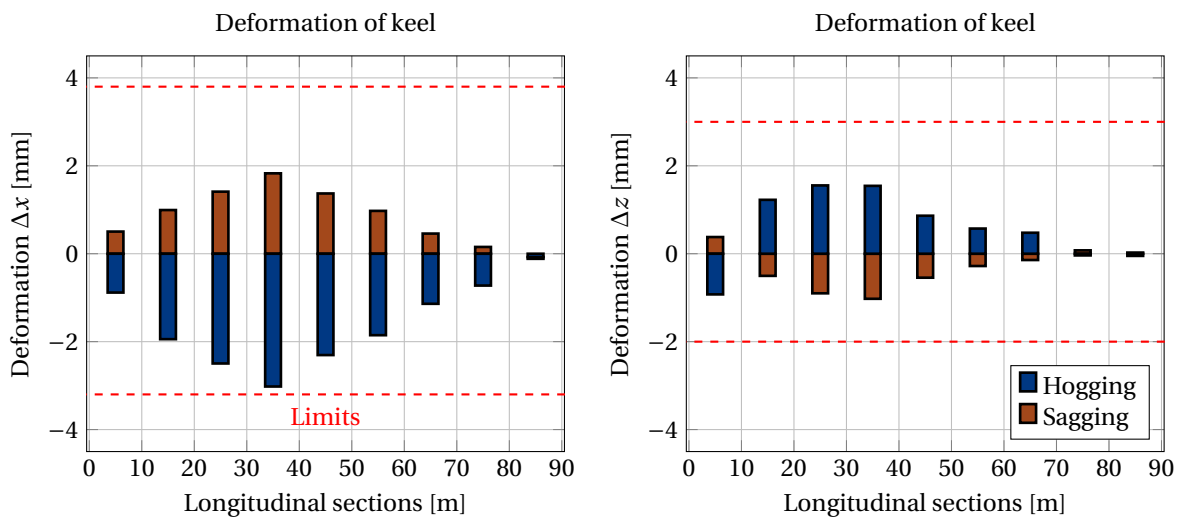


Figure 4.34: Magnitude of the deformation components Δx and Δz of the keel for longitudinal intervals of 10 m.

have to be equal for each longitudinal section, because some locations in the yacht might be more relevant for comfort issues than others.

In addition to the deformation components Δx and Δz , the torsional deformation component Δu_z can be calculated with the longitudinal rotation θ_x in Figure 4.30 according to the method described in Section 4.5.2. For the torsion, the outer locations of the hull are taken in the y -direction or at starboard/port side of the hull (due to symmetry the y -coordinates of starboard and port side are similar) at a height of the waterline, which corresponds to the outer width of the hull. The results are given in Figure 4.35.

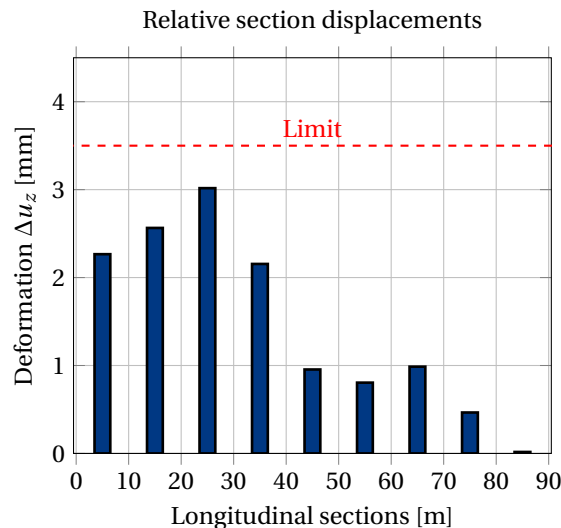


Figure 4.35: Magnitude of the deformation component Δu_z at the outer hull width at the waterline due to torque for longitudinal intervals of 10 m.

Again, the location where the wide body starts is clearly visible by the lower bars for $L > 40$ m, since the torsional stiffness increases there. Also, the locations of largest deformation corresponds to the location where the torsional constant is relatively low (see Figure 4.6) and a peak in torque distribution is present (see Figure 3.12). The sections with the largest deformation are hence not a surprise, though it does give direct overview of what magnitudes of deformation can be expected. Same holds for the vertical bending response, if the deformations are still within limits, the graphs can be directly communicated to other disciplines in the design process. Previously, the empirical relations provided (coarse) insights in the longitudinal stiffness of a yacht, which could be only read by structural engineers. Now, the deformation bar graphs can clearly indicate what the deformations are that other disciplines need to take into account. Everything that is installed in the yacht, from technical air-conditioning systems to marble interior has to account for these deformations, since they are inevitable in the elastic hull structure. The purpose is thus twofold: one, structural engineers can make a risk assessment by comparison with magnitudes that previously were causing discomfort in yachts and two, once the deformation is within limits, the deformations can be directly communicated to all disciplines to take them into account from the start of the detailed engineering phases. The latter considers for example clearances for interior, which is discussed in more detail in Section 4.6.2.

A last note on the analysis performed is that the superstructure is not taken into account in the beam model right now and though the largest stiffness is generated by the hull, the superstructure still has some influence. More research is required to the influence of the superstructure to make general statements, since the superstructure can be quite different. For this yacht, the peak magnitude of the global response decreases by approximately 22% as seen in Figure 4.36 if the superstructure is incorporated. The local deformations for the vertical bending therefore also decrease by a similar percentage for the real yacht.

4.6.2. Clearance analysis

The analysis in Section 4.6.1 is useful to get an overall view of the longitudinal stiffness, in this section this approach is extent to a room which can be compared to actual locations on the yacht. The generation of a deformed room contour was already shown in Figure 4.17. This section presents the results for an example room taken in the test yacht to determine either if the structure locally additional stiffness and what clearance or connections should be adopted. As discussed before, it is not possible to determine accurately what the

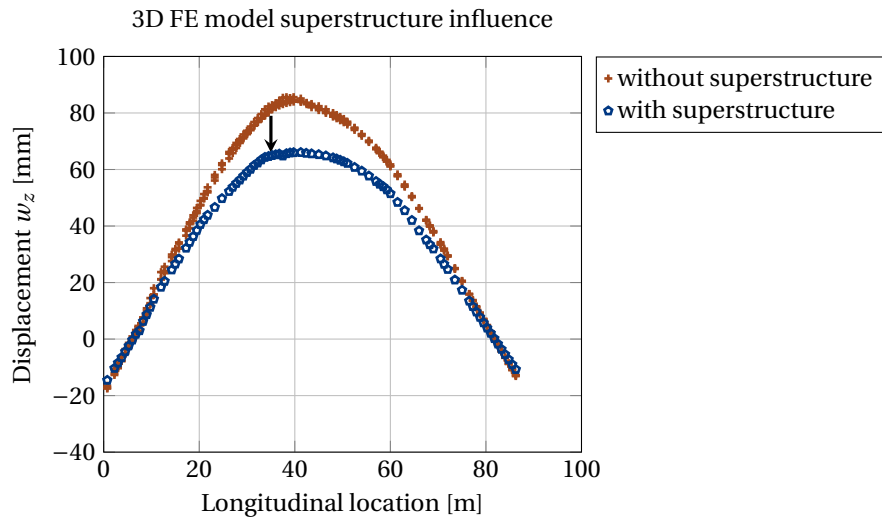


Figure 4.36: Influence of the superstructure on the vertical displacement for the hogging load case.

tilting of the walls is, so this analysis is just focused on the expansion, bulging and rotation of the decks that are part of the room.

In Figure 4.37 a room of length L is given with the interior represented by two rectangles on the bottom and top representing generic interior elements, such as floors or ceiling plating. The room is located over the full width of the yacht, hence the torsion component is determined at the y-coordinates at port side and starboard.

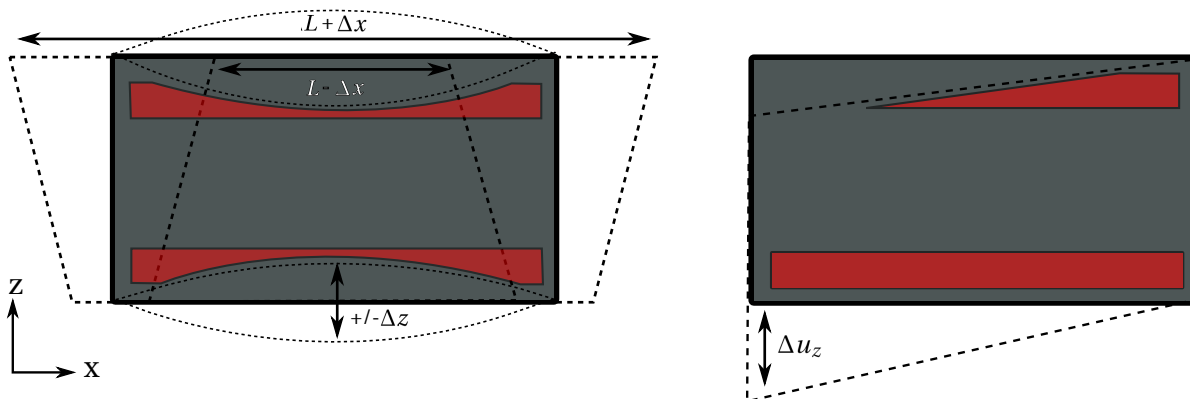


Figure 4.37: A side view of the room deformations for bending deformation components Δx , Δz and torsion component Δu_z . Interior elements are indicated by the rectangles at the top and bottom of the room.

Anything that is installed in the room needs to accommodate for the deformation of the structure in some way or another. If rigid connections are used, the interior elements themselves will deform and be damaged or create noise, which is desirable to minimise for the highest level of experienced comfort. If flexible connections are used, the deformation components in Figure 4.37 give an indication of the range of flexibility such a connection is required to have.

A random location is chosen on the test case yacht to demonstrate what the results can be of the deformations. The longitudinal location of the room is at $x = 25-35$ m, the floor at 4.2 m above the keel and a room height of 2.5 m. With the displacement field in Eq. (4.7), the room contour of this room is calculated for discrete number of points as seen in Figure 4.38 and to indicate the deformation components, the scale is adjusted in the right figure to visualize the bulging Δ_z of the ceiling. The walls are included to sketch a complete picture, however as indicated before, the actual wall rotations are not necessarily accurate in the current beam model.

The deformation components due to vertical bending and torsion of the room contour in Figure 4.38 are given in Table 4.3. These are the extreme components for vertical bending (occurring for the EDW

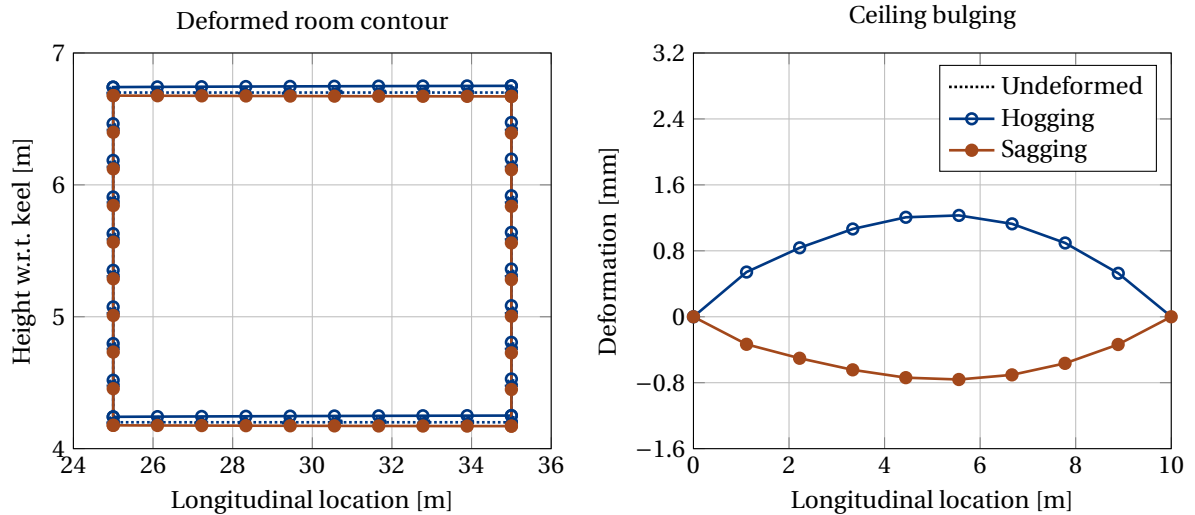


Figure 4.38: The vertical bending deformation of a room for the hogging and sagging states of the hull girder.

with heading 180°) and torsion (occurring for the EDW with heading 60°). The components Δx and Δz can be scaled according to the ratio of the vertical bending displacements w_z for the EDW 180° response and the EDW 60° response. E.g. for negative torsion the ratio of the peak vertical displacements is approximately $21 \text{ mm}/51 \text{ mm} = 41\%$, hence the bending components (Δx and Δz) that occur at the same moment the maximum torsion deformation component (Δu_z) is achieved are 41% of the values given in Table 4.3. It highly depends on the interior element under consideration how the deformation components in Table 4.3 should be combined, hence this is left for the users of the approach given in this work to decide.

Table 4.3: Deformation components for a room at $x=25\text{-}35 \text{ m}$, with floor height at 4.2 w.r.t. keel and room height of 2.5 m

Component	Ceiling	Floor	Units
Δx	+ 2.5/-1.4	+0.5/-0.3	mm
Δz	+1.2/-0.7	+1.2/-0.7	mm
Δu_z	+/-1.8		mm

In the selected room, the floor expansion and contraction are rather small since the floor is located close to the neutral axis of the yacht. The ceiling deformation is larger, since it is located further away from the neutral axis. The interior elements connected to the ceiling or their connection, have to allow for at least 2.5 mm of expansion and 1.4 mm of contraction, as well as an upward bulging of 1.2 mm and a downward bulging of 0.7 mm . Also, at port side or starboard at the maximum width of the yacht the floor and ceiling the relative vertical movement of the floor is 1.8 mm . Thus interior elements that are placed along the length of the yacht, must account for this down or upward movement.

4.7. Solutions for response improvements

For the structural engineers at Feadship it is important to know what can be done in order to improve the local response. In this section the qualitative influence of the main structural parameters is discussed on the global and local response. Also, some parameters are mentioned that do have an influence, however are unlikely to be changed driven by the structural design.

- **Moment of inertia:** Considering the importance of the vertical bending, the moment of inertia I_{yy} is the most important parameter to increase the longitudinal stiffness of the yacht. The layout of the yacht, however, is usually governed by the desired layout of the customer, which is rarely the most efficient structural solution. Improvement on the moment of inertia is normally obtained by increase of deck thickness or the decks themselves are located further outward. Additionally, hull girders can be placed or increased in height and thickness.
- **Shear area:** It is demonstrated that the influence of the shear deformations had a significant influence on the vertical displacement for the test case yacht and therefore improvement of the cross-sectional

shear area can be helpful to increase the longitudinal stiffness. The shear area A_z is largely dependent on the amount over vertical material in a cross-section, but also whether this is properly connected to the deck above to transfer the loads. Additional longitudinal stiffness can thus be gained by longitudinal bulkheads or walls that connect floors.

- **Torsional constant:** The torsional constant is largely affected by the size of the largest closed cross-sectional outline in the cross-section. Adding longitudinal bulkheads to increase the amount of closed-cells is not effective as they are largely unloaded in torsion [51]. Thus increasing the area of the largest closed cross-section is the best option to improve the torsion. Additionally, small improvements can be made by creating closed-cross-sections at the hull with double walls, such as is done for large container ships [33].
- **Material properties:** The Young's modulus and shear stiffness of the material used in the hull have a major influence on the local deformations. The higher stiffness and strength of steel makes it the most used material for the hull, however to meet higher customer requirements, aluminium is more often chosen. While aluminium alloys are available that provide enough strength, stiffness is largely unaltered and therefore the longitudinal stiffness of the hull can become insufficient for the Feadship comfort standards. This puts emphasis on creating tools and methods that provide more insight in the longitudinal stiffness of the yacht, which is the motivation of this thesis work.
- **Mass:** The mass of the yacht and its distribution affect the magnitude of the loads on the structure and therefore a yacht with a lower mass requires less construction. This means that weight saving can be beneficial to increase the comfort on board of a Feadship. Normally, though, weight savings are performed for different reasons than structural comfort, such as for achieving the contracted top speed.
- **Length:** The length of the yacht is not a driver for the structural design, although it influences the response and the longer the yacht is the larger the absolute deformations become. Increasing trends in the superyacht industry are larger yachts and with larger room sizes, which impose new risks on the construction. Again, this is also a large part of the motivation for this thesis.

Once the deformations are within acceptable limits, their magnitude is still inevitably non-zero, due to the elastic nature of the material. Therefore, the last solution is to adopt appropriate clearances and/or flexible connections to allow any type of interior instalment without resulting in creaking or damage to maximise the comfort on board of Feadship superyachts.

4.8. Summary

The yacht hull without superstructure is modelled as a beam with 1D timoshenko beam elements that include shear deformations and torsion deformation. The nodes of the beam model allow displacements and rotations in six degrees of freedom at each node, stored in the component vectors \mathbf{w} and $\boldsymbol{\theta}$. The bending, axial and rotational deformations are all decoupled. The Finite Element (FE) routine of the beam model is programmed in Python and verified with an exact agreement of a model made in the Siemens NX 11 software with 1D beam elements. The input of the beam elements is based on material properties and cross-sectional properties, which are determined by the NX section method that calculates the properties based on cross-sectional outlines directly obtained from a 3D model of the yacht. A check is performed with properties determined by Special Service Craft (SSC) software provided by Lloyd's register with a good agreement for the moment of inertia I_{yy} .

The global response of the beam is validated by comparison of the displacements and rotations of a complete detailed 3D FE model consisting of shell and beam elements. The used loading conditions are the Lloyd's register rule design loads for the hogging and sagging wave bending moments including the Still Water Bending Moment (SWBM) for the half-loaded loading condition. Overall, the global response showed a good agreement for the vertical and horizontal bending response and the longitudinal rotation due to an applied torque. The horizontal bending is small in magnitude and is considered not relevant to regard in relation to risk analysis for longitudinal stiffness. The global response showed better agreement if the cross-sectional properties are determined with the NX section method than determined with the SSC software. The decrease in performance for the SSC properties is largely a result of a conservative calculation of the vertical shear area A_z used in the SSC software. Additionally it is found that the shear deformations account for approximately 20% of the total vertical displacement of the hull.

The local response in the yacht hull is derived from the global response by using the equations for the displacement field of a cross-section obtained from linear beam theory. The local deformation components that can be calculated for the vertical bending are the longitudinal expansion (Δx) and bulging (Δz) of horizontal elements (the decks). The components are validated by taking longitudinal sections with length ΔL and comparing the results with the 3D FE model. A good accuracy for all components is found at heights varying from the keel to the highest vertical location (the outer decks). The rotation/tilting of the walls can not be determined, since a cross-section does not rotate as a rigid body, due to the shear stiffness difference between the decks. The displacement field for the rotation of the cross-section due to torsion can only partly be used, because the non-prismatic nature of the yacht hull results in a center of twist location that does not correspond to the neutral point of a cross-section. The location of the center of twist is shown to be at the vertical plane of symmetry of the yacht (xz -plane) and therefore it is possible to determine the vertical deformation component u_y from the displacement field. The relative vertical displacements in torsion for different longitudinal sections showed good agreement with the 3D FE model.

The wave-induced loads determined in Chapter 3 are combined with the beam model to obtain a global response for realistic load cases to obtain the magnitude of deformations that can actually occur. A method is presented to compare the local deck expansion Δx and bulging Δz at the outer vertical locations and the relative vertical displacement due to torsion with still-to-be-formulated limit values to get an indication of the longitudinal bending and torsional stiffness of the yacht. This approach is extended for a specific room to indicate the clearances and/or provide information to decide on the connection methods that should be applied for interior instalment.

At last, a qualitative discussion is given on what parameters can be adjusted to improve the global and/or local response and concluded that the comfort is maximised once the deformations are within acceptable limits and appropriate clearances and connections are used in the design.

5

Conclusions

The aim of this research work was to establish a method that could increase the knowledge on the longitudinal bending and torsion stiffness of Feadship superyachts to be able to perform better risk assessment during the preliminary design phase. The method consists of three main steps, with the first step the creation of operational wave-induced load distributions that represent the loading conditions that Feadships encounter in normal use. The second step is the modelling of the yacht structure excluding the superstructure as a 1D beam with Timoshenko elements that includes bending, shear and torsion deformations. The model is validated with a 3D Finite Element (FE) model with good agreement for both the global and local responses. The third step combines the derived load distributions with the beam model and provides insight in the global hull girder bending of the yacht in operational conditions and local deformation components indicate structural risks and clearances that should be adopted. The method can be applied to previously built yachts to link the experienced level of comfort on board to the local deflection components to set-up local deflection limits for new (unconventional) yachts to determine whether their initial structural design in the preliminary design phase is sufficiently stiff. Also initial estimates can be made on the clearances that have to be adopted in a location of interest where the deflections might be problematic for the interior. The research objective was formulated as follows:

To include the effect of operational wave-induced loads on a yacht structure in the preliminary design phase by creating a structural model that incorporates major structural elements and identifies structural limit states that can indicate excessive local deformations and/or predict required interior clearances.

The developed routines allow for the determination of the wave-induced load distributions of a yacht and can generate a global and local structural response that can be a realistic initial estimate on local deformations and clearances, therefore the research objective of this thesis is met.

In Chapter 1 the research questions are formulated that guided this thesis work and have been answered throughout this document. The conclusions in relation to the two main research questions are as follows:

I What is the relevant operational wave-induced load distribution of a yacht in relation to the longitudinal stiffness and how does it compare to the rule design loads?

The spectral analysis of the response spectra created by a linear response analysis allows for the determination of maxima or most probable maximum values of the internal vertical and horizontal bending moment and torque on transverse cross-sections along the length of a yacht. For the demonstrated test case in this work at cruise speed, the maximum peak response for the vertical bending moment occurred for (long-crested) seas with heading angle $\beta = 180^\circ$ and mean zero-crossing period $T_z = 6.1$ s, for the horizontal bending moment for heading angle $\beta = 120^\circ$ and mean zero-crossing period $T_z = 3.8$ s and for the torque for heading angle $\beta = 60^\circ$ and mean-zero crossing period $T_z = 4.4$ s. The longitudinal locations for which the maxima occur are amidships for the vertical and horizontal bending moment and at approximately 25% of the length between perpendiculars L_{pp} from the aft perpendicular for the torque, which is in accordance with literature. A regular equivalent design wave can be used to create moment and/or torque load distributions by choosing the aforementioned maximum peak responses as target response for the regular wave to cause. This makes

sure that the most extreme load is reached for that sea state and the corresponding load distributions can be applied to the structural models. The wave-induced vertical bending moment distribution is similar in shape to the Lloyd's Register rule design bending moment curve, though lower in magnitude, since the rule design loads are used for (ultimate) strength assessment. The wave-induced torque is compared to the Bureau Veritas rule design torque and is similar in magnitude. Also, it has an unsymmetric torque distribution, as opposed to the symmetric rule design torque. Additionally, the horizontal bending moment peak is lower than the vertical bending moment, but in magnitude still significant. Despite the latter, both the beam model and the 3D FE model showed that the resulting structural response is insignificant compared to the vertical bending moment deformations. Therefore the horizontal bending moment is not deemed relevant for the longitudinal stiffness assessment of Feadships provided that the geometry does not deviate too much from the used test case in this thesis. The relevant load distributions are thus the vertical bending moment and the torque and can be calculated according to a sea state that represents experimental conditions or design sea states to determine limit values of the structural response. All load distributions compare well to the classification load distributions and are deemed sufficiently accurate for the preliminary design.

II Can the response of the 1D beam model be used to indicate structural risks in new designs and/or obtain useful predictions for interior clearance?

The 1D beam model consists of material stiffness and cross-sectional properties that represent the yacht hull without superstructure. The cross-sectional property input is obtained by using cross-sectional outlines of the hull structure for which Siemens NX 11 is able to determine the properties (the NX section method) with good agreement with currently available methods. Also, this method computes the torsional constant for that is required for the torsional response of the beam model. The use of the properties determined by the NX section method gives better agreement with the 3D FE model global response than if the Special Service Craft (SSC) software is used to determine the properties, which is to a largest extent caused by the conservative estimation of the vertical shear area in the SSC software. Good agreement is found between the global response of the beam model and the detailed 3D FE model for the vertical and horizontal bending and the longitudinal torsion. The shear deformations had a significant contribution of 20% to the vertical displacement in vertical bending, hence for accurate local response analysis, the shear deformations should be taken into account. The global response is used to derive local deformation components that describe the bulging and expansion/contraction of horizontal structural elements under vertical bending and for torsion the deformation component that can be derived is the relative vertical deformation between longitudinal locations. All deformation components showed good agreement with the 3D FE model and it can be concluded that the local response can be calculated with sufficient accuracy for the preliminary design. The local deformation components at locations where the deflections can be critical for the client comfort can be compared to limit values derived from previous yachts to indicate that the stiffness of a new yacht is too low and appropriate actions should be taken. The same deformation components can be used to get initial information on the clearances or connections that should be applied for the interior. All of the above results in the affirmative answer of the second main research question.

The developed routines for the determination of the wave-induced load distributions in combination with the 1D structural beam model and the local response analysis results in more detailed insights in the longitudinal stiffness distribution of Feadship superyachts. This is useful during internal communication in concurrent design sessions, providing a clear picture of the influence of the structural stiffness on other disciplines. Most importantly, it enables Feadship to increase the level of comfort onboard of the yachts to make sure they can maintain the strong market position in the global superyacht industry.

6

Recommendations for future work

This thesis work covered a wide range of topics to provide a complete overview of what can be achieved with more insight in longitudinal stiffness of superyachts. Most of these topics can be subjected to further research especially with focus on the practical applicability for Feadships. Several research topics are identified that can increase the potential of this work or are required for practical application of this method.

In this work it was shown that good accuracy is obtained for deformation components with a relatively simple representation of the yacht structure. The deformations need to be compared with limit values to indicate any risks in a new design and therefore the investigation if this limit values is necessary. For example, yachts that have been shown to experience comfort related issues due to an insufficient longitudinal stiffness can be analysed with the methods in this thesis work to set-up the actual limits. This can be a combination of user experience to indicate critical locations with experimental measurements of the deformations. The application of this method to other yachts is therefore the most important step to be made to increase the potential of this work and to be of direct practical use to Feadship.

The experimental measurements on board of the yacht is recent topic at Feadship that is performed and direct comparison of the deformations can be useful to check the validity of the beam model in this work in reality, but also the 3D FE models that are used for validation in this work. The 3D FE models are also a simplification of reality and deviations are very well possible. The locations of the strain measurements have to take into account limitation of the beam model that local effects of e.g. cut-outs that change the stress field around it can not be taken into account.

The beam model in this work is a simple representation of reality, which can be improved upon to create a more detailed deformation field. Suggestions were already provided in the literature review in Section 2.5 to use methods like the coupled-beam method to create a model that can more accurately determine deformations between the decks. Also, the superstructure can then be incorporated, which is relevant, because the superstructure usually contains many of the (luxurious) owner area's for which discomfort due to creaking is most critical. Although promising, this is an extensive step, because the model should be able to adapt easily for the different layouts of the custom yachts to be of practical use and research has to be performed to the required stiffness of the springs or elements between the decks. Therefore it is advised to test the beam model in this work first and if the insights of the comparison with previous yachts is not sufficient to invest in the more complicated models.

The complete 3D FE models are currently used at the end of the detailed design phase to demonstrate the structural strength for certification and perform as a design check before the yacht gets into commissioning. The complete models take a long time to complete and are therefore not often used in the direct design process of the yacht itself. It might be useful to investigate the ability to use the global response of the beam model in this work to use as boundary conditions for partly FE models. In that case, only a portion of the ship can be modelled in detail, which takes less time and the displacements and rotations from the beam model can be imposed as boundary conditions to study the stress concentrations for sections that have e.g. geometric discontinuities that pose a risk to the design.

The structural model alone is not the only factor that determines the accuracy of the response, also the magnitude of the loads is a large factor. The load case analysis for operational loads can be improved by a more complete analysis called a long-term analysis. In this analysis the probability of the occurrence of sea states and the operational profile of a yacht is combined to create a complete envelope of load distributions. This

means a higher certainty is obtained that the design loads cover all the possible loading scenario's. If (partly) non-linear methods are also included, which are applicable in sea states with $H_s > 4$ m the load distributions can even replace the Lloyd's Register rule loads for strength analysis, which means the loads are more applicable to Feadships. This allows for less conservative designs, resulting in a lighter structure and thus increasing the yacht performance.

In this work, a regular design wave is used to derive the load distributions, which is actually a wave that is never occurring in reality. In literature it was found that using an irregular design wave, more realistic and reliable loads were obtained [19]. This is especially true for concurrent values of the vertical bending moment and torque, because the time moment of occurrence of the two defines whether local deformations cancel each other or occur in addition to each other. Additionally, the irregular waves can be developed that are short-crested, which matches reality even more. The research to more applicable design waves can be directly used in combination with the method in this work. Also, if multiple loading conditions are to be analysed, the beam model is computationally efficient enough to evaluate a larger amount of loading conditions.

The ship particulars used as input for the strip method solver SHIPMO are preliminary estimates and for example the mass distribution is used as input as mass elements with a certain radius of gyration. Currently, initial estimates are used that are based on rules of thumb for the magnitude of these radii and more accurate estimates of these values can improve the accuracy of the internal load RAO's that are calculated.

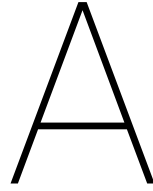
Bibliography

- [1] Andersen, L. and Nielsen, S. R. [2008], *Elastic Beams in Three Dimensions*, DCE Lecture Notes, Aalborg University, Department of Civil Engineering, Structural Mechanics.
- [2] Bai, Y. and Jin, W.-L. [2015], *Marine structural design*, 2 edn, Butterworth-Heinemann, Amsterdam.
- [3] Balduzzi, G., Aminbaghai, M., Sacco, E., Füssl, J., Eberhardsteiner, J. and Auricchio, F. [2016], 'Non-prismatic beams: A simple and effective timoshenko-like model', *International Journal of Solids and Structures* **90**, 236–250.
- [4] Bertram, V. [2012], *Practical ship hydrodynamics*, 2 edn, Butterworth-Heinemann, Amsterdam and London.
- [5] Bittencourt, M. L. [2014], *Computational solid mechanics: Variational formulation and high order approximation / Marco L. Bittencourt*, 1st edn, CRC Press, Boca Raton.
- [6] Bosboom, J. and Stive, M. [2015], *Coastal dynamics I*, 0.5 edn, Delft Academic Press, Delft.
- [7] Bureau Veritas [2017], 'Hull structure and arrangement for the classification of cargo ships less than 65 m and non cargo ships less than 90 m: Nr 600 dt r02 e'.
- [8] Bureau Veritas [2018], 'Rules for the classification of steel ships: Part b - hull and stability'.
- [9] Cai, X. [2016], Ship Response Estimation in Early Design Stage, Master thesis, KTH Royal Institute of Technology, Stockholm.
- [10] Chakrabarti, S. K. [2005], *Handbook of offshore engineering*, 1 edn, Elsevier, Amsterdam and London.
- [11] Clauss, G. F., Klein, K. and Dudek, M. [2010], Influence of the bow shape on loads in high and steep waves, in '29th International Conference on Ocean, Offshore and Arctic Engineering: Volume 4', ASME.
- [12] Cowper, G. R. [1966], 'The shear coefficient in timoshenko's beam theory', *Journal of Applied Mechanics* **33**(2), 335–340.
- [13] Crandall, S. H. and Mark, W. D. [1963], *Random vibration in mechanical systems*, 2 edn, Academic Press, New York.
- [14] de Hauteclocque, G., Derbanne, Q. and El-Gharbaoui, A. [2012], Comparison of different equivalent design waves with spectral analysis, in 'Volume 1: Offshore Technology', ASME, p. 353.
- [15] Det Norske Veritas - Germanischer Lloyd [2015], 'Rules for classification: Part 3 hull, chapter 3 hull design loads'.
- [16] Det Norske Veritas - Germanischer Lloyd [2017], 'Recommended practice dnvgl-rp-c205: Environmental conditions and environmental loads'.
- [17] Duncan, W. J., Ellis, D. L. and Scruton, C. [1933], 'Xv. the flexural centre and the centre of twist of an elastic cylinder', *The London, Edinburgh, and Dublin Philosophical Magazine and Journal of Science* **16**(104), 201–235.
- [18] Fagerberg, L. [2003], Wrinkling of Sandwich Panels for Marine Applications, Phd thesis, KTH Aeronautical and Vehicle Engineering, Stockholm, Sweden.
- [19] Fang, M.-C., Fang, C.-C. and Wu, C.-H. [2007], 'Prediction of design wave loads of the ocean structure by equivalent irregular wave approach', *Ocean Engineering* **34**(10), 1422–1430.
- [20] Folso, L. and Rizzuto, E. [2003], Equivalent waves for sea loads on ship structures, in 'Volume 2: Safety and Reliability; Pipeline Technology', ASME, pp. 423–431.

- [21] Fonseca, N. and Soares, C. G. [2004], 'Experimental investigation of the nonlinear effects on the vertical motions and loads of a containership in regular waves', *Journal of Ship Research* **48**(2), 118–147.
- [22] Fricke, W. and Robert, B. [2012], *Proceedings of the 18th International Ship and Offshore Structures Congress*, Vol. 2, Schiffahrts-Verlag "Hansa" GmbH & Co. KG, Hamburg.
- [23] Fung, Y. C. [2002], *An introduction to the theory of aeroelasticity*, Dover Publications, New York, NY.
- [24] Gere, J. M. and Goodno, B. J. [2009], *Mechanics of materials*, 7 edn, Cengage Learning, Toronto ON and Clifton Park NY.
- [25] Gerritsma, J. and Beukelman, W. [1964], 'The distribution of the hydrodynamic forces on a heaving and-pitched shipmodel in still water', *International Shipbuilding Progress* **11**(123), 506–522.
- [26] Heder, M. and Ulfvarson, A. [1991], 'Hull beam behaviour of passenger ships', *Marine Structures* **4**, 17–34.
- [27] Holthuijsen, L. H. [2007], *Waves in oceanic and coastal waters*, 1 edn, Cambridge University Press, Cambridge.
- [28] Hughes, O. F., Paik, J. K. and Béghin, D. [2010], *Ship structural analysis and design*, 2 edn, Society of Naval Architects and Marine Engineers, Jersey City, N.J.
- [29] Hutchinson, J. R. [2001], 'Shear coefficients for timoshenko beam theory', *Journal of Applied Mechanics* **68**(1), 87.
- [30] Iijima, K., Shigemi, T., Miyake, R. and Kumano, A. [2004], 'A practical method for torsional strength assessment of container ship structures', *Marine Structures* **17**(5), 355–384.
- [31] Jang, C. D. and Hong, S. Y., eds [2009], *Proceedings of the 18th International Ship and Offshore Structures Congress - Loads*, Vol. 1, Seoul, Korea.
- [32] Jensen, J. J. [1983], 'On the shear coefficient in timoshenko's beam theory', *Journal of Sound and Vibration* **87**(4), 621–635.
- [33] Jensen, J. J. [2001], *Load and Global Response of Ships*, Vol. 4 of *Ocean Engineering Book Series*, Elsevier.
- [34] Jensen, J. J. and Pedersen, P. T. [1978], 'Wave-induced bending moments in ships - a quadratic theory', *The Royal Institution of Naval Architects* pp. 151–165.
- [35] Journée, J. M. [1992], 'Quick strip theory calculations in ship design', *Conference on Practical Design of Ships and Mobile Structures* **1**.
- [36] Journée, J. M. and Adegeest, L. J. [2003], 'Theoretical manual of strip theory program "seaway for windows": Ship hydromechanics laboratory, delft university of technology, tud report no.1370'.
- [37] Journée, J. M., Massie, W. W. and Huijsmans, R. H. [2015], *Offshore Hydromechanics: Delft University of Technology*, 3 edn, Interfaculty Center for Offshore technology.
- [38] Kring, D., Huang, Y.-F., Sclavounos, P., Vada, T. and Braathen, A. [1997], Nonlinear ship motions and wave-induced loads by a rankine method, in 'Twenty-First Symposium on Naval Hydrodynamics', pp. 54–63.
- [39] Lin, F. [2016], 'Hydroelasticity analysis in frequency domain and time domain', *Journal of Shipping and Ocean Engineering* **6**(2).
- [40] Lloyd's Register [2015], 'Direct calculations for special service craft of metallic construction, august 2015'.
- [41] Lloyd's Register [2018a], 'Rules and regulations for the classification of special service craft, july 2018'.
- [42] Lloyd's Register [2018b], 'Structural design assessment: Primary structure of passenger ships, january 2018'.
- [43] Lloyd's Register Group Limited [2018], 'Special service craft (ssc) software: Version 2018'.

- [44] Ma, M., Zhao, C. and Hughes, O. [2014], 'A practical method to apply hull girder sectional loads to full-ship 3d finite-element models using quadratic programming', *Ships and Offshore Structures* **9**(3), 257–265.
- [45] Ma, S., Ge, W.-p., Ertekin, R. C., He, Q. and Duan, W.-y. [2018], 'Experimental and numerical investigations of ship parametric rolling in regular head waves', *China Ocean Engineering* **32**(4), 431–442.
- [46] Maritime Research Institute Netherlands, MARIN [2018], 'Shipmo software: Version 2018'.
- [47] Megson, T. H. G. [2013], *Aircraft structures for engineering students*, Elsevier aerospace engineering series, 5 edn, Butterworth-Heinemann, Oxford and Waltham, MA.
- [48] Naar, H., Varsta, P. and Kujala, P. [2004], 'A theory of coupled beams for strength assessment of passenger ships', *Marine Structures* **17**(8), 590–611.
- [49] Ochi, M. K. [1981], 'Principles of extreme value statistics and their application', *The Society of Naval Architects and Marine Engineers* pp. 15–30.
- [50] Oñate, E. [2009], *Structural analysis with the finite element method: Linear statics*, Vol. 1 of *Lecture notes on numerical methods in engineering and sciences*, Springer, Dordrecht and London.
- [51] Oñate, E. [2013], *Structural analysis with the finite element method: Linear statics*, Vol. 2 of *Lecture notes on numerical methods in engineering and sciences*, Springer, Dordrecht and London.
- [52] Paik, J. K. [2018], *Ultimate limit state analysis and design of plated structures*, 2 edn, John Wiley & Sons, Hoboken, New Jersey.
- [53] Pedersen, T. [2000], *Wave Load Prediction - a Design Tool*, PhD thesis, Technical University of Denmark, Lyngby.
- [54] Perez, T. [2005], *Ship motion control: Course keeping and roll stabilisation using rudder and fins*, *Advances in industrial control*, 1 edn, Springer, Berlin and London.
- [55] Phelps, B. P. [1997], 'Determination of wave loads for ship structural analysis: Dstn aeronautical and maritime research laboratory'.
- [56] Pierson, Jr., W. J., Neumann, G. and James, R. W. [1971], *Practical methods for Observing and Forecasting Ocean Waves by means of Wave Spectra and Statistics: U.S. Naval Oceanographic Office*, 3 edn.
- [57] Pilkey, W. D. [2002], *Analysis and design of elastic beams: Computational methods*, 1 edn, Wiley, New York and Chichester.
- [58] Rajendran, S., Fonseca, N. and Guedes Soares, C. [2015], 'Effect of surge motion on the vertical responses of ships in waves', *Ocean Engineering* **96**, 125–138.
- [59] Rajendran, S., Fonseca, N. and Soares, C. G. [2016], 'Prediction of extreme motions and vertical bending moments on a cruise ship and comparison with experimental data', *Ocean Engineering* **127**, 368–386.
- [60] Reddy, J. N. [2015], *An introduction to nonlinear finite element analysis: With applications to heat transfer, fluid mechanics, and solid mechanics*, 2 edn, Oxford University Press, Oxford.
- [61] Roy, J., Munro, B., Walley, S. and Meredith, A. [2008], 'Longitudinally vs. transversely framed structures for large displacement motor yachts', *20th HISWA symposium*.
- [62] Salvesen, N., Tuck, E. and Faltinsen, O. [1970], 'Ship motion and sea loads', *The Society of Naval Architects and Marine Engineers* **6**, 250–287.
- [63] Shama, M. [2013], *Buckling of Ship Structures*, 1 edn, Springer Berlin Heidelberg, Berlin, Heidelberg.
- [64] Siemens Product Lifecycle Management Software Inc. [2016], 'Nx nastran 11: Element library reference'.
- [65] Siemens Product Lifecycle Management Software Inc. [2018], 'Siemens nx, version 11'.

- [66] Soares, C. G. and Garbatov, Y. [2015], *Proceedings of the 19th International Ship and Offshore Structures Congress*, CRC Press/Balkema, Leiden, The Netherlands.
- [67] Soares, C. G. and Garbatov, Y. [2017], *Progress in the analysis and design of marine structures: Proceedings of the 6th International Conference on Marine Structures (MARSTRUCT 2017), May 8-10, 2017, Lisbon, Portugal*, CRC Press, Boca Raton.
- [68] Soares, C. G. and Santos, T. A. [2016], *Maritime technology and engineering III: Proceedings of the 3rd International Conference on Maritime Technology and Engineering (MARTECH 2016, Lisbon, Portugal, 4-6 July 2016) / edited by Carlos Guedes Soares, T.A. Santos*, CRC Press, Boca Raton.
- [69] Soares, C. G. and Schellin, T. E. [1996], 'Long term distribution of non-linear wave induced vertical bending moments on a containership', *Marine Structures* **9**, 333–352.
- [70] Soares, C. G. and Schellin, T. E. [1998], 'Nonlinear effects on long-term distributions of wave-induced loads for tankers', *Journal of Offshore Mechanics and Arctic Engineering* **120**, 65–70.
- [71] Sun, X. S., Yao, C. B., Xiong, Y. and Ye, Q. [2017], 'Numerical and experimental study on seakeeping performance of a swath vehicle in head waves', *Applied Ocean Research* **68**, 262–275.
- [72] Tan, S. G. [1995], 'Seakeeping considerations in ship design and operations: Maritime research institute netherlands (marin)', *Regional Maritime Conference, Indonesia*.
- [73] Temarel, P., Bai, W., Bruns, A., Derbanne, Q., Dessi, D., Dhavalikar, S., Fonseca, N., Fukasawa, T., Gu, X., Nestegård, A., Papanikolaou, A., Parunov, J., Song, K. H. and Wang, S. [2016], 'Prediction of wave-induced loads on ships: Progress and challenges', *Ocean Engineering* **119**, 274–308.
- [74] Tupper, E. C. [2013], *Introduction to Naval Architecture: Formerly Muckle's Naval Architecture for Marine Engineers*, 1 edn, Elsevier Science & Technology Books, Jordan Hill, England.
- [75] van Sluijs, M. F., Cox, G. G. and Andrew, R. N. [1981], *Final report and recommendations of the 16th ITTC Seakeeping Committee: International Towing Tank Conference*, Leningrad.
- [76] Vernon, T. A. and Nadeau, Y. [1987], *Thin-walled beam theories and torsion application ship hulls: Defence Research Establishment Atlantic*, Technical Memorandum, Canada.
- [77] Wang, C. M., Reddy, J. N. and Lee, K. H. [2000], *Shear deformable beams and plates: Relationships with classical solutions*, 1 edn, Elsevier, Amsterdam and New York.
- [78] Wijker, J. [2004], *Mechanical Vibrations in Spacecraft Design*, 1 edn, Springer Berlin Heidelberg, Berlin, Heidelberg.
- [79] Xia, J., Wang, Z. and Jensen, J. [1998], 'Non-linear wave loads and ship responses by a time-domain strip theory', *Marine Structures* **11**(3), 101–123.
- [80] Young, W. C., Budynas, R. G. and Roark, R. J. [2002], *Roark's formulas for stress and strain*, 7 edn, McGraw-Hill, New York and London.
- [81] Zhao, C., Ma, M. and Hughes, O. [2013], Applying strip theory based linear seakeeping loads to 3d full ship finite element models, in 'Ocean Engineering', Vol. 5.



Two-noded Timoshenko beam element

The two-noded Timoshenko beam element is a 1D beam element with twelve degrees of freedom, six at each node. It can account for loads in three-dimensional space and includes shear deformations and torsion. Both Oñate [51] and Andersen and Nielsen [1] give a (part of the) derivation for the element stiffness matrix K_e , the element load vector f_e and element degrees of freedom vector w_e . The notation of Andersen and Nielsen [1] is more concise and given here with the possible element loading types and directions given in Figure A.1.

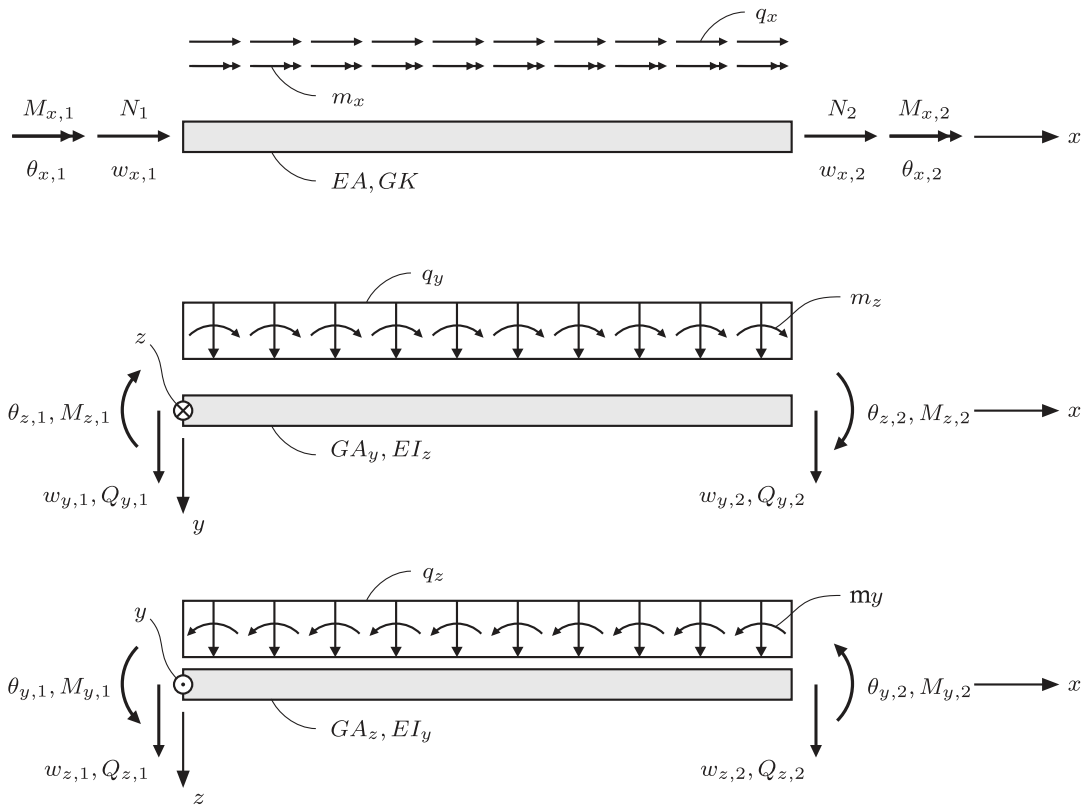


Figure A.1: Timoshenko beam element loaded in three directions with definition of degrees of freedom, nodal reaction forces, element loads and sectional properties. [1]

The element equilibrium equations may be expressed in matrix form seen in Eq. (A.1).

$$r_e = K_e w_e + f_e \quad (\text{A.1})$$

The 12-dimensional column vectors r_e , w_e and f_e containing the reaction forces, element degrees of freedom and loads, respectively, can be found in Eq. (A.2). The constants Φ_y and Φ_z are given in Eq. (A.3).

$$\mathbf{r}_e = \begin{bmatrix} \mathbf{r}_{e1} \\ \mathbf{r}_{e2} \end{bmatrix} = \begin{bmatrix} N_1 \\ Q_{y,1} \\ Q_{z,1} \\ M_{x,1} \\ M_{y,1} \\ M_{z,1} \\ N_2 \\ Q_{y,2} \\ Q_{z,2} \\ M_{x,2} \\ M_{y,2} \\ M_{z,2} \end{bmatrix}, \quad \mathbf{w}_e = \begin{bmatrix} \mathbf{w}_{e1} \\ \mathbf{w}_{e2} \end{bmatrix} = \begin{bmatrix} w_{x,1} \\ w_{y,1} \\ w_{z,1} \\ \theta_{x,1} \\ \theta_{y,1} \\ \theta_{z,1} \\ w_{x,2} \\ w_{y,2} \\ w_{z,2} \\ \theta_{x,2} \\ \theta_{y,2} \\ \theta_{z,2} \end{bmatrix}, \quad \mathbf{f}_e = \begin{bmatrix} \mathbf{f}_{e1} \\ \mathbf{f}_{e2} \end{bmatrix} = \begin{bmatrix} -\frac{1}{2}q_x l \\ -\frac{1}{2}q_y l + m_z \\ -\frac{1}{2}q_z l - m_y \\ -\frac{1}{2}m_x l \\ \frac{1}{12}q_z l^2 - \frac{1}{2}\frac{\Phi_z}{1+\Phi_z}m_y l \\ -\frac{1}{12}q_y l^2 - \frac{1}{2}\frac{\Phi_y}{1+\Phi_y}m_z l \\ -\frac{1}{2}q_x l \\ -\frac{1}{2}q_y l - m_z \\ -\frac{1}{2}q_z l + m_y \\ -\frac{1}{2}m_x l \\ -\frac{1}{12}q_z l^2 - \frac{1}{2}\frac{\Phi_z}{1+\Phi_z}m_y l \\ \frac{1}{12}q_y l^2 - \frac{1}{2}\frac{\Phi_y}{1+\Phi_y}m_z l \end{bmatrix}. \quad (\text{A.2})$$

$$\Phi_y = 12\frac{EI_z}{GA_y l^2}, \quad \Phi_z = 12\frac{EI_y}{GA_z l^2}. \quad (\text{A.3})$$

The element stiffness matrix \mathbf{K}_e is given by Eq. (A.4), with the definitions $k_{ij}^{z/y}$ given by equations Eq. (A.5) and Eq. (A.6).

$$\mathbf{K}_e = \begin{bmatrix} \frac{EA}{l} & 0 & 0 & 0 & 0 & 0 & -\frac{EA}{l} & 0 & 0 & 0 & 0 & 0 \\ 0 & k_{11}^z & 0 & 0 & 0 & k_{12}^z & 0 & k_{13}^z & 0 & 0 & 0 & k_{14}^z \\ 0 & 0 & k_{11}^y & 0 & k_{12}^y & 0 & 0 & 0 & k_{13}^y & 0 & 0 & k_{14}^y \\ 0 & 0 & 0 & \frac{GK}{l} & 0 & 0 & 0 & 0 & 0 & -\frac{GK}{l} & 0 & 0 \\ 0 & 0 & k_{12}^y & 0 & k_{22}^y & 0 & 0 & 0 & k_{23}^y & 0 & 0 & k_{24}^y \\ -\frac{EA}{l} & 0 & 0 & 0 & 0 & 0 & \frac{EA}{l} & 0 & 0 & 0 & 0 & 0 \\ 0 & k_{13}^z & 0 & 0 & 0 & k_{23}^z & 0 & k_{33}^z & 0 & 0 & 0 & k_{34}^z \\ 0 & 0 & k_{13}^y & 0 & k_{23}^y & 0 & 0 & 0 & k_{33}^y & 0 & 0 & k_{34}^y \\ 0 & 0 & 0 & -\frac{GK}{l} & 0 & 0 & 0 & 0 & 0 & \frac{GK}{l} & 0 & 0 \\ 0 & 0 & k_{14}^y & 0 & k_{24}^y & 0 & 0 & 0 & k_{34}^y & 0 & k_{44}^y & 0 \\ 0 & k_{14}^z & 0 & 0 & 0 & k_{24}^z & 0 & k_{34}^z & 0 & 0 & 0 & k_{44}^z \end{bmatrix} \quad (\text{A.4})$$

$$\begin{bmatrix} k_{11}^z & k_{12}^z & k_{13}^z & k_{14}^z \\ k_{22}^z & k_{23}^z & k_{33}^z & k_{34}^z \\ k_{33}^z & k_{34}^z & k_{44}^z & \end{bmatrix} = \frac{EI_z}{(1+\Phi_y)l^3} \begin{bmatrix} 12 & 6l & -12 & 6l \\ (4+\Phi_y)l^2 & -6l & (2-\Phi_y)l^2 & \\ & 12 & -6l & \\ & & (4+\Phi_y)l^2 & \end{bmatrix} \quad (\text{A.5})$$

$$\begin{bmatrix} k_{11}^y & k_{12}^y & k_{13}^y & k_{14}^y \\ k_{22}^y & k_{23}^y & k_{33}^y & k_{34}^y \\ k_{33}^y & k_{34}^y & k_{44}^y & \end{bmatrix} = \frac{EI_y}{(1+\Phi_z)l^3} \begin{bmatrix} 12 & -6l & -12 & -6l \\ (4+\Phi_z)l^2 & 6l & (2-\Phi_z)l^2 & \\ & 12 & 6l & \\ & & (4+\Phi_z)l^2 & \end{bmatrix} \quad (\text{A.6})$$

B

Siemens NX 11 cross-sectional property performance

The tool in Siemens NX11 that determines the cross-sectional properties is verified by comparing its performance to the analytical calculation of the cross-sectional properties of two simple cross-sections: a box and an I-beam cross-section, as seen in Figure B.1. A thin-walled cross-section is taken with the properties as given in Table B.1, because the analytical equations are derived for thin-walled cross-sections (except for the area A , and area moments of inertia I_{yy} and I_{zz})

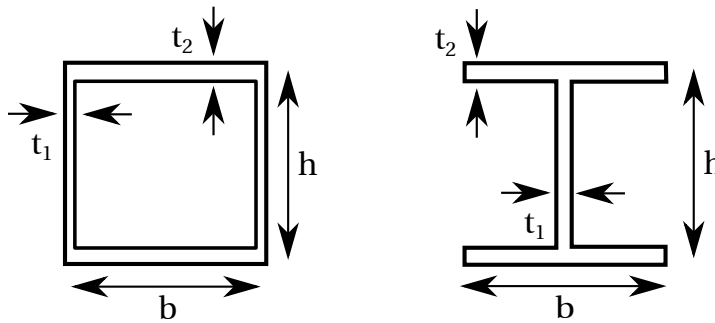


Figure B.1: The box and I-beam cross-sections used for tool verification.

Table B.1: Geometry parameters of cross-sections

Parameters	Box	I-beam	Unit
h	100	150	mm
b	100	100	mm
t_1	1	1	mm
t_2	1	1	mm

For the box section, the area A and second moment of inertia's I_{yy} and I_{zz} are calculated as given by equations Eq. (B.1), Eq. (B.2) and Eq. (B.3), respectively.

$$A = 2t_1(h + t_2) + 2t_2(b - t_1) \quad (\text{B.1})$$

$$I_{yy} = \frac{1}{6}t_1(h + t_2)^3 + 2\left(\frac{1}{12}(b - t_1)t_2^3 + (b - t_1)t_2\left(\frac{h}{2}\right)^2\right) \quad (\text{B.2})$$

$$I_{zz} = \frac{1}{6}t_2(b - t_1)^3 + 2\left(\frac{1}{12}(h + t_2)t_1^3 + (h + t_2)t_1\left(\frac{b}{2}\right)^2\right) \quad (\text{B.3})$$

The torsional constant is taken as Eq. (B.4) as defined by Gere and Goodno [24].

$$J = \frac{2b^2 h^2 t_1 t_2}{b t_1 + h t_2} \quad (\text{B.4})$$

No analytical equations are found for the warping stiffness C_w , since warping stiffness is usually insignificant compared to the torsional stiffness for closed-cross-sections. For both the box section and the I-section, the shear correction factors k_z is calculated with the equations as derived by Cowper [12].

For the I-beam section, the area and second moment of inertia's are calculated as given by Eq. (B.5), Eq. (B.6) and Eq. (B.7), respectively.

$$A = 2bt_1 + (h - t_1)t_2 \quad (\text{B.5})$$

$$I_{yy} = \frac{1}{12} t_2 (h - t_1)^3 + 2 \left(\frac{1}{12} b t_1^3 + b t_1 \left(\frac{h}{2} \right)^2 \right) \quad (\text{B.6})$$

$$I_{zz} = \frac{1}{6} t_1 b^3 + \frac{1}{12} (h - t_1) t_2^3 \quad (\text{B.7})$$

The torsional constant and warping constant are taken as Eq. (B.8) and Eq. (B.9) as defined by Young et al. [80].

$$J = \frac{2b^2 h^2 t_1 t_2}{b t_1 + h t_2} \quad (\text{B.8})$$

$$C_w = \frac{h^2 t b^3}{24} \quad (\text{B.9})$$

The results for the comparison of the NX 1D element section method and the analytical equations can be seen in Table B.2. From the results it can be concluded that the NX method calculates the cross-sectional properties of thin-walled sections within acceptable accuracy¹.

Table B.2: Error percentage of the NX 1D element section method compared to the analytical equations for the respective cross-sections.

Parameters	Box	I-beam
A	0.0%	0.0%
I_{yy}	0.0%	0.0%
I_{zz}	0.0%	0.0%
J	0.4%	0.0%
C_w	-	0.0%
k_z	3.9%	2.0%

¹Note that for larger geometries with the same thickness (i.e. h and b increased by a factor of 10) the results are the same